LUT UNIVERSITY
LUT School of Energy Systems
LUT Mechanical Engineering

Alex Rosu

ROTOR BALANCING AND ALIGNING WITH ACTIVE MAGNETIC BEARINGS: A CASE STUDY OF MUSK DRIVETRAIN SIMULATOR

Lappeenranta 14.05.2021

Supervisor: D. Sc. (Tech.) Eerik Sikanen
Examiners: Professor Jussi Sopanen
Adjunct professor D. Sc. (Tech.) Rafal Jastrzebski

TIIVISTELMÄ

LUT-Yliopisto
LUT School of Energy Systems
LUT Kone

Alex Rosu

Roottorin tasapainotus ja linjaus aktiivimagneettilaakereilla: MUSK-voimansiirto simulaattorin tapaustutkimus

Diplomityö

2021

98 sivua, 47 kuvaa ja 9 taulukkoa

Ohjaaja: TkT Eerik Sikanen
Tarkastajat: Professori Jussi Sopanen
Dosentti Rafal Jastrzebski

Hakusanat: Aktiivi tilan seuranta, aktiivimagneettilaakeri, säätö, joustava roottori, suurnopeus, linjausvirhe, simulaatio, epätasapaino

Jotta voidaan löytää ratkaisu useisiin maailmanlaajuisiin kestävyyshaasteisiin, kuten luonnonvarojen niukkuuteen, ympäristön pilaantumiseen ja ilmastonmuutokseen, on tärkeää kohdistaa tutkimusta luotettaviin ja energiatehokkaisiin koneisiin. Yksi konetyyppi, joka kuuluu tähän kestävien koneiden ryhmään, on suurnopeuskone, jota on tukemassa aktiiviset magneettilaakerit (AMB). Kuten tavallisten pyörivien koneiden tapauksessa, myös AMB:ien tukema kone voi altistua voimakkaalle tärinälle epätasapaino- ja linjausvirheiden vuoksi toimintasyklinsä aikana. Tämä tärinä voi lyhentää koneen käyttöikää ja aiheuttaa samalla lisäkäyttökustannuksia, ellei sitä valvota kunnolla. Epätasapainon ja linjausvirheiden aiheuttaman tärinän estämiseksi onkin mahdollista käyttää koneelle sopivia ohjausalgoritmeja.

Tämän tutkielman päätavoitteena on ollut suorittaa kestävyyden arviointi valitulle joustavalle AMB-roottorin voimansiirtojärjestelmälle. Arviointia suoritettaessa epätasapaino- ja linjausvirheitä on sijoitettu järjestelmän eri paikkoihin virtuaalisin keinoin. Arviointitestit on suoritettu turvallisessa virtuaalisessa testausympäristössä hyödyntämällä todellisen järjestelmän Simulink-mallia. Järjestelmän dynaamisten vasteiden tutkimiseen ja analysointiin on käytetty aikatason analyysimenetelmää. Tärkeimmät tulokset osoittavat, että epätasapaino ei ole yhtä vakava vika kuin kytkimen virheellinen suuntaus tutkitussa järjestelmässä sen tarkasteltavalla toiminta-alueella. Linjausvirhe on erityisen kriittinen järjestelmän roottorin nostovaiheessa, kun roottorilla on mahdollisuus olla kosketuksessa turvalaakereidensa kanssa. Koska kytkimen linjausvirhe on todistettavasti kriittisempi vika, on tarpeen soveltaa erilaisia toimia, jotka voisivat minimoida sen. Yksi ehdotettu lähestymistapa on suunnitella vankempi kytkin kytkemään roottori ajettuun koneeseen. Tämä antaisi mahdollisuuden saavuttaa järjestelmän yleiseen luotettavuuteen liittyviä etuja.

ABSTRACT

LUT University
LUT School of Energy Systems
LUT Mechanical Engineering

Alex Rosu

Rotor balancing and aligning with active magnetic bearings: a case study of MUSK drivetrain simulator

Master's thesis

2021

98 pages, 47 figures and 9 tables

Supervisor: D. Sc. (Tech.) Eerik Sikanen
Examiners: Professor Jussi Sopanen
Adjunct professor D. Sc. (Tech.) Rafal Jastrzebski

Keywords: Active condition monitoring, active magnetic bearing, control, flexible rotor, high-speed, misalignment, simulation, unbalance

To provide a solution to several global sustainable challenges such as scarce of natural resources, environment pollution, and climate change, it is important to focus a research on reliable and energy-efficient machines. One type of machine which belongs to this group of sustainable machines, is a high-speed rotating machine which is supported by active magnetic bearings (AMBs). As is the case with ordinary rotating machines, the machine supported by AMBs can also be subjected to high vibration due to unbalance and misalignment faults during its operation cycle. This vibration can decrease the service-life of the machine while simultaneously causing additional operation costs if not monitored properly. To suppress vibrations caused by unbalance and misalignment defects, it is possible to apply suitable controlling algorithms for the machine.

The main objective of this thesis has been to perform a robustness evaluation for a selected flexible AMB-rotor drivetrain system. While performing the evaluation, unbalance and coupling misalignment faults have been placed at different locations on the system by virtual means. The evaluation tests have been carried out in a safe virtual testing environment by utilizing the Simulink model of the real system. For studying and analyzing the dynamic responses of the system, a time domain analysis approach has been utilized. The main results are indicating that an unbalance is not as severe fault than a coupling misalignment in the investigated system within its studied operation range. The misalignment fault is especially critical during the lift-off phase of the rotor of the system when there is a possibility for the rotor to contact with its safety bearings. Because a coupling misalignment is evidently more critical fault, it is necessary to apply different actions which could minimize it. One suggested approach is to design more robust coupling to connect a driving rotor with a driven machine. This would allow to achieve benefits related to the overall reliability of the system.

ACKNOWLEDGEMENTS

I would like to first of all thank Jussi Sopanen for allowing me to be part of his research team during these past few years. This has allowed me to gain valuable working experience and also additional knowledge from the field of rotor dynamics while I have been pursuing my master's degree. I am also grateful for my supervisor Eerik Sikanen for his overall support during this master's thesis project. His support has been especially very helpful whenever I have had more technical questions regarding different aspects of rotor dynamics which are linked to the case study part of this work. Rafal Jastrzebski has also earned my gratitude for answering my questions regarding the control and simulations and also electrical aspects of this work. But perhaps the most important people whom I still value the most are my family and friends. They are truly the people who have kept me going during all my years of study. And because of this I will be forever in their debt.

Alex Rosu

Alex Rosu

Lappeenranta 14.05.2021

TABLE OF CONTENTS

TIIVISTELMÄ
ABSTRACT
ACKNOWLEDGEMENTS
TABLE OF CONTENTS
LIST OF SYMBOLS AND ABBREVIATIONS
1 INTRODUCTION 11
1.1 Background and motivation 12
1.2 Research problem 14
1.3 Objective 16
1.3.1 Research questions 17
1.3.2 Hypotheses 17
1.4 Scope 18
1.5 Structure of thesis 18
2 UNBALANCE AND MISALIGNMENT IN AMB-ROTOR SYSTEMS 19
2.1 Modelling of flexible rotor 19
2.2 Principle of unbalance 20
2.3 Misalignment 24
2.3.1 Misalignment in drivetrain couplings 24
2.3.2 Misalignment between rotor and AMB actuator 32
2.3.3 Sensor runout and non-collocation 38
2.3.4 Misalignment of safety bearings 40
3 VIBRATION COMPENSATION TECHNIQUES FOR AMB 41
3.1 Conventional methods of balancing and aligning 41
3.1.1 Balancing of rigid rotors 42
3.1.2 Balancing of flexible rotors 43
3.1.3 Rotor drivetrain alignment 45

3.2 Balancing and aligning by using AMBs 46
3.2.1 Decentralized and centralized PID control 47
3.2.2 LQG control method 50
3.2.3 Unbalance control strategies with AMBs 53
3.2.4 Load capacity of AMB 59
3.3 Vibration evaluation criteria 60
4 ROBUSTNESS EVALUATION OF THE SELECTED SYSTEM THROUGH TIME DOMAIN SIMULATIONS 63
4.1 Introduction of MUSK drivetrain 64
4.2 Implementing unbalance and misalignment on the simulation model 69
4.3 Case 1: With unbalance but without misalignment 73
4.4 Case 2: With unbalance and misalignment 79
5 DISCUSSION ABOUT THE RESULTS 86
6 FINAL CONCLUSIONS 90
LIST OF REFERENCES 92

LIST OF SYMBOLS AND ABBREVIATIONS

Roman symbols:

$\mathbf{A}$	System state matrix
A	Cross-section area of magnetic pole
a	Ratio between maximum displacement and minimum clearance of air gap
a_k	Knee frequency point
$\mathbf{B}$	Control matrix
C_0	Nominal air gap
C	Arbitrary coefficient
$\mathbf{C}$	System output matrix
C_{min}	Minimum axial or radial clearance of air gap
$C_{PID}(t)$	Generated control signal by PID controller
D_{max}	Maximum displacement
$\mathbf{D}_M$	Damping matrix
d	Displacement
$E(t)$	Error signal
e	Eccentricity
F	Resultant force due to coupling misalignment
F_{AMB}	Force due to active magnetic bearing
F_{AMB_m}	Force due to misaligned active magnetic bearing
F_m	Constant force
$\boldsymbol{F}_{MA}$	Combined misalignment load vector
$\boldsymbol{F}(t)$	Excitation force vector
F_{ub}	Unbalance force
$\mathbf{G}$	Disturbance input matrix
$\mathbf{G}_M$	Gyroscopic matrix
$G_{notch}(s)$	Second order transfer function of notch filter
$G_{PID}(s)$	Transfer function of PID controller
I_1	Injection point for the controller's input in unbalance control schematic
I_2	Injection point for the controller's output in unbalance control schematic
I_z	Rotor's mass moment of inertia in the direction of z-axis

$\mathbf{K}$	Stiffness matrix of rotor
K_d	Coefficient of PID controller's derivative term
$\mathbf{K}_f$	Gain matrix of Kalman filter
K_i	Coefficient of PID controller's integral term
K_p	Coefficient of PID controller's proportional term
$\mathbf{K}_r$	Optimal state feedback matrix gain
k_a	Force-displacement stiffness
k_b	Stiffness of coupling bolt
k_i	Force-current stiffness
k_{ma}	Modified force-displacement stiffness
k_{mi}	Modified force-current stiffness
i_0	Bias current
i	Control current
J_{LQR}	Cost function of linear quadratic regulator
M	Moment
$\mathbf{M}$	Mass matrix of rotor
m_u	Residual unbalance mass
N	Number of turning coils
O_1	Center point of right shaft
O_2	Center point of left shaft
P	Location point of connecting bolt
$\mathbf{Q}$	Weighing matrix on system's states
$\boldsymbol{q}(t)$	Displacement vector
R	Radius of right shaft's center point with respect to the location of coupling bolt
$\mathbf{R}$	Weighing matrix on system's inputs
r	Radius of left shaft's center point with respect to the location of coupling bolt
s	Laplace frequency parameter
T	Motor torque
T_R	Bending moment on a rotor due to angular misalignment across coupling
T_z	Torque along the longitudinal axis of rotor
t	Time
U_2	Modified controller's output in unbalance control schematic
$\boldsymbol{u}(t)$	Control input vector

V_2	Original sensor signal in unbalance control schematic
$\mathbf{V}$	Measurement noise covariance matrix
$\boldsymbol{v}(t)$	Measurement noise vector
$\mathbf{W}$	System disturbance covariance matrix
$\boldsymbol{w}(t)$	System disturbance vector
x_{nc}	Offset between active magnetic bearing and displacement sensor
$\boldsymbol{x}(t)$	System state vector
$\hat{\boldsymbol{x}}$	State estimate vector
$\boldsymbol{y}(t)$	System output vector
z_{max}	Maximum axial movement of rotor

Greek symbols:

α	Phase shift of unbalance
β	Angular misalignment
γ	Angle between two adjacent magnetic coils
ΔE	Total misalignment
ΔL	Axial distance between non-driven and driven shafts
Δt	Time step
Δy	Parallel misalignment in y-axis
λ	Global magnetic permeability
μ_0	Magnetic permeability in vacuum
ξ_{notch}	Damping ratio of notch filter
τ_d	Time constant
ω	Angular speed of rotor
ω_f	Excitation frequency
ω_{notch}	Central frequency of notch filter
$\dot{\omega}$	Angular acceleration

Abbreviations:

ACM	Active condition monitoring
AMB	Active magnetic bearing
FEM	Finite element method
LQG	Linear quadratic gaussian
LQR	Linear quadratic regulator
MATLAB	Matrix laboratory
MIMO	Multi-input and multi-output
ODE	Ordinary differential equation
PID	Proportional-Integral-Derivative
R&D	Research and Development
RoBeDyn	Rotor-Bearing Dynamics
SCM	Smart condition monitoring
SISO	Single-input and single-output
UFFC	Unbalance force counteracting control
UFRC	Unbalance force rejection control
UPM	Unbalanced magnetic pull

1 INTRODUCTION

Growing interest to machines with higher power-density and higher energy-efficiency has led a drive in international research towards high-speed technology during the past few decades. Most of the applications regarding high-speed technology are related to rotating electrical machines of which peripheral speed lies between 60 – 370 m/s. These applications are commonly related to turbomachines such as high-speed turbines, compressors, or pumps. One of the additional benefits of high-speed technology is that in some applications it can also be improving the reliability of machine since there is no need to use an intermediate transmission system anymore to deliver the power, but instead the power can be delivered directly to the driven end of machine. Additionally, the trend in electrifying the future transport methods has also influenced the interest for researching and developing high-speed applications. (Gerada D. et al. 2014, p. 2946-2952.)

To eliminate typical wear related problems caused by high frictional forces between a stator and rotor machine elements of a high-speed machinery and to make the necessity of using lubrication between the relatively moving machine elements unnecessary, the technology related to active magnetic bearing (AMB) has been invented. Since AMB magnetically levitates and thus supports a rotor inside the stator without allowing machine elements to have any mechanical contact with each other, most of friction, and the necessity of using lubrication and seals are eliminated compared to the case when traditional bearings are used. Other advantages of AMB are its capability to withstand high temperatures, its applicability to be used in vacuum environments, and its suitability in controlling vibration and noise characteristics of a rotor. (Muminovic A. J. et al. 2020, p. 113.)

Unbalance defect in rotating machines is one of the oldest problems which is known often to be challenging to compensate. When a rotor is unbalanced, it may lead to also another common fault in the system which is a coupling misalignment. Both defects are considered harmful to the rotor drivetrain since they are capable to cause severe vibration in the system and therefore subjecting the machine to numerous critical component failures which would then lead to downtime and increased costs for the company. When either of these defects are present in the system, a rotor may also experience unbalanced magnetic pull (UMP) effect

due to eccentric air gap in the stator. This induces additional vibration to the system afflicting the system's reliability and robustness further . Since AMBs are recognized to be suited for suppressing the vibration caused by these defects, AMBs are quite often used in the industry to actively control and stabilize the rotor in such cases. (Kuppa & Lal 2019, p. 1; Corne, Knockaert & Desmet 2017, p. 2; Kim et al. 2020, p. 212361) An example of a rotor drivetrain supported by three radial AMBs is presented in Figure 1.

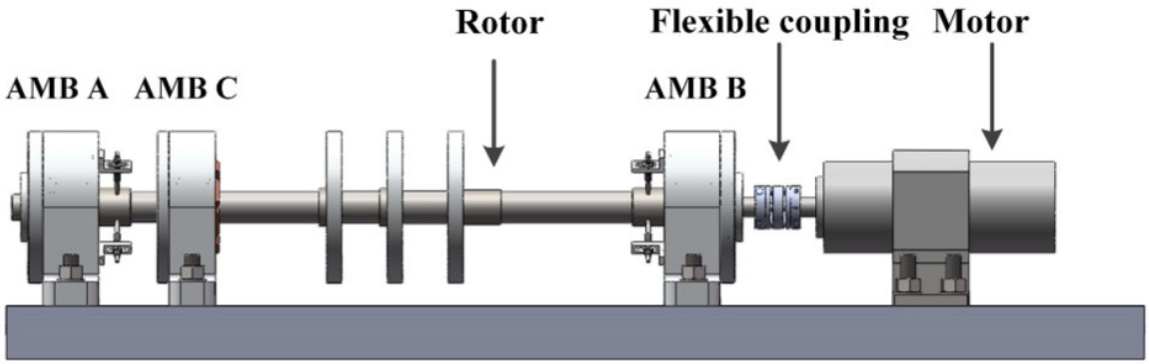

Figure 1. A rotor drivetrain supported by three radial AMB bearings (Ran, Hu & Wu 2018, p. 4).

1.1 Background and motivation

Because there is a need of tackling the problem for finding ways to design robust and efficient controller system to achieve automatic balancing and vibration suppression in AMB-rotor systems, an interest for doing the research revolving around this topic has been growing with steady rate during the past years. During initial years of the research, the utilization of control methods related to classic control theory such as simple PID (Proportional-Integral-Derivative) control and state feedback control for rigid AMB-rotor systems have been studied. After the evolution of control theory, research interest has been grown towards more adaptive methods which utilize intelligent optimization algorithms. (Huang, Zheng & Zhang 2019, p. 2888.) These methods have also been proofed to be suitable for controlling the systems which consist of flexible rotors (Gerada D. et al. 2014, p. 113).

Because the deployment of AMBs for minimizing vibrations in supported flexible rotor systems is still relatively unexplored research area as is seen in Figure 2, it will act as the basis on which this research topic will be built on. From Figure 2 it can be noticed that during

year 2019 there has been a peak regarding the published documents related to this research area. The following statistical graph about the current trend revolving this research area has been obtained from the Scopus database by using keywords: Active magnetic bearing; flexible; and rotor.

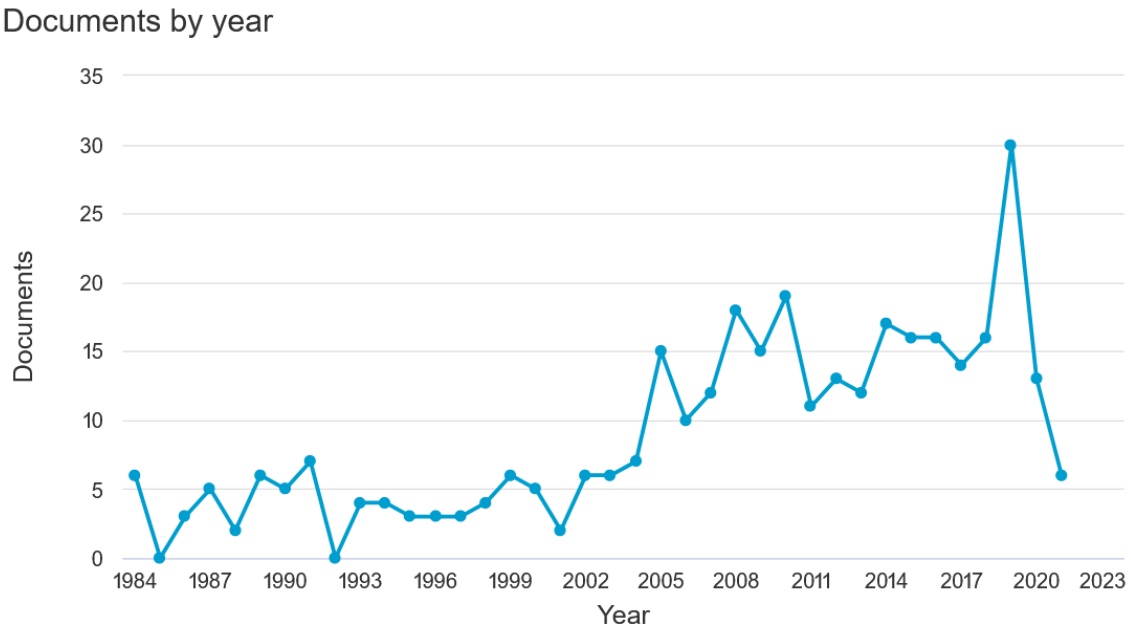

Figure 2. A graph which shows the research trend regarding utilization of AMBs for stabilizing flexible rotor systems (Scopus 2021).

The motivation for this research topic is to contribute to the research of integrating AMB related technology with the high-speed applications so that the demands of industry about the future applications can be met. The high-speed applications with integrated AMBs also consume fewer material resources, require less maintenance and they are participating in reducing environment pollution (SpinDrive 2021). Thus, AMBs can also be considered as suitable solutions for fighting against arising problems related to sustainability and environment. Hence, this research field is also important from the point of view of future society and should be studied further. This also acts as one of the main motivations for this thesis topic.

The outcome of this thesis can be used in research facilities which are not only focused on finding but who also wishes to implement sustainable and eco-friendly solutions for future applications. Most of these referred future applications are related to energy-efficient

electrical machines such as high-speed electric engines, flywheel energy storage systems, high-speed tooling in machining and turbomachinery related to pumps, gas compressors, and air blowers (Gerada D. et al. 2014, p. 2946-2949). The results of this research could also be used in industry by certain research and development (R&D) branches which are interested to implement more capable controlling and vibration compensation solutions in their own prototypes.

1.2 Research problem

AMB is an open-loop unstable system meaning that without a precise feedback control the attempt for levitating a rotor safely during its operation becomes unstable. That is why the design of a controller for AMB systems plays a key role in AMB's performance. Usually, a feedback signal to the controller is provided by a displacement sensor which is measuring the rotor's position. With the help of power amplifier, this signal is then used by the controller to activate the coils of AMB which is enough to adjust the rotor's position. Because the controller is one of the most critical components of AMB systems, there has been much research revolving around how to utilize different types of controlling methods and also what kind of an effect do they have on the dynamics of rotating machinery which are supported by AMBs. (Srinivas, Tiwari & Kannababu 2018, p. 539-540.) Figure 3 shows the main working principle of rotor magnetic levitation.

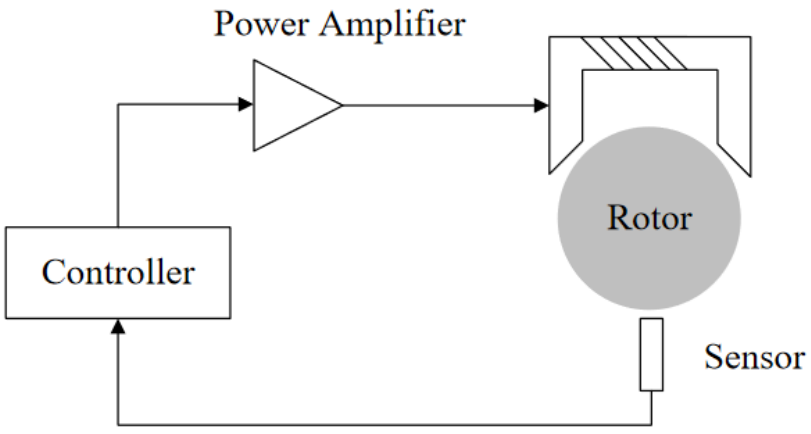

Figure 3. The working principle of rotor magnetic levitation (S.Y. Zhang et al. 2017, p. 3).

Currently, most of AMB applications are controlled by PID controllers which are suitable for rigid rotors with low operational speeds, and which are operating under their first bending natural frequency. However, for more advanced applications such as flexible rotor systems there is an increased requirement for the reliability and robustness of controller. This is true especially in the cases where the rotor is operating above its critical speeds while also gyroscopic forces are affecting system's performance. Different controlling methods can be generally divided into single-input and single-output (SISO) systems and into adaptive multi-input multi-output (MIMO) systems. Because of their simplicity, SISO systems are usually implemented in slowly rotating applications while adaptive MIMO systems are used with more advanced applications. (Srinivas et al. 2018, p. 539-541.)

Designing a suitable controlling method for a certain rotating machinery also requires an accurate numerical model of the corresponding physical system which is based on finite element method (FEM). To match better with the physical counterpart, the numerical model can be updated by doing experimental tests on the physical system and measuring its dynamic responses. This kind of method for fine tuning the accuracy of numerical model is called modal updating. (Srinivas et al. 2018, p. 540.)

Previously, a research regarding the utilization of AMBs for different rotor systems has focused on different ways for identifying and suppressing vibration which may occur because of mass unbalance of the rotor (Srinivas et al. 2018, p. 541). Vibration may also be caused by the rotor's misalignment, base excitations, bearing or gear faults, initial and propagating cracks or by the torsional and bending loads (Srinivas et al. 2018, p. 565). Of the presented faults, unbalance and misalignment have been identified to be the most common occurring defects which can be found from affecting almost all rotating machines (Mogal & Lalwani 2015, p. 114).

A condition monitoring has also become an important area where AMBs could be applied. In condition monitoring, the rotor's parameters are observed while the rotor is operating. In case a certain parameter of the operating rotor changes significantly, this would indicate that there is some kind of possible fault in the system. Traditionally when a fault is detected the machinery is stopped temporarily and the component which has a fault is repaired or replaced depending on the fault's severity. Although a faulty component can be identified and

replaced by this method, this type of condition monitoring tends to cause some downtime and extra costs. (Srinivas et al. 2018, p. 541-543.)

Compared to traditional monitoring, active monitoring is a method which is used to monitor the machinery's operation in real-time. By applying active condition monitoring (ACM) it is possible to reduce the downtime significantly since the faults can be detected early and the maintenance can be scheduled not to interfere any processes. ACM can also provide numerical data about the fault which is causing problems. ACM however requires an accurate simulation model of the physical system in order to be performed properly and also for the measured condition data to be valid. Smart condition monitoring (SCM) is a new ACM technique in which parameters of the system are not only monitored but they are also controlled in order to prevent connected faults from occurring. In this technique AMBs can also be used as exciters for identifying probable faults of the system. Therefore, they have a role in actively monitoring the machine's optimal performance even though the information on how to use AMBs as tools in ACM is still lacking. (Srinivas et al. 2018, p. 543-565.)

Certain challenges related to the implementation of AMBs still need further investigation. One of the practical challenges is the estimation and suppression of residual unbalances in case of flexible rotors which is relatively limited. The reason for this limitation is the greater power requirement which also increases the size of AMB when larger residual unbalances are needed to be identified and suppressed. A higher mechanical bandwidth of flexible rotor compared to rigid rotor is also creating a challenge for controller designers since the mechanical response of flexible rotors is relatively large when they are subjected to excitation forces with high frequencies. MIMO controlling systems are suitable for decreasing the magnitude of mechanical response of flexible rotors, but MIMO systems are hindered by their complexity which has caused challenges to implement them in commercial applications so far. (Srinivas et al. 2018, p. 548-566.)

1.3 Objective

The objective of this thesis is to simulate and monitor if the chosen investigated machine is capable to operate optimally in the presence of either unbalance or misalignment fault or possibly during the case when they are both present. This study is performed after the numerical models of the studied flexible AMB-rotor system have been connected with the

suitable AMB control model. The suitable control model should be capable to handle the system in such a way which allows it to operate safely and reliably even in the presence of defects which could cause otherwise harmful vibration in the system.

The machine on which the case study will be applied is an innovative energy-efficient high-speed application which contributes to sustainability and thus offers social and environmental benefits. The interest to study the machine's optimal performance comes from the fact that to being able to be launched in the market, it is important to guarantee that the machine is working properly and safely. This also increases the companies' potentiality of obtaining commercial value from the application.

1.3.1 Research questions

Although the research is mainly focused on studying the system's robustness against probable unbalance and misalignment disturbances, there are still certain research questions which will be guiding the whole process of this thesis work. These research questions are:

i. What are the main reasons for vibration to occur in certain AMB-rotor system?
    - How the excitation forces could be modelled based on these reasons?

ii. Why certain vibration compensating techniques are more suitable to be applied for the studied application than the others?
    - What are the main criteria for that?

iii. Why is it important for monitoring the optimal performance of the investigated high-speed application?
    - How the machine's optimal performance can be monitored effectively?

1.3.2 Hypotheses

The main hypothesis of this thesis is that the optimal performance of the machine within its operation speed range can be achieved by the chosen algorithms which are implemented for compensating vibration due to unbalance and misalignment. This is possible because of their capability to adapt to changing conditions. One of the hypotheses is also that the machine is

capable to perform optimally even when both unbalance and misalignment are affecting the system's dynamics at the same time.

1.4 Scope

The focus of this thesis work is to study different compensating techniques for the investigated flexible AMB-rotor application which would guarantee its reliable and safe operation. Because of this, the numerical models of the studied flexible AMB-rotor system are expected to be sufficiently complete before the case study is applied. Therefore, the creation and verification of the mentioned models will not be part of this research. Also, since the verification of the mentioned models have already been done in frequency domain, it allows the analysis to be switched to time domain which is more useful for studying the system's performance over time. This will provide information on whether the performance of the machine remains robust even if it is disturbed by excitation forces originating from possible unbalance and misalignment faults.

1.5 Structure of thesis

Rest of the thesis is organized such that in section 2 the principles and types of unbalance and misalignment in AMB-rotor systems are described. The analytical models for estimating potential excitation forces generated by the mentioned faults are also expressed during this section. In section 3 traditional methods of balancing and aligning are firstly covered after which the focus turns to how AMBs can be used specifically to perform the compensation. Section 4 focuses on the case study in which the robustness level of the investigated AMB-rotor drivetrain system is studied and analyzed in time domain by imposing unbalance and misalignment faults to the system through several simulations. Finally, section 5 assesses the validity and reliability level of the results while also their novelty, concrete and general value is explained. In this section future work suggestions are also given. The final conclusions of the work are derived in section 6.

2 UNBALANCE AND MISALIGNMENT IN AMB-ROTOR SYSTEMS

This section concentrates on describing the possible sources of unbalance and misalignment in an AMB-rotor system. Before diving into different theory aspects of the mentioned defects, the modelling process of a flexible rotor is firstly introduced briefly to understand how the dynamic response of a rotor is related to excitation forces while also being dependent on the system's own properties. While the theory of unbalance and misalignment is described, the defects are categorized into their different types to understand how they are varying. Additionally, the suitable methods for estimating the excitation forces caused by unbalance and misalignment defects are explained during this section.

2.1 Modelling of flexible rotor

The modelling process of any type of rotor can begin from defining the equation of motion which is based on Newton's second law (Vuojolainen 2020, p. 33):

$$\mathbf{M}\ddot{\boldsymbol{q}}(t) + (\mathbf{D}_M + \omega\mathbf{G}_M)\dot{\boldsymbol{q}}(t) + \mathbf{K}\boldsymbol{q}(t) = \boldsymbol{F}(t) \tag{2.1}$$

where $\mathbf{M}$, $\mathbf{D}_M$ and $\mathbf{K}$ are the matrices of rotor's inertia, damping and stiffness properties whereas $\mathbf{G}_M$ is a matrix which considers gyroscopic effects. The degrees of freedom of rotor with respect to its center of mass are included in the displacement vector $\boldsymbol{q}(t)$ while angular speed of the rotor is dictated by ω. Vector $\boldsymbol{F}(t)$ represents on the other hand excitation forces which can be caused for example due to unbalance and misalignment defects. Equation (2.1) is suitable for rotors which are axially symmetric, and which are rotating with a constant speed. In the modelling process, it is also assumed that the measured displacements are relatively small. The model of flexible rotor can be constructed by using FEM modelling process where the rotor is subdivided into finite number of separate elements which each have their own properties and local coordinates. The used elements are based on Timoshenko beam theory in which both rotational inertia and the shear deformation are considered. (Vuojolainen 2020, p. 33-35.)

2.2 Principle of unbalance

If the rotor's mass axis is not perfectly distributed along its length, the rotor is dictated to be unbalanced. Unbalance can also be considered as a misalignment between the rotor's principal axis of polar moment of inertia and its rotation axis. Unbalance is the most important defect to compensate in rotating machineries to ensure the machine's smooth operation. (Adams Jr. 2007, p. 753.) Figure 4 presents one example case how the mass of the rotor can be unevenly distributed along its axial length.

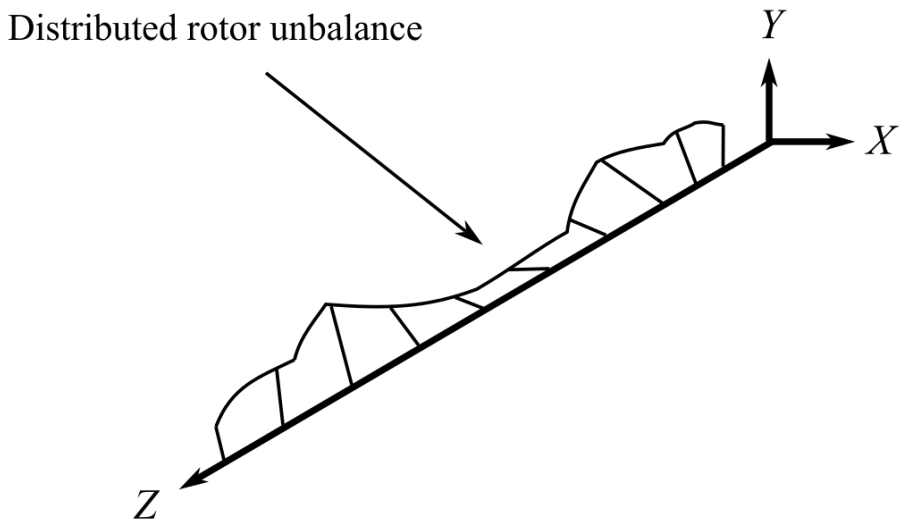

Figure 4. Uneven mass distribution along the axial length of a rotor (Mod. Adams Jr. 2007, p. 753).

The uneven mass distribution in a rotor is typically caused by manufacturing inaccuracies in casting process such as unintentional porosity. Utilizing raw material of which density varies, the applied manufacturing tolerances and material wear out or increase during the rotor's operation are also likely reasons for unbalance to occur. (Saleem, Diwakar & Satyanarayna 2012, p. 8.) Human errors in design and assembly phase, and feature varieties such as keyways, keys, bolts, nuts, and welds which are attached to the rotor during balancing may also have a role in causing an unbalance. It is common that the rotor's mass distribution tends to also change over time because of the changing environment conditions in which the rotor has to operate. These varying environment conditions could be alternating environment temperatures, corrosive substances and deposit build up which all have an effect on the rotor's mass distribution. (Ozoegwu et al. 2012, p. 50.)

Unbalance causes synchronous vibration which matches with the rotor's rotational frequency (Kumar, Diwakar & Satyanarayna 2012, p. 3415). The components of centrifugal force in the rotor's *x*- and *y*-axis due to unbalance can be modelled as follows (Kumar & Tiwari 2020, p. 3):

$$F_{ub_x} = m_u e\omega_f{}^2 \cos(\omega_f t + \alpha);$$
$$F_{ub_y} = m_u e\omega_f{}^2 \sin(\omega_f t + \alpha) \tag{2.2}$$

where m_u is the residual unbalance on a rotor, e is amount of eccentricity, ω_f is the excitation frequency of unbalance while α is the phase shift of unbalance as is shown in Figure 5.

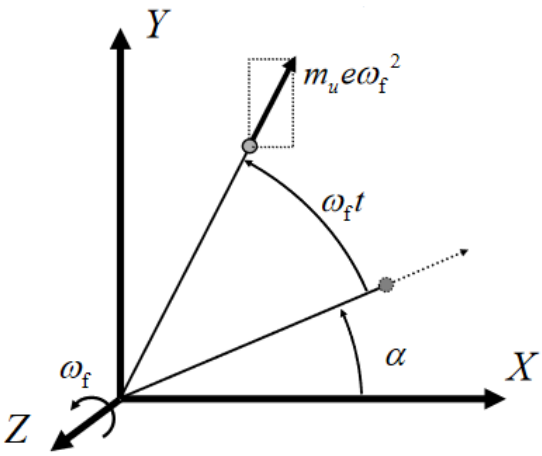

Figure 5. Residual unbalance on a rotor (Mod. Kärkkäinen 2007, p. 31).

By looking at equation (2.2), it can be concluded that certain residual unbalance will not be causing any excitation force to the rotor if the rotor is not rotating. But if the rotor is accelerating, unbalance force can increase quickly in a non-linear fashion since it is proportional to the square of rotor's spin speed. Eccentricity and phase shift have also an effect on the magnitude of excitation force caused by unbalance. Equation (2.2) can be presented even in a more compact form by using a vector representation:

$$\begin{bmatrix} F_{ub_x} \\ F_{ub_y} \end{bmatrix} = m_u e\omega_f{}^2 \begin{bmatrix} \cos(\omega_f t + \alpha) \\ \sin(\omega_f t + \alpha) \end{bmatrix} \tag{2.3}$$

Unbalance can be categorized into different types based on whether residual unbalance exist on a single plane or multiple planes. Categorization is also heavily influenced by the loading effect on a rotor due to unbalance. Vuojolainen, Jastrzebski & Pyrhönen (2018, p. 3) recognize four main types of unbalance which are:

- Static unbalance
- Couple unbalance
- Quasi-static unbalance
- Dynamic unbalance

When a rotor is statically unbalanced, it has a residual unbalance existing on a single plane at a certain distance from the rotor's center of mass. This causes the rotor's principal axis of inertia to be shifted radially from the rotor's axis of rotation (Bloch & Geitner 2019, p. 269) while the residual unbalance subjects rotor to radial load during its operation as shown in Figure 6.

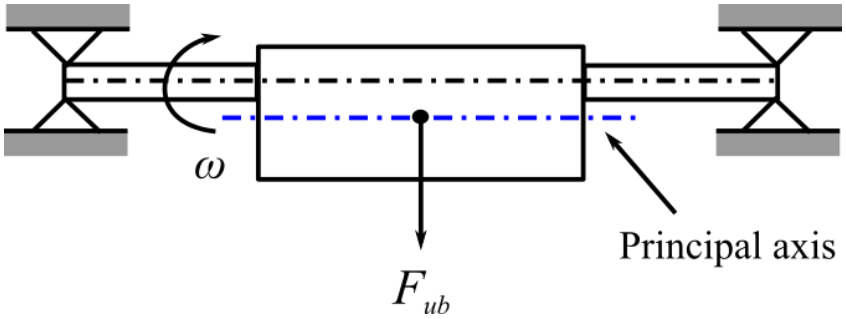

Figure 6. A rotor with static unbalance (Mod. Tiwari 2018, p. 30).

A rotor experiences couple unbalance when two equal residual unbalance masses are laying on two separate planes, 180° out of phase from each other (Bloch & Geitner 2019, p. 271). Because of the arrangement how the two unbalance masses are positioned on a rotor, couple unbalance can create a moment of couple which causes rotor to wobble during its operation. This is illustrated in Figure 7 in which the principal axis and rotation axis have a shared center point, but the principal axis is inclined influenced by the moment *M*.

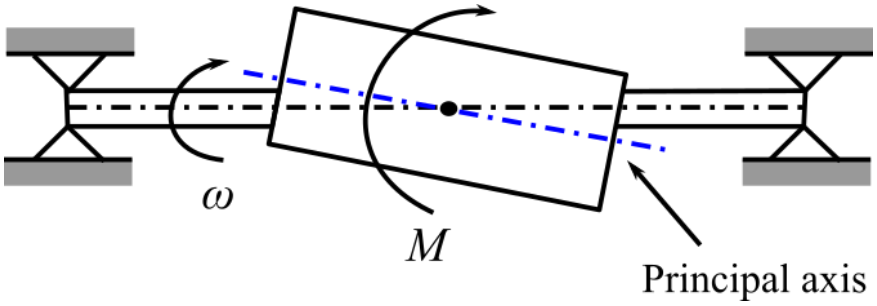

Figure 7. A rotor with couple unbalance (Mod. Tiwari 2018, p. 30).

Quasi-static unbalance is on the other hand considered to be a mix of static unbalance and couple unbalance. In this type of unbalance the rotor's principal axis intersects with its rotation axis only at one particular point. (Bloch & Geitner 2019, p. 272-273.) With quasi-static unbalance a rotor is subjected to both radial and moment loads while it is spinning as is illustrated in Figure 8.

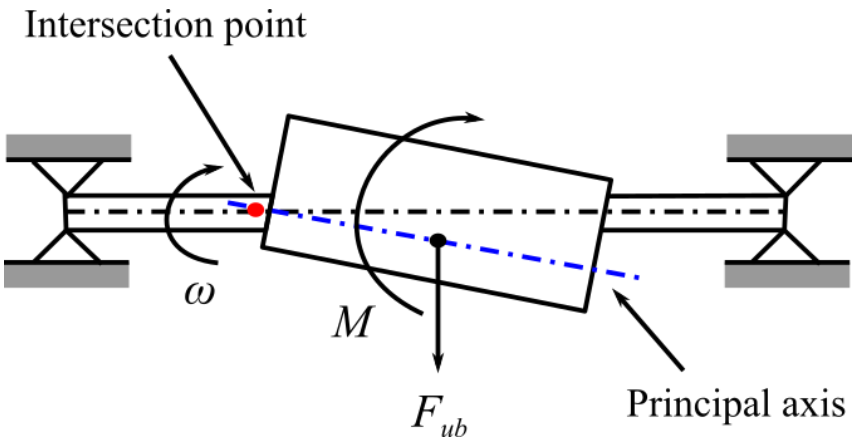

Figure 8. A rotor with quasi-static unbalance (Mod. Tiwari 2018, p. 30).

Of all unbalance types, dynamic unbalance can be most often recognized as the source of vibration if a rotor is unbalanced. Dynamic unbalance is similar to quasi-static unbalance. (Bloch & Geitner 2019, p. 273.) What differentiates dynamic unbalance from quasi-static type however is that the principal axis is not intersecting with the rotation axis at any point as is shown in Figure 9. As with the case of quasi-static unbalance, a rotor is subjected to both radial and moment loads while the rotor is spinning.

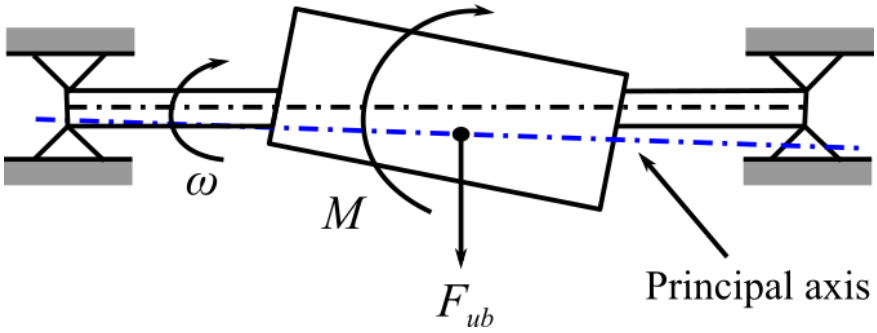

Figure 9. A rotor with dynamic unbalance (Mod. Tiwari 2018, p. 30).

2.3 Misalignment

Beside unbalance, misalignment defect is one of the most common faults which can cause severe vibration to occur in a rotating machinery. The reasons for misalignment can be derived from manufacturing or assembly errors, deformation of shafts and bearings caused by an external static and cyclic loading or by a thermal loading. Sensor runout and non-collocation are also one of the typical sources for vibration to occur in AMB-rotor drivetrains since they have an effect on the system controller's dynamics. Regardless of whether the coupling is rigid or flexible, misalignment subjects machinery to axial and radial vibrations which may cause instability to the system by inducing wear on machinery's bearings or by causing shafts to bend. Because misalignment can be originated from imbalance conditions, machinery could experience 1X synchronous vibration (once per revolution). Misalignment has been identified to cause vibration occurring at higher harmonics as well, mostly at 2X. (Behera D. P, Behera R. & Naikan 2014, p. 2476–2478; Darbandi et al. 2016, p. 111; Kulesza 2015, p. 1522.)

2.3.1 Misalignment in drivetrain couplings

The main function of a drivetrain coupling is to connect a driving shaft with a driven shaft so that the power can be delivered to the machine component which requires it. Utilized couplings are often flexible in order to provide a capability to compensate a small inevitable misalignment between the two shafts. Misalignment in the drivetrain coupling can occur when the centerlines of these shafts are not perfectly aligned with each other. Misalignment in drivetrain couplings can usually be prematurely monitored by monitoring different parameters in the system such as torque, current and acoustics levels and also from vibration signals. Although other methods have been used quite often for investigating misalignment

level between the linked shafts, collecting this data from the vibration response has not yet been studied that detailly. (Desouki et al. 2020, p. 1-2.)

Misalignment in drivetrain couplings can usually be divided into two types which are parallel and angular misalignment. In case of parallel misalignment, rotating machinery has at least two shafts of which centerlines are parallel but not collinear as is seen in Figure 10. In the figure, O_1 and O_2 are representing the center point of each shaft end respectively, whereas Δy is the total parallel misalignment in the direction of shaft's y-axis.

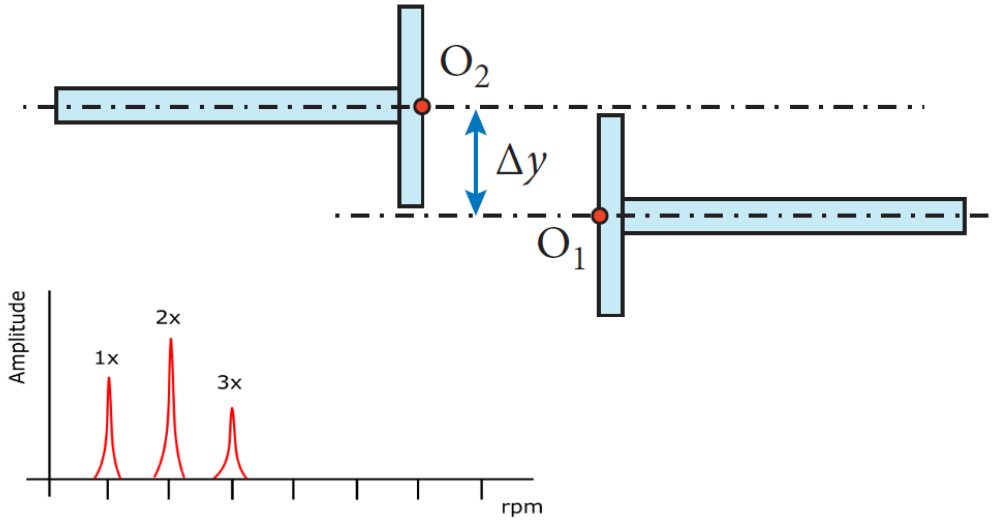

Figure 10. Parallel misalignment between the two connected shafts and its vibration characteristics (Mod. Desouki et al. 2020, p. 3).

Compared to angular misalignment, parallel misalignment compels vibration to dominate in radial direction instead of axial direction. When this type of misalignment is present, vibration has 180° phase difference over the coupling, and its second harmonic component (2X) prevails more likely over the first component (1X). What dictates how much larger the second harmonic component is relative to the first component depends on the structure of the used coupling. It can also be often found that radial vibration can occur in higher harmonic components such as 3X as well. (Behera D. P et al. 2014, p. 2477–2478.)

The radial forces experienced by the coupling are commonly combination of static and dynamic loads which are often practically difficult to estimate. The reason for this is that in practice it is unlikely that certain type of drivetrain coupling has the same internal geometry

than with other types of couplings. This has been a limiting factor for estimating the internal forces in different variety of couplings, since applying a same force estimation model with variety of couplings is not possible. (Desouki et al. 2020, p. 7.)

In a case where the coupling is a disc coupling, the movement diagram of the parallel misalignment can be illustrated as shown in Figure 11.

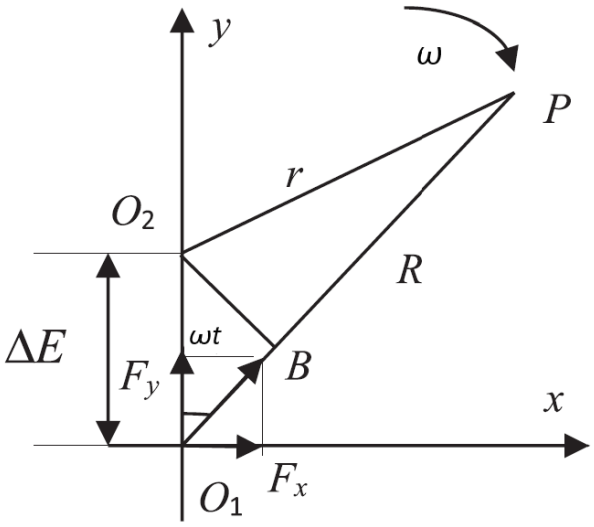

Figure 11. The movement diagram of parallel misalignment defect (Mod. Wang & Gong 2019, p. 366).

In Figure 11, R is the radius of the right shaft's center point O_1 while r is the radius of left shaft's center point O_2. Radiuses of both center points are measured with respect to the location point of connecting bolt P on the coupling. F_x and F_y are on the other hand the force components on the bolt applied by both left and right shafts in x- and y-axes. Total misalignment between the two shafts is denoted by ΔE which in this case includes only parallel misalignment Δy, while the angle between the bolt's rotation speed and misalignment is designated with ωt.

If it is assumed that r is relatively larger compared to ΔE and that r is equal to distance PB, the distance O_1B can be defined as (Wang & Gong 2019, p. 366):

$$O_1B = R - r = \Delta E\cos(\omega t) \tag{2.4}$$

Displacement of the two half couplings *d* is the same if the size of the couplings and their material are matching with each other. This allows *d* to be expressed with the following equation (Wang & Gong 2019, p. 366):

$$d = \frac{O_1B}{2} = \frac{\Delta E\cos(\omega t)}{2} \tag{2.5}$$

If the stiffness of the bolt in the direction of O_1B is k_b, then the resultant force acting on the two half-couplings can be written as (Wang & Gong 2019, p. 366):

$$F = \frac{k_b \Delta E\cos(\omega t)}{2} \tag{2.6}$$

As has been mentioned, this force gets to resolved into separate components which are affecting in *x*- and *y*-axes. Therefore, the force components can be expressed as (Wang & Gong 2019, p. 366):

$$\begin{aligned} F_x &= F\sin(\omega t) = k_{bx}\frac{\Delta E}{2}\cos(\omega t)\sin(\omega t) = k_{bx}\frac{\Delta E}{4}\sin(2\omega t); \\ F_y &= F\cos(\omega t) = k_{by}\frac{\Delta E}{2}\cos(\omega t)\cos(\omega t) = k_{by}\frac{\Delta E}{4}(1 + \cos 2\omega t) \end{aligned} \tag{2.7}$$

in which k_{bx} and k_{by} are describing the coupling stiffnesses in the directions of *x*- and *y*-axes.

From the defined force equations for parallel misalignment, it is possible to verify that the forces in the coupling are indeed occurring twice per shaft rotation while their applied direction is also changing. Therefore, in case of parallel misalignment second harmonic of vibration is prevalent as has been described before. The corresponding internal forces on the left-side of the coupling are simply equal but opposite to the coupling forces on the right-side which is determined by Newton's third law (Wang & Gong 2019, p. 366).

When the centerlines of shafts are intersecting at certain point, but are not collinear, then the shafts are angularly misaligned as is seen in Figure 12.

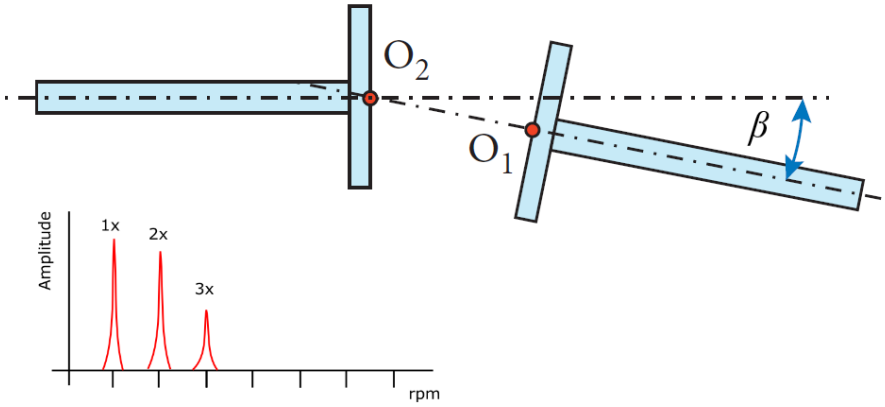

Figure 12. Angular misalignment between two connected shafts and the caused harmonics (Mod. Desouki et al. 2020, p. 3).

In Figure 12, angular misalignment between the two connected shafts is denoted by β. Vibration caused by angular misalignment is dominating in axial direction, and it has 180° phase difference across the coupling. Additionally, angular misalignment does not have one specific harmonic component which prevails over other components, but instead axial vibration is occurring on each 1X and 2X harmonic components evenly. As with the case of parallel misalignment, it is possible sometimes to also identify 3X or higher harmonic components when the two shafts are angularly misaligned. (Behera D. P et al. 2014, p. 2477-2478.)

In the presence of an angular misalignment fault, the driving torque from the motor T gets resolved to separate components T_z and T_R. The component T_z is acting along the rotor's axis while T_R is acting perpendicular to the rotor's axis causing it to bend in lateral direction as is shown in Figure 13.

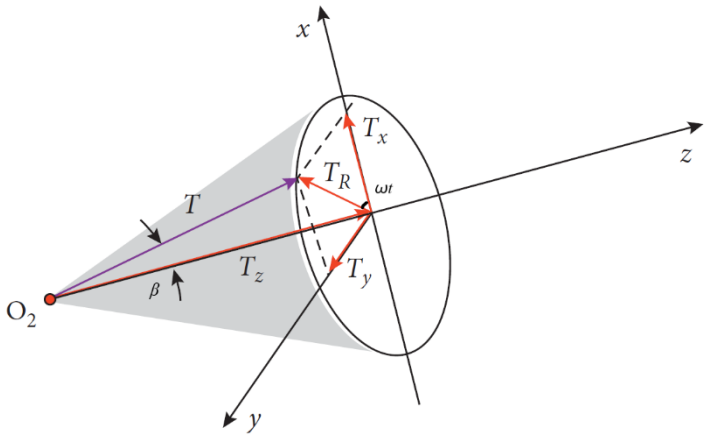

Figure 13. The resolved components of driving torque T when the connected shafts are angularly misaligned (Mod. Desouki et al. 2020, p. 9).

The mentioned torque and moment components can be estimated by the following equations (Desouki et al. 2020, p. 8):

$$T_z = T\cos(\beta); \qquad T_R = T\sin(\beta) \tag{2.8}$$

The bending moment T_R can be resolved further to its two own rectangular moment components which are acting in x- and y-axes (Desouki et al. 2020, p. 8):

$$T_x = T\sin(\beta)\cos(\omega t); \qquad T_y = T\sin(\beta)\sin(\omega t) \tag{2.9}$$

Equation set (2.9) can be derived further by considering the speed ratio of angularly misaligned shafts which can be dictated as (Desouki et al. 2020, p. 8):

$$\frac{\omega_2}{\omega_1} = \frac{C_1}{1 + C_2\cos(2\omega t)} \tag{2.10}$$

In equation (2.10), C_1 and C_2 are arbitrary coefficients which are determined from (Desouki et al. 2020, p. 8):

$$C_1 = \frac{4\cos(\beta)}{3+\cos(2\beta)};$$
$$C_2 = \frac{1-\cos(\beta)}{3+\cos(2\beta)} \tag{2.11}$$

By substituting the defined coefficients into equation (2.10), differentiating it and applying some minor rearrangements, the expression for determining acceleration $\dot{\omega}$ at center point O_2 becomes (Desouki et al. 2020, p. 8):

$$\dot{\omega} = \frac{2C_1C_2\omega^2\sin(2\omega t)}{(1+C_2\cos 2\omega t)^2} \tag{2.12}$$

Now, the torque component along the longitudinal axis of the rotor T_z can be written as (Desouki et al. 2020, p. 8):

$$T_z = I_z\dot{\omega} = I_z\frac{2C_1C_2\omega^2\sin(2\omega t)}{(1+C_2\cos 2\omega t)^2} \tag{2.13}$$

where I_z is the shaft's polar moment of inertia around its z-axis.

Finally, by using the defined equations for the torque T_z (2.8 and 2.13), the equation set (2.9) for calculating the moment components T_x and T_y can be rewritten into following form (Desouki et al. 2020, p. 8):

$$T_x = T_z\tan(\beta)\cos(\omega t);$$
$$T_y = T_z\tan(\beta)\sin(\omega t) \tag{2.14}$$

The torque along the rotor's axis and the bending moment components affecting to the right-side of the coupling are equal but opposite to the defined torque and moments on the coupling's left-side (Desouki et al. 2020, p. 8).

In some cases, there is a chance that the rotor drivetrain assembly can have both parallel and angular misalignment existing at the same time. This kind of case is referred as combined misalignment and it is illustrated in Figure 14.

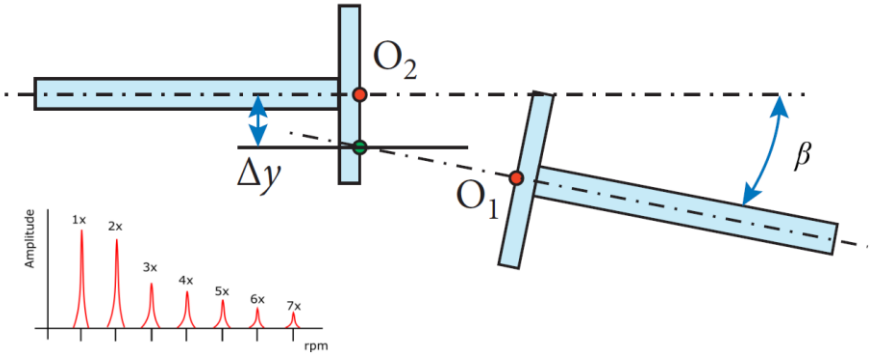

Figure 14. Combined misalignment between two connected shafts and the caused harmonics (Mod. Desouki et al. 2020, p. 3).

If either parallel or angular misalignment is substantial, it may cause high amplitude of vibration to be present at several harmonics (4X to 8X). Alternatively, it can create several additional harmonics at higher frequencies. This unique vibration response makes it possible to identify and estimate the amount of looseness within the connected shafts. (Behera D. P. et al. 2014, p. 2477.)

In case of combined misalignment, total misalignment ΔE can be evaluated by summing together the individual displacements caused by parallel misalignment Δy and and angular misalignment β as is seen from the equation (Desouki et al. 2020, p. 7):

$$\Delta E = \Delta y + \Delta L \tan(\beta) \tag{2.15}$$

In equation (2.15), ΔL is the axial distance between the driven and non-driven shafts which is measured from the center of articulation point for both shaft ends.

The acting forces and torques on the left-side of the coupling are now defined as a common load vector $\boldsymbol{F}_{MA}$ (Desouki et al. 2020, p. 8):

$$\boldsymbol{F}_{MA}(t) = \begin{bmatrix} F_x = k_{b_x}\frac{\Delta E}{4}\sin(2\omega t) \\ F_y = k_{b_y}\frac{\Delta E}{4}(1+\cos 2\omega t) \\ F_z = 0 \\ T_z = I_z\frac{2C_1C_2\omega^2\sin(2\omega t)}{(1+C_2\cos 2\omega t)^2} \\ T_x = T_z\tan(\beta)\cos(\omega t) \\ T_y = T_z\tan(\beta)\sin(\omega t) \end{bmatrix} \quad (2.16)$$

The magnitudes of the loads on the right-side of the coupling are simply opposite to the left coupling side (Desouki et al. 2020, p. 8).

2.3.2 Misalignment between rotor and AMB actuator

The rotor should be centered inside the supporting AMB housing all time during its operation such that the air-gap's distance is equal along the entire circumference of stator. In case a rotor deviates from this magnetic center, the magnetic flux distribution becomes non-symmetric and concentrates at location where the air-gap is smallest. Because of non-uniform and concentrated magnetic flux distribution, UMP is created which causes rotor to move in the direction of a displacement. This magnetic attraction force is proportional to the square of air-gap flux density which can cause severe vibration to occur when the rotor is accelerating. (Chiba et al. 2005, p. 302-303.)

Deviation which can lead to UMP is usually caused either by possible assembly and manufacturing errors or by some mechanical fault at the rotor's surface level which are introducing eccentricity to the system. One example of a possible assembly error is the angular misalignment of one of the two AMB actuators which is tilted with an angle β with respect to the common center axis of the machine assembly as shown in Figure 15. (Bouaziz A. et al. 2015, p. 210.) This leads the size of nominal air gap C_O to be increased by the amount of eccentricity e on the tilted actuator side which causes UMP to occur. UMP occurs since the supporting forces due to actuators on both side of the rotor becomes unequal influenced by the non-uniform air gap.

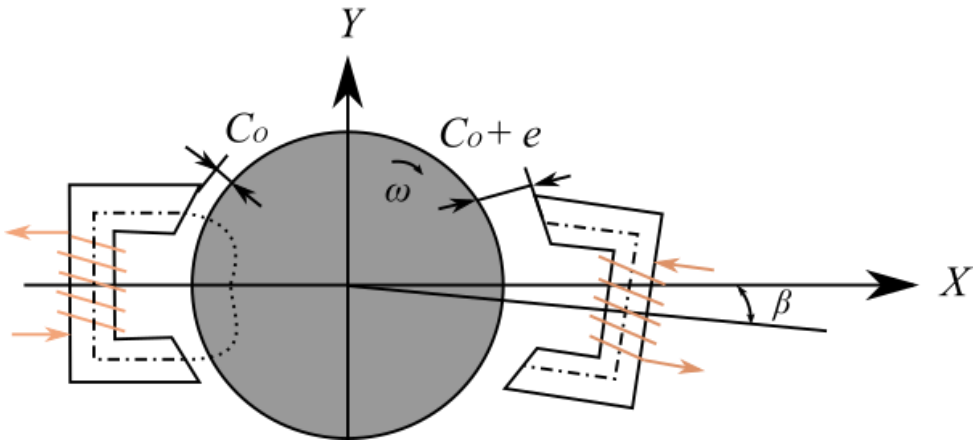

Figure 15. Angular misalignment of AMB actuator (Mod. Bouaziz A. et al. 2015, p. 211).

Another misalignment defect related to AMBs is a case in which one of the two AMB actuators has shifted relative to the center axis of other AMB in parallel fashion. This is influenced by an occurring mechanical defect at the air gap level. Because of this offset, certain amount of eccentricity e is created between the actuators as is illustrated in Figure 16. With this defect the upper air gap of the left misaligned AMB becomes $C_0 + e$ while the actuator's lower air gap becomes C_0 - e. (Bouaziz A. et al. 2015, p. 211.)

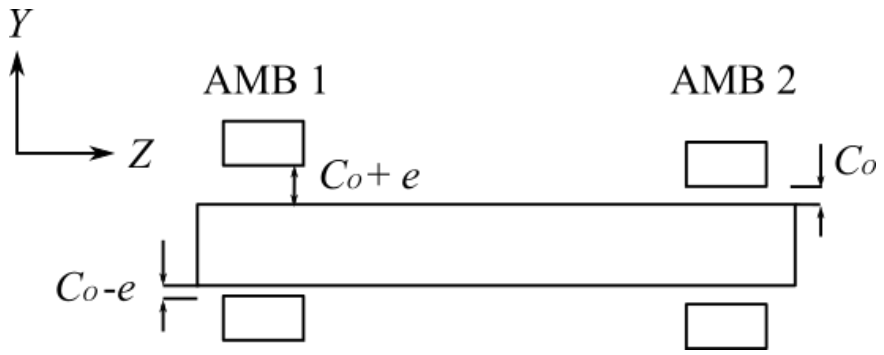

Figure 16. Parallel misalignment of AMB actuator (Mod. Bouaziz A. et al. 2015, p. 211).

It is also possible that the component which has eccentricity in the AMB-rotor system is the rotor and not the AMB actuator. This kind of eccentricity is specifically referred as rotor eccentricity of which there are three different types existing as shown in Figure 17.

The three types of rotor eccentricity are (Schlensok & Henneberg 2004, p. 1071):

- Static eccentricity
- Dynamic eccentricity
- Mixed eccentricity

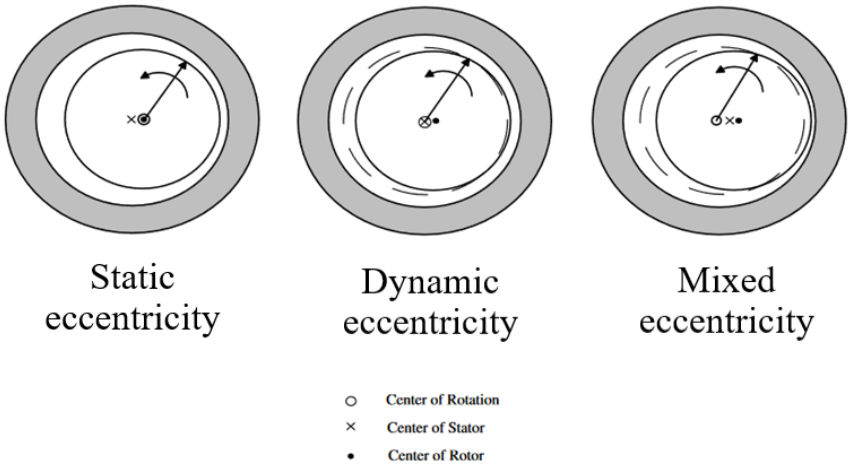

Figure 17. Types of eccentricity (Mod. Safa et al. 2014, p. 97).

With static eccentricity, the rotation axis is fixed to the rotor while the rotor is positioned to the other side of the machine. Therefore, the air-gap is asymmetric around circumference of the electrical machine and does not alter when the rotor rotates. In addition to the fixed air gap, the minimum and maximum values of force excitations are also spatially fixed since the excitations are linked to the location of rotation axis which does not move. (Schlensok & Henneberg 2004, p. 1071.)

In the case of rotor eccentricity, where the rotor is positioned to the other side of the machine, but the rotation axis is fixed with the stator axis, the rotor is dynamically eccentric. Because the rotational axis is not fixed to the rotor center anymore, the rotor rotates along the circumference of the machine which also makes the air gap to rotate along with it. The minimum and maximum values of force excitations are also not fixed spatially with this type of rotor eccentricity. (Schlensok & Henneberg 2004, p. 1071.)

Compared to the two other rotor eccentricity types, mixed eccentricity is the type of eccentricity which is occurring most often. In this eccentricity type, the rotational axis is located neither at rotor axis nor stator axis but instead it lies somewhere between them. This leads the force excitations to be mix of fixed and rotating excitations. (Schlensok & Henneberg 2004, p. 1071.)

To estimate the resulting effect of UMP force due to the certain misalignment between the rotor and AMB, let's first consider the case when there is no misalignment defect meaning that the rotor and stator are aligned perfectly with each other. The electromagnetic force applied on the rotor in *y*-axis due to two opposed magnetic poles of AMB in this condition can be defined as (Kumar & Tiwari 2021, p. 410):

$$F_{AMB_{my}} = \lambda \left\{ \frac{\left(i_0 + i_y\right)^2}{\left(C_0 - d_y\right)^2} - \frac{\left(i_0 - i_y\right)^2}{\left(C_0 + d_y\right)^2} \right\} \tag{2.17}$$

in which i_0 is biasing current, i_y and d_y are control current and displacement in *y*-axis. Global magnetic permeability is designated with λ and it can be determined from the following equation (Kumar & Tiwari 2021, p. 410):

$$\lambda = \frac{A\mu_0 N^2 \cos\left(\frac{\gamma}{2}\right)}{4} \tag{2.18}$$

where A is the cross-section area of AMBs magnetic pole, μ_0 is permeability of vacuum (4π x 10^{-7} H/m), N is the number of coil windings and γ defines the angle between electromagnet's two adjacent magnetic poles.

If it is assumed that $C_0 >> d_y$ and $i_0 >> i_y$, equation (2.17) can be linearized by using Taylor's series expansion into the following form (Kumar & Tiwari 2021, p. 411):

$$F_{AMB_y} = k_a d_y + k_i i_y \tag{2.19}$$

in which k_a and k_i are constants that are linked to force-displacement and force-current stiffnesses respectively, and are expressed as (Kumar & Tiwari 2021, p. 411):

$$k_a = \frac{4\lambda i_0^2}{C_0^3}; \qquad k_i = \frac{4\lambda i_0}{C_0^2} \tag{2.20}$$

The force due to AMB in x-axis in a case where there is no misalignment defect, can be estimated similarly as in y-axis, from the equation (Kumar & Tiwari 2021, p. 411):

$$F_{AMB_x} = k_a d_x + k_i i_x \tag{2.21}$$

where the displacement and controlling current measured in the x-plane are denoted by d_x and i_x.

As has been mentioned earlier, when the rotor or AMB is misaligned, air gap becomes non-uniform. If the misalignment occurs like is shown in the earlier figure 17, the air gap closer to the lower electromagnet decreases while the air gap at proximity to the upper electromagnet increases. Therefore, the applied force on the rotor due to AMB in y-axis is altered and can be written as (Kumar & Tiwari 2021, p. 411):

$$F_{AMB_{my}} = \lambda \left\{ \frac{\left(i_0 + i_y\right)^2}{\left(C_0 - e - d_y\right)^2} - \frac{\left(i_0 - i_y\right)^2}{\left(C_0 + e + d_y\right)^2} \right\} \tag{2.22}$$

By not considering the high-order terms of d_y^2 in equation (2.22) based on the assumption that $d_y << (C_0 - e)$ and $d_y << (C_0 + e)$, and also by making further simplifications it is possible to obtain (Kumar & Tiwari 2021, p. 412):

$$F_{AMB_{my}} = \lambda\left\{\frac{4C_0 i_0^2 d_y}{(C_0-e)^2(C_0+e)^2} + \frac{4i_0 i_y (C_0^2+e^2)}{(C_0-e)^2(C_0+e)^2} + \frac{4C_0 e i_y^2 + 4e d_y i_y^2 + 4i_0 e d_y i_y + 4C_0 e i_0^2}{(C_0-e)^2(C_0+e)^2}\right\} \tag{2.23}$$

If the terms with high-order such as i_y^2, $d_y i_y^2$, and $d_y i_y$ are neglected, the equation (2.23) is linearized into (Kumar & Tiwari 2021, p. 412):

$$F_{AMB_{my}} = \lambda\left\{\frac{4C_0 i_0^2 d_y}{(C_0-e)^2(C_0+e)^2} + \frac{4i_0 i_y (C_0^2+e^2)}{(C_0-e)^2(C_0+e)^2} + \frac{4C_0 e i_0^2}{(C_0-e)^2(C_0+e)^2}\right\} \tag{2.24}$$

As a final step, the equations of k_a and k_i (2.20) are substituted to equation (2.24) which leads to the following expression (Kumar & Tiwari 2021, p. 412):

$$F_{AMB_{my}} = k_{ma} d_y + k_{mi} i_y + F_m \tag{2.25}$$

in which

$$k_{ma} = \frac{k_a}{(1-e_1^2)^2};\quad k_{mi} = \frac{k_i(1+e_1^2)}{(1-e_1^2)^2};\quad F_m = \frac{F_a e_1}{(1-e_1^2)^2};\quad F_a = \frac{4\lambda i_0^2}{C_0^2};\quad e_1 = \frac{e}{C_0} \tag{2.26}$$

In a case where similar misalignment occurs in *x*-axis, the applied force on the rotor by AMB is similarly (Kumar & Tiwari 2021, p. 412):

$$F_{AMB_{mx}} = k_{ma} d_x + k_{mi} i_x + F_m \tag{2.27}$$

By comparing the defined AMB force equations (2.19 and 2.25) in *y*-axis which are corresponding to different alignment conditions, it is noticeable that the main differences between the equations are the modifications to the force-displacement stiffness constant k_a

and force-current stiffness constant k_i parameters. The earlier constants have been replaced with the new constants k_{ma} and k_{mi}. Additionally, a term F_m which is a force constant has also been added to the AMB force model. Thus, in a case where there is an eccentricity in the system, the rotor is subjected to larger radial force due to AMB.

One should keep in mind that when the rotor is dynamically eccentric or if it has mixed eccentricity, the size of air gap does not remain constant as is expressed in the presented equations. Instead, it is varying as a function of rotor's rotation since the air gap rotates along with a rotor. This makes the estimation of AMB force more complex by using only analytical methods compared to the case where the air gap remains static. In practice, in cases like these AMB force is usually estimated by utilizing numerical methods such as FEM computation which allows to take other factors also into account in the system modelling like eddy-current losses and magnetic saturation effect in the stator coil windings. However, different analytical methods for estimating AMB force due to eccentricity are considered to be sufficient if one is only interested about the approximation of the eccentricity effect on the rotor's dynamic performance. Since analytical methods are also saving some computing resources, numerical methods are usually utilized only for studying more complex phenomena related to eccentricity and UMP effect. (Donát 2012, p. 84.)

2.3.3 Sensor runout and non-collocation

In order to keep the rotor stabilized in its required position, proximity sensors are used of which the most common type of sensor is an eddy-current sensor. The working principle of this type of sensor is based on the sensed eddy currents which are induced on the rotor's conductive surface by the high-frequency alternating current from the sensor's electromagnetic coil. (Darbandi et al. 2016, p. 111.) Other type of displacement sensor of which operation principle is similar as with the eddy-current type but is commonly applied with rotors of which surface is made of ferromagnetic material is called inductive sensor. (Schweitzer & Maslen 2009, p. 101).

If the rotor has a surface which is eccentric and its material is non-homogeneous, the radial displacement of the rotor maybe measured with some noise which can generate a periodic control input if the disturbed measured signal is fed to the controller in a feedback loop. Thus, this harmonic disturbance can act as one source which deviates the rotor from its

steady-state position and causes eccentricity in the system. This type of disturbance is commonly referred as sensor runout and it has the potentiality of applying some harmonic disturbances such as harmonic currents to the system which can be synchronous with the rotor's angular speed or which are multiple integers of the rotor's rotational frequency. Harmonic currents are undesired since they act as a source of noise and reaction forces in the machine's foundation. They may also cause irregular power losses in the actuator's coils which can cause a hazardous situation to occur especially with higher rotational frequencies. (Darbandi et al. 2016, p. 111-112.)

Other issue with the proximity sensors is related to possible non-collocation of sensor and AMB actuator which is influenced by the limitations of structural and functional reasons. One of those reasons is related to the electromagnetic interference between the sensor and the electromagnetic coils of AMB. When the proximity sensor is not locating at the same axis as AMB actuator axis the rotor may become destabilized due to the reason that the rotor's position is measured at different plane than at which the rotor's position is controlled as illustrated in figure 19. Because of this offset, a phase lag could exist between the measurement plane and the plane of applied control force. This has the potentiality to destabilize the system if not considered. (Kulesza 2015, p. 1522 -1523.) In Figure 18, the offset between AMB actuators and sensors is denoted by x_{nc}.

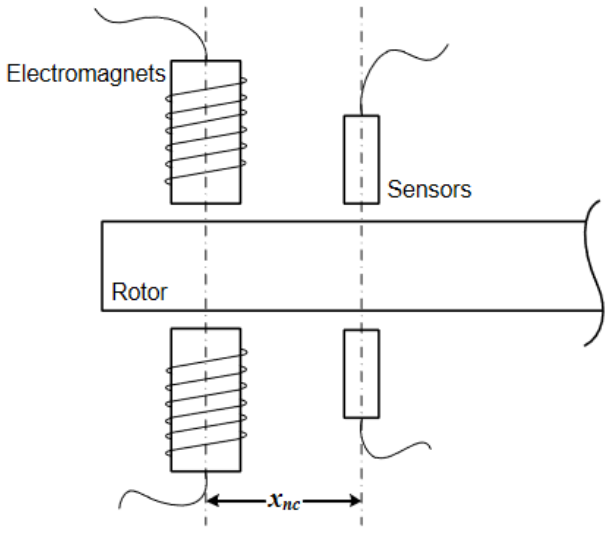

Figure 18. Non-collocation of AMB actuator and displacement sensors (Wroblewski 2011, p. 16).

2.3.4 Misalignment of safety bearings

The purpose of safety bearings is to support the rotor in case of a sudden power loss or if AMB fails to provide non-contact support for the rotor while it is in service. Thus, auxiliary bearings have a significant role in AMB-rotor system and should be assembled and working properly for these types of cases. However, these bearings can also have a misalign defect in which case the bearing is eccentric to the rotor and other auxiliary bearings. This misalignment defect usually increases after every emergency drop and is affecting greatly the dynamics of rotor during the drop-down event which is why it should be considered and monitored. (Kärkkäinen 2007, p. 3-20.)

Kärkkäinen (2007, p. 65) has dictated that if the misalignment would occur in horizontal direction, it would be more critical to the rotor's stability than if the misalignment would be occurring in vertical direction. When the horizontal misalignment becomes too great, it can decrease the life-cycle of both safety bearing and rotor. The reason for the life-cycle decrement are the high contact forces during the drop-down event to which the components are subjected. Contact forces are created when the rotor is forced to whirl inside the bearing due to the misalignment of safety bearing. In practice, controlling this misalignment is difficult because during a design phase it has to be taken care of that a safety bearing is concentric not only with the rotor but also to other safety bearings as well. Additionally, it has to be ensured that AMBs are aligned with safety bearings and with the rotor so that the whole system is concentric. (Kärkkäinen 2007, p. 65-82; Halminen et al. 2015, p. 702-704.)

Since modelling the dynamics of rotor and safety bearings during the drop down event is out of scope of this work, the likely contact forces in that kind of event are not expressed in this chapter. However, one should be still aware that the misalignment of safety bearings have also an effect on the magnitude of vibrational forces which the rotor may need to withstand in case of a power loss event or other event that prevents AMB from providing supporting action on the rotor. If the misalignment is neglected, both the rotor and safety bearings could experience severe damage depending on the magnitude of defect during the collision event.

3 VIBRATION COMPENSATION TECHNIQUES FOR AMB

In this section, conventional methods for compensating unbalance and misalignment defects in different rotor drivetrain systems are first introduced. Then, the focus is shifted to the theory of how AMBs can be specifically utilized for keeping the system stabilized under the mentioned fault conditions. Finally, the vibration evaluation criteria defined by ISO 14389-2 standard, which can be used for checking if the vibration level experienced by AMB-rotor system is at the sufficient level, is presented at the end of this section.

3.1 Conventional methods of balancing and aligning

To ensure that a rotating machinery is operating smoothly, it is important to find suitable methods for compensating the vibrations induced by possible unbalance and misalignment defects. In addition to smooth operation, numerous other reasons for balancing and aligning have also been recognized. Overall, the following benefits for the unbalance and misalignment compensation can be listed (Diouf & Herbert 2014, p. 8; Verma, Sarangi & Kolekar 2014, p. 125):

- Vibration suppression
- Assuring longer service-life of rotor and other components of the system
- Mitigating the effect of structural stresses on bearings and couplings
- Mitigating noise
- Providing a higher-quality product by the better efficiency of machine

It should be regarded that in practice obtaining perfect alignment and balanced conditions for certain rotating machinery is not that easy for various of technical reasons which have been explained in the earlier section. But regardless of this fact, the faults should still be maintained within acceptable range in order to achieve the most optimal behavior for the machine.

Most of rotors can be balanced either in the factory environment or in the field based on the recognized industrial standards which are similar to one another. But since rotors can differ based on their material and manufacturing processes, the execution of balancing can be still different for an individual rotor. Selecting a suitable balancing method is also heavily

influenced by whether the rotor is rigid or flexible and what type of unbalance exists on the rotor. From the past experiences, the different specifications, and tolerances regarding the tolerable level of unbalance and the consequent vibration have been identified and developed. (Diouf & Herbert 2014, p. 7-11.)

3.1.1 Balancing of rigid rotors

Rigid rotors are usually balanced with a single balancing plane or with two balancing planes. If a rigid rotor has a complex construction, it could also be required to use more than two balancing planes. (Vuojolainen et al. 2018, p. 3.) In case of static unbalance however, unbalance is compensated theoretically by adding an equal balancing weight at the same radial plane where the unbalance exists but with 180° opposite phase angle. The inserted balancing weight creates a centrifugal force which is equal but opposite to the radial load caused by static unbalance. Therefore, with the added balancing weight it is possible to compensate the effect of static unbalance by only using a single-plane. (Diouf & Herbert 2014, p. 9-10.) Figure 19 illustrates the procedure of single-plane balancing method.

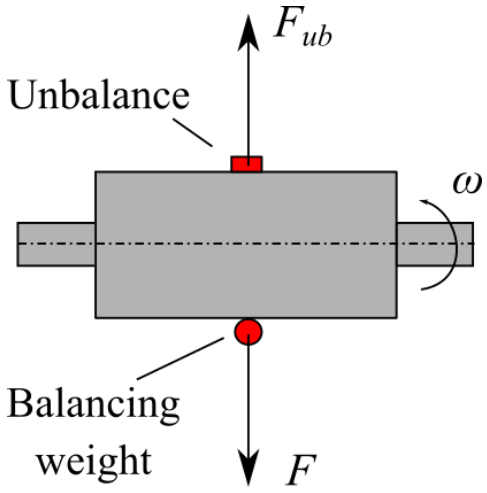

Figure 19. Single-plane balancing procedure.

In order to balance a rotor which has couple unbalance, a pair of balancing weights needs to be attached to the rotor as shown in Figure 20. This pair of balancing weights is positioned on the rotor with an opposite phase angle with respect to the couple unbalance in order to create a counter moment which can compensate the couple moment due to unbalance. Thus,

two planes are at least required for correcting couple unbalance defect. (Diouf & Herbert 2014, p. 10.)

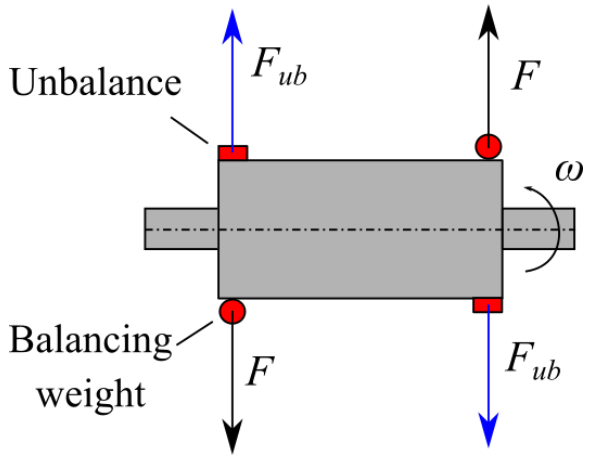

Figure 20. Two-plane balancing procedure.

For balancing dynamic unbalance, one should consider using static and couple balancing methods simultaneously. Since the mentioned type of unbalance is combination of both unbalance types it cannot be corrected effectively by using only one of the corrective methods. In practice, in order to correct dynamic unbalance balancing weights with different size and relative angular position are placed on the rotor at two separate planes. (Vaughan 2013, p. 3-4.)

3.1.2 Balancing of flexible rotors

Rigid rotors and flexible rotors can be distinguished depending on their operating range. Any rotor which over-reaches its first bending critical speed is considered as flexible while the rotors which are operating below their bending critical speed are considered as rigid. Typically, a flexible rotor has one or numerous critical speeds at which the rotor bends with a particular flexural bending mode if its operation speed reaches the corresponding critical speed. Because flexible rotor's bending modes are speed dependent, a flexible rotor should be balanced at its full operating speed range in order for the rotor to withstand deformations caused by each possible bending mode which are included within its operation range. This is the reason why a certain flexible rotor should be balanced with more than two balancing planes. This also makes the balancing procedure of a flexible rotor commonly more demanding compared to balancing of a rigid rotor. The number of balancing planes and their

optimal locations is determined by the rotor's critical speeds and the corresponding mode shapes and their effect on the rotor's vibration response. (Adams Jr. 2007, p. 755; Diouf & Herbert 2014, p. 11.)

Figure 21 represents the first two bending mode shapes of a certain flexible rotor. In the first bending mode, the rotor experience maximum vibration at its midspan. This mode can be corrected effectively by applying a suitable correction weight at the same plane where the vibration has its highest amplitude but with 180° phase shift with respect to the mode's amplitude. In addition to the first bending mode, the rotor also has the second mode in which maximum vibration is occurring at two different planes: ¼ and ¾ span of the rotor. As with the case of first mode, the second mode can also be corrected by applying suitable correction weights at span locations where the peaks of vibration exist but with the opposite phase angles. (Adams Jr. 2007, p. 755.)

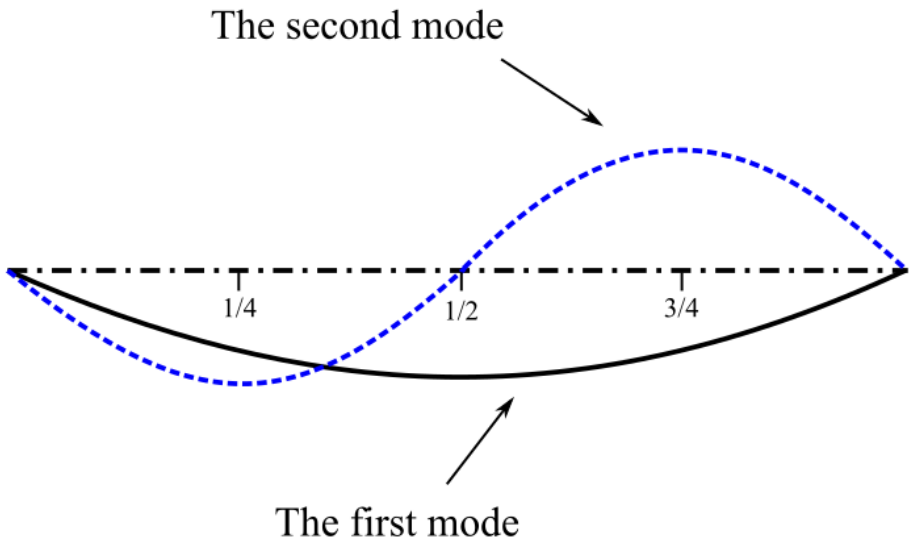

Figure 21. The first two flexural bending mode shapes of a flexible rotor.

What complicates the design of this balancing procedure, however, is that by applying a correction weight at the location of ¾ span, vibration of the first bending mode increases. This is due to correction weight which has been positioned at close proximity to the initial unbalance which causes the first mode to occur. Therefore, the initial unbalance and correction weight are together exciting the first mode which increases the overall vibration. This could possibly cause more severe consequences than if the correction weight at ¾ span

location would not have been inserted on the rotor to fix the second mode at the first place. This is why one should usually design the balancing procedure of flexible rotor with care.

A machine which consists of a flexible rotor assembly with multiple different components usually require each component to be first balanced individually since individual components have their own critical speeds and modes. After the rotor is assembled, the final balancing is performed on the full assembly. In some cases, balancing of flexible rotors can be a simpler procedure if the rotor is operating below 80% of the first critical speed or if it is supported by soft bearings. In these types of cases the rotor can be balanced with a low-speed balancing machine by using only two correction planes as with the case of rigid-body balancing. It should be considered however that to balance a flexible rotor sufficiently by using only rigid-body balancing methods, an information of where most of the unbalance is concentrated at the rotor is still required. (Adams Jr. 2007, p. 755-756.)

3.1.3 Rotor drivetrain alignment

The principle of rotor drivetrain alignment is based on the process of adjusting driving and driven shafts which are initially misaligned to be collinear again. This collinear condition should apply in both vertical and horizontal planes for the system. Usually, the tolerance level which indicates the maximum allowed misalignment is specified by the machine component designers. In industry, common alignment techniques have been concentrated earlier mostly on traditional mechanical inspection techniques which include visual inspection and utilization of basic measurement tools such as straightedges, calipers, gages, and spirit levels. These techniques are relatively simple methods, but they lack accuracy which is why they are mainly suitable only for identifying misalignment defect but not for correcting it. (Lijesh & Harani 2015, p. 1142; Subbiah & Littleton 2018, p. 197 – 213.)

Recently, a more sophisticated, and improved rotor drivetrain alignment method which is based on utilization of laser optics has grown some research interest. In this method, displacements of drivetrain coupling, and shafts are measured with laser transmitters and detecting receivers as shown in Figure 22.

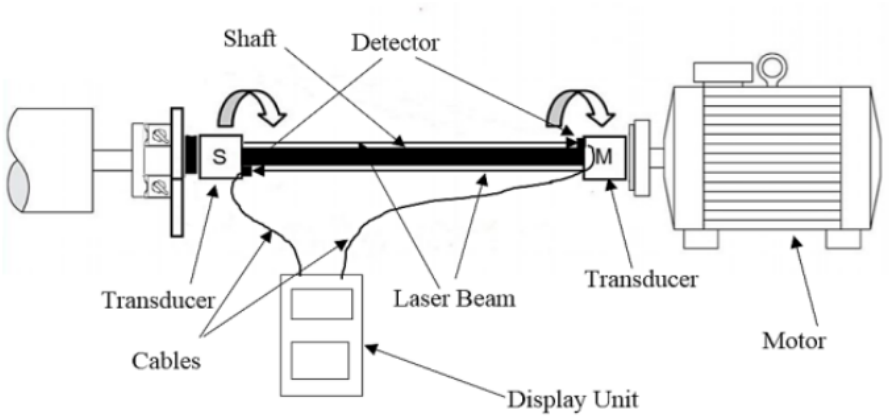

Figure 22. Principle of laser alignment system (Lijesh & Harani 2015, p. 1143).

After the data about the displacements has been collected, the measurements are compared to the reference point that relates to the system's condition without misalignment. By using the reference data, it is possible to monitor the elevation changes in the system in real-time during the system's operation. This enables performing a correcting alignment action simultaneously while displacements are measured. This is not possible with the common tools which are limiting the measurements and corrective action to be performed separately. Although more expensive, laser measurement tools achieve the alignment of drivetrain in more quickly fashion with higher accuracy when compared to earlier mechanical inspection techniques. Because of the method's high accuracy, longer life-cycles of the system's machine elements can be ensured while energy cost reduction and higher power rates can also be achieved by the overall better efficiency of the system. (Lijesh & Harani 2015, p. 1142-1143; Subbiah & Littleton 2018, p. 216.)

3.2 Balancing and aligning by using AMBs

AMBs with their active control are very suitable for suppressing vibration due to different source of vibration such as unbalance and drivetrain misalignment. But, as has been mentioned in the introduction chapter, AMB-rotor systems are open-loop unstable systems which typically need a feedback controller in order to be stable within their operation range. Most of commercial AMB systems are controlled with SISO types of controllers such as PID controllers of which working principle is simple. Because of their simple construction they are easily adjustable and implementable. These types of controllers are also highly efficient for stabilizing rigid rotors. (Yoon, Lin & Allaire 2013, p. 75-80.)

The design and implementation of PID controller for controlling flexible AMB-rotor systems is not however as that easy. For these purposes, advanced MIMO controllers are more suitable. MIMO controllers offer higher robustness and better performance compared to PID controllers, although they are not as common in the industry applications as PID controllers because of their complexity. Due to some limitations of PID controllers which MIMO controllers do not possess, their usage in the industry is expected to grow in the future, however. (Yoon et al. 2013, p. 81-87.) In addition to different levitation control methods, AMBs also utilize unique unbalance control feature to specifically compensate loads and transmitted vibration or to minimize harmonic displacements due to unbalance in AMB-rotor systems (ISO 14389-4 2012, p. 5).

3.2.1 Decentralized and centralized PID control

In a simplest term, the working principle of PID controller is having the rotor's displacement to be measured with a displacement sensor which is then fed as an input to the PID controller. The PID controller then compares this displacement information to the rotor's reference position and creates an error signal $E(t)$ which relates to the difference between the reference and actual rotor's position. The error signal is then used to generate a control signal $C_{PID}(t)$ to drive the coils of AMB. The generated control signal $C_{PID}(t)$ by the PID controller can be expressed as (Muminovic A. J. et al. 2020, p. 115):

$$C_{PID}(t) = K_p E(t) + K_d \frac{dE(t)}{dt} + K_i \int_0^t E(t)dt \tag{3.1}$$

In equation (3.1), the first proportional term relates to the force which has a similar effect than a mechanical spring whereas the derivative term acts like a damping force. The integral term on the other hand decreases the steady-state error caused by certain constant disturbance. The force which rotor experiences due to PID controller is the combination of all three terms presented in equation (3.1). Therefore, the controller can be understood as a system which resembles a spring-damper that can be adjusted as required. Since PID controller is a dynamic system, it is usually described with the transfer function as shown (Yoon et al. 2013, p. 75):

$$G_{PID}(s) = K_p + \frac{K_d(s)}{\tau_d s + 1} + \frac{K_i}{s} \tag{3.2}$$

where τ_d is a small time constant which has been included to the derivative term to transform it as a proper transfer function.

Magnetically suspended rotors can generally be controlled with either decentralized PID controller or with tilt-and-translate (centralized) PID controller. The way how these two different PID-controllers differ from each other is that with the case of first type controller, the control of each axis of the rotor in each bearing is separate and is measured by a single displacement sensor. Therefore, with this kind of control arrangement, PID controllers are not communicating with each other in order to keep the system stable. This is the main differentiating factor which distinguish decentralized PID control from centralized PID control. The arrangement of decentralized PID control can be seen in Figure 23.

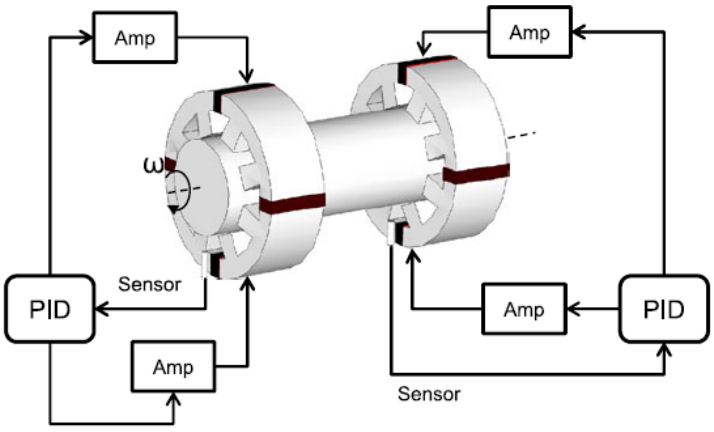

Figure 23. The arrangement of decentralized PID control assuming that a bias-current is fed to the amplifiers (Yoon et al. 2013, p. 78).

Because of the described control arrangement, decentralized PID control is simple, but on the other hand the performance of the system is limited. This is influenced by the rotor's lateral dynamics at each bearing location which are coupled. Since the dynamics at one end of the rotor can be highly affected if the force is applied at the other end of rotor, decentralized PID is uncapable to offer the best performance due to the reason that each sensor/actuator pair is controlled independently. (Yoon et al. 2013, p. 77.)

Centralized PID control has been designed to overcome the issues which are present in decentralized PID. With centralized PID control structure, the inputs and outputs of several bearings are combined together by the controllers. The aim of this control arrangement is to acquire the set of rigid tilt and translating modes from the decoupled rotor dynamics. This decoupling of rotor dynamics is necessary since the parallel and conical modes of the rotor which dominate the rotor's lateral dynamics cannot be controlled simultaneously. In order to stabilize these rigid modes, it is required that the modes will be first decoupled so that they can be stabilized individually with separate PID controllers. (Yoon et al. 2013, p. 77-78.) The principle of centralized PID control arrangement is illustrated in Figure 24.

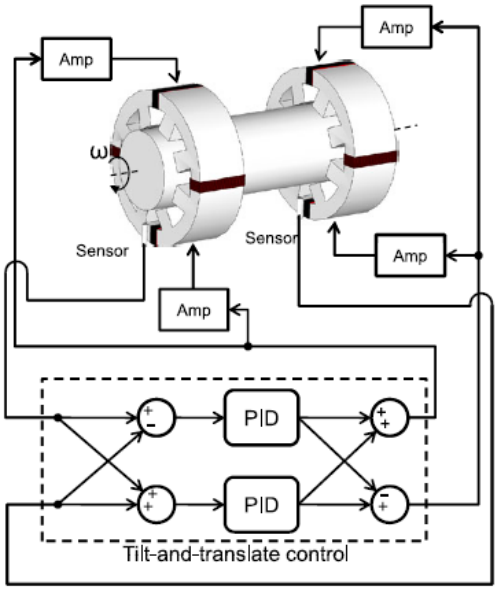

Figure 24. The arrangement of centralized PID control assuming that a bias-current is fed to the amplifiers (Yoon et al. 2013, p. 79).

In the figure, the rotor's tilt and translation are measured by using the gathered displacement information from both sensor location. This information is then converted to translation measurement by summing the two measured signals together while the tilting is computed as the difference between the signals. When the measurements have been obtained, they are fed to the PID controllers of which outputs are then combined to control each AMB actuator in the system. The conical mode can be controlled by feeding the output from the controllers to the actuators with the opposite signs. The translation mode on the other hand is controlled by feeding the output to the actuators with the equal signs. (Yoon et al. 2013, p. 78.)

Although the working principle of PID controllers is simple which is the reason they are most often used in commercial applications, they still have certain limitations. One limitation is related to stabilization of flexible rotors which have more complex dynamics than in the case of rigid rotors. Because of this, additional signal filters are usually required to help the PID controller to damp the rotor oscillation at higher resonances. However, the design procedure of these filters is not self-intuitive. (Yoon et al. 2013, p. 80.)

Non-collocation of displacement sensors and AMB actuators is another limiting factor in case of PID controllers. For rigid rotors, non-collocation does not cause that much of an issue since the deformation of the modes is relatively small. Thus, any measurement error regarding the rotor's displacement at the sensor location with respect to the actual displacement at the bearing location will also be small. The deformation of the modes belonging to a flexible rotor can however be relatively large at certain sections on the rotor. If there is a particular point between the locations of sensor and AMB in which the mode's slope is zero (nodal point), 180° phase shift exists between the measured and actual rotor's oscillation. Since PID controllers are counting on single feedback measurement from the sensor to create the control signal, this could lead the system to become unstable. (Yoon et al. 2013, p. 80-81.)

3.2.2 LQG control method

In the case of MIMO controllers, all the measurements measured by the sensors are first gathered to one location after which the control signals to the actuators is computed by the single algorithm. Therefore, with this kind of control structure all AMBs are cooperating in order to keep the rotor stabilized. One type of MIMO controller is a linear quadratic gaussian (LQG) controller which is similar to related linear quadratic regulator (LQR) controller which both are based on optimal control theory. (Yoon et al. 2013, p. 81).

What differentiates LQG controller from LQR controller however is that LQG utilizes Kalman state estimator which aims to estimate the system state over time from certain output measurement. Thus, LQG controller can be considered as LQR controller which estimates the system's state with the help of Kalman filter. (Yoon et al. 2013, p. 81.) LQG controller is capable to provide a good performance and stability for the controlled system even though

some system disturbances and measurement noise might be present or in a case where the system model might have some minor inaccuracies (Shabaninia & Jafari 2012, p. 1).

For the design process of this controller, the dynamics of linear system can be expressed in a state-space representation (Shabaninia & Jafari 2012, p. 3) as follows:

$$\begin{aligned} \dot{\boldsymbol{x}}(t) &= \mathbf{A}\boldsymbol{x}(t) + \mathbf{B}\boldsymbol{u}(t) + \mathbf{G}\boldsymbol{w}(t); \\ \boldsymbol{y}(t) &= \mathbf{C}\boldsymbol{x}(t) + \boldsymbol{v}(t) \end{aligned} \tag{3.3}$$

in which $\boldsymbol{x}(t) \in R^n$, $\boldsymbol{u}(t) \in R^m$, and $\boldsymbol{y}(t) \in R^q$ represent the system's states, control inputs and outputs vectors, respectively, whereas $\mathbf{A} \in R^{(\mathrm{n\ x\ } n)}$, $\mathbf{B} \in R^{(\mathrm{n\ x\ } m)}$, $\mathbf{G} \in R^{(\mathrm{n\ x\ } p)}$ and $\mathbf{C} \in R^{(\mathrm{q\ x\ } n)}$ are representing the system state, control input, inputs of disturbance and output matrices, respectively. In equation (3.3), the system noise $\boldsymbol{w}(t)$ and the measurement noise $\boldsymbol{v}(t)$ are Gaussian white noise processes with p and q vector dimensions. The mean value of both noises is zero and the covariance matrices which are associated to them can be defined as (Shabaninia & Jafari 2012, p. 3):

$$\begin{aligned} E = \{\boldsymbol{w}\boldsymbol{w}^{\mathrm{T}}\} = \mathbf{W} \geq 0, \;\; E = \{\boldsymbol{v}\boldsymbol{v}^{\mathrm{T}}\} = \mathbf{V} > 0, \\ E = \{\boldsymbol{w}\boldsymbol{v}^{\mathrm{T}}\} = 0 \end{aligned} \tag{3.4}$$

where E is an expectation operator, and $\mathbf{W}$ and $\mathbf{V}$ are covariance matrices related to system and measurement noises, respectively. Now, in LQR control problem the aim is to minimize the quadratic cost function J_{LQR} which can be written as (Yoon et al. 2013, p. 81):

$$J_{LQR} = \int_0^\infty (\boldsymbol{x}^{\mathrm{T}}\mathbf{Q}\boldsymbol{x} + \boldsymbol{u}^{\mathrm{T}}\mathbf{R}\boldsymbol{u})\mathrm{d}t \tag{3.5}$$

where the weighing matrices of the function are denoted by $\mathbf{R} = \mathbf{R}^{\mathrm{T}} > 0$ and $\mathbf{Q} = \mathbf{Q}^{\mathrm{T}} \geq 0$.

This is realized by letting the control signal vector $\boldsymbol{u}$ to be a linear function of the state $\boldsymbol{x}$ vector (Shabaninia & Jafari 2012, p. 4):

$$\boldsymbol{u} = -\mathbf{K}_r \boldsymbol{x} \tag{3.6}$$

where $\mathbf{K}_r$ is the optimal state feedback matrix gain. To estimate system state $\boldsymbol{x}$ from the output observation $\boldsymbol{y}$, Kalman filter can be designed which follows the state equation (Shabaninia & Jafari 2012, p. 4):

$$\frac{d}{dt}\hat{\boldsymbol{x}} = \left(\mathbf{A} - \mathbf{K}_f \mathbf{C}\right)\hat{\boldsymbol{x}} + \mathbf{B}\boldsymbol{u} + \mathbf{K}_f \boldsymbol{y} \tag{3.7}$$

in which $\mathbf{K}_f$ is the gain matrix of Kalman filter and $\hat{\boldsymbol{x}}$ is optimal estimate vector of the state vector $\boldsymbol{x}$ which is selected such that it minimizes the function (Shabaninia & Jafari 2012, p. 3):

$$E\{[\boldsymbol{x} - \hat{\boldsymbol{x}}]^{\mathrm{T}}[\boldsymbol{x} - \hat{\boldsymbol{x}}]\} \tag{3.8}$$

After the suitable estimate has been found, it is treated as it would be the true measurement of the state in order to find a solution to the LQG control problem. By implementing LQR controller with a state estimator $\hat{x}$ leads to the LQG control law (Yoon et al. 2013, p. 82):

$$\boldsymbol{u} = -\mathbf{K}_r \hat{\boldsymbol{x}} \tag{3.9}$$

The block diagram of LQG controller, which is composed of Kalman filter and LQR controller, is shown in Figure 25.

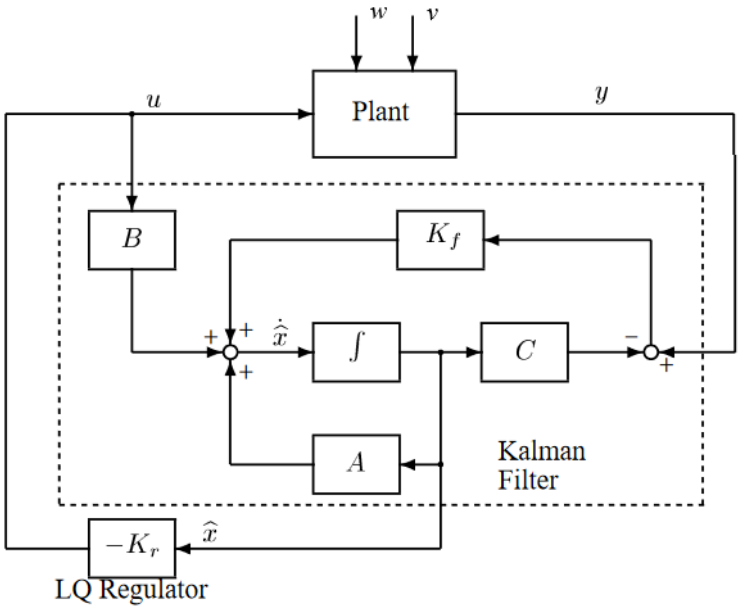

Figure 25. The LQG controller composed of Kalman filter and LQR controller (Mod. Skogestad & Postlethwaite 2005, p. 378).

With the help of Kalman filter, LQG control allows the estimation of system states even though they might be non-measurable due to different sources of noise. However, selecting suitable weighting functions while designing the controller is not a trivial task and quite often tends to depend on the skill and experience level of the designer. Additionally, because of the controller's high sensitivity to plant uncertainties, unmodelled plant dynamics might cause some issues. If some of the aspects which are relevant have been ignored during the modelling process, Kalman filter is uncapable to provide the accurate required estimations of the system's states in order to keep the system stabilized. (Yoon et al. 2013, p. 82.)

3.2.3 Unbalance control strategies with AMBs

Compared to traditional bearings such as ball and journal bearings, AMB is capable to adjust actively system's response due to possible unbalance conditions. This is one of the most important features of AMB which distinguish it from the conventional bearings. Unbalance control feature can be classified mainly into two different control strategies (Schweitzer & Maslen 2009, p. 215 - 216):

- Cancelling or rejecting the bearing reaction forces which are synchronous with the rotor's speed. This lets the rotor to rotate around its inertia axis, assuming that the air gap is sufficiently large in the stator housing for allowing such motion.

- Cancellation or rejection of unbalance vibration due to residual unbalance by compensating the centrifugal force with a suitable counterforce which lets the rotor to rotate around its geometrical axis.

Additional unbalance control strategy is related to minimizing resonance vibration by providing optimal synchronous damping forces on the rotor while it passes through its bending critical speeds. The three different unbalance control strategies with their different terms as they are presented in literature and industry while also the benefits and disadvantages of each strategy are shown in Table 1 which is taken from ISO 14389-4.

Table 1. Unbalance control strategies with their common terms and the positive and negative resulted control system properties of each strategy (Mod. ISO 14839-4 2012, p. 36).

Unbalance control strategy	**Control system terms used in industry/literature**	**Resulting control system properties**
Cancellation / rejection of synchronous bearing reaction force	• Unbalance compensation • Automatic balancing system (ABS) • Automatic balancing control • Adaptive feed forward compensation • Adaptive feedforward compensation • Adaptive vibration control (AVC) • Adaptive unbalance control • Automatic vibration rejection (AVR) • Feed forward compensation (FFC) • Inertial auto centering control • Unbalance force rejection control (UFRC)	+ Elimination of synchronous bearing reaction forces + Reduction of housing vibrations + Reduction of machine noise emissions + Avoidance of dynamic power amplifier saturation + Reduction of power consumption (reactive power) + Cost reduction (lower installed power) -Cannot be applied when passing bending resonance speeds

Table 1 continues. Unbalance control strategies with their common terms and the positive and negative resulted control system properties of each strategy (Mod. ISO 14839-4 2012, p. 36).

Unbalance control strategy	Control system terms used in industry/literature	Resulting control system properties
Cancellation / rejection of unbalance vibration	• Peak of gain control • Unbalance force counteracting control (UFCC)	+ Attenuation of unbalance-induced vibrations / displacements / orbits by suitable compensation forces + Suitable for high-precision positioning applications - May need high bearing forces and high amplifier power when used in the presence of large residual rotor unbalance or near bending resonance speeds
Damping force generation	• Optimum damping control (ODC)	+ Reduces vibration by offering peak damping at the synchronous frequency (used only for passing bending critical speeds - May need high bearing forces and high amplifier power in the presence of large residual rotor unbalance

All the listed unbalance control methods can be treated mathematically as generalized notch filters as is shown in Figure 26 since the methods are united by the process of injecting signals which have narrow band, and which are synchronous with the rotor's speed in order to compensate the residual unbalance. The only differentiative factor regarding the presented methods is related to how the signals are generated, at which point in the control loop they are fed and what kind of process is utilized for allowing the signals to adapt to the unbalance which may be unknown. (ISO 14389-4 2012, p. 35.)

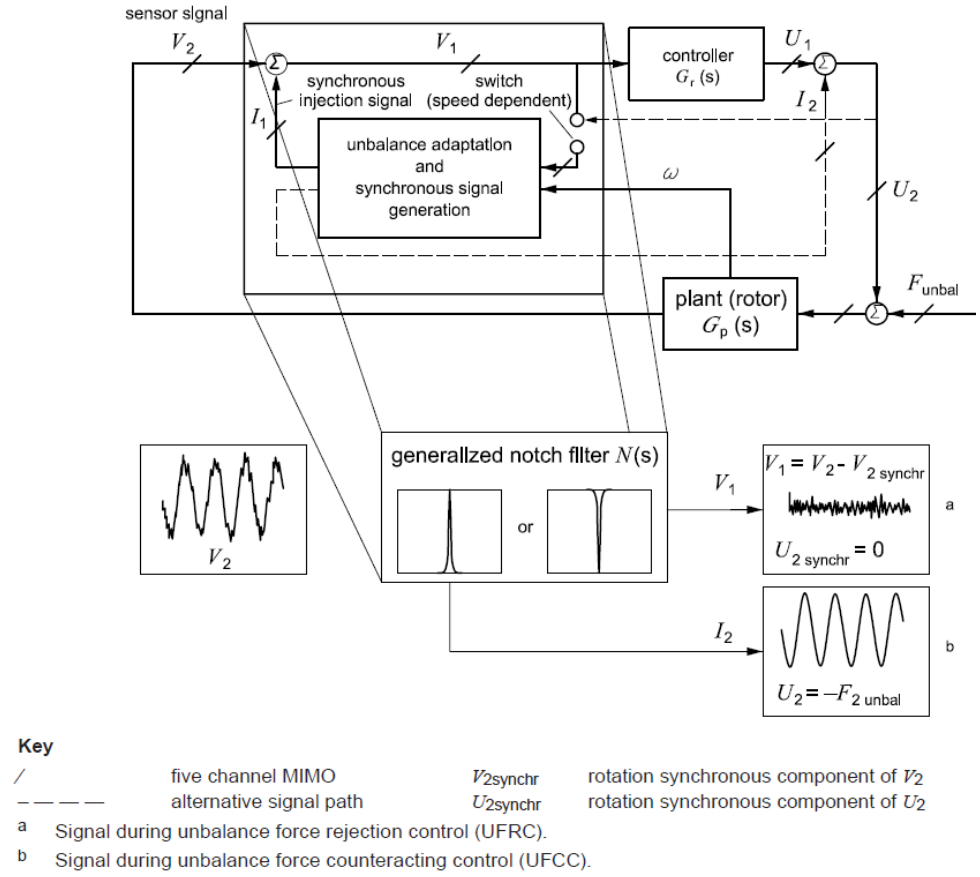

Figure 26. The unbalance control feature of AMB in which the principle of UFRC and UFCC control methods is presented (ISO 14389-4 2012, p. 37).

Of the presented unbalance control methods, the most often used method is UFRC method which is usually activated after the rotor's speed has reached a certain activation point. Typically, this speed is set below to the rotor's normal operating speed while it can also be set to speeds lower than the critical speeds corresponding to the rotor's rigid body modes in order to help it to transverse the resonance points. This also applies for UFCC unbalance control method. (Schweitzer & Maslen 2009, p. 216 – 220; ISO 14389-4 2012, p. 39.) As is illustrated in Figure 26, the injection point of compensation signal can be either at the input or at the output of controller. For the UFRC control scheme, the compensation signal is preferred to be injected to the input of the controller I_1 since it allows to gain better benefits than injecting the signal to the controller's output I_2. This reason is linked to the removal of synchronous components from the sensor signal V_2 which leads to better handling of numerical computation when digital control algorithm is considered. (ISO 14389-4 2012, p. 35.)

In case of UFRC method, regardless of whether the compensation signal is injected to the input or output of the controller, the generalized notch filter provides the signal in such a way which allows the rotor to rotate around its inertia axis. This is achieved by subtracting any synchronous rotation component from the sensor signal V_2 which leads the controller's output U_2 also not to contain any synchronous component. This minimizes reaction forces of the bearings and housing vibrations. In UFCC unbalance control method on the other hand, the notch filter most often injects the compensation signal to the controller's output which generates a counterforce to counteract the excitation force due to unbalance which minimizes the rotor's deviations and allows it to spin around its geometrical axis. (ISO 14389-4 2012, p. 35.)

In Figure 27, the responses of rotor's harmonic displacement and magnetic bearing current which have been measured in time domain are shown. For this specific example, UFRC unbalance control method has been selected as compensation method since the minimization of the response of synchronous bearing reaction force current is dictated to be more critical than minimizing rotor's displacement response. Also, the rotation speed of the rotor has been set as 200 Hz while the activation point of UFRC is illustrated by the label *a*.

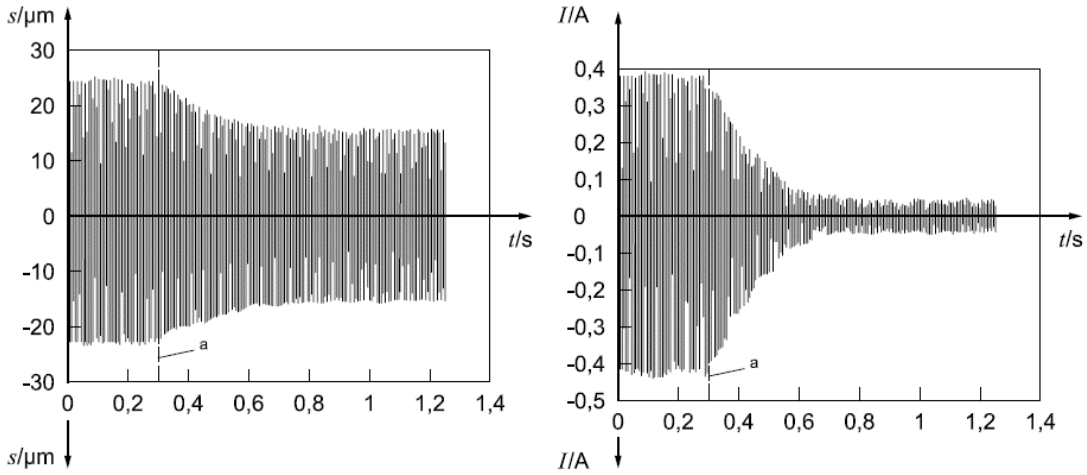

Figure 27. The responses of rotor's displacement and synchronous bearing force current when UFRC unbalance control method is implemented (ISO 14389-4 2012, p. 38).

As can be verified from Figure 27, after UFRC is activated at moment $t = 0.3$ s the response of synchronous bearing force current minimizes drastically. The remaining signals in the force current response are only related to measurement and control noise. This proofs that

by using UFRC method for compensating residual unbalance on a rotor, the synchronous bearing forces to the foundation of machine and vibration noise can be eliminated almost completely. By looking at Figure 27 it is also visible that UFRC is beneficial in reducing the displacement response of the rotor by some amount. (ISO 14389-4 2012, p. 37.)

Generalized notch filters allow the rotor to operate in stable condition over its entire speed range which is possible by adjusting the phase angle of the filter to be suited for different rotor speed ranges. (Liu et al. 2019, p. 1.) Because of this, the filters can also be used for achieving stability of flexible modes which are lightly damped. In commercial applications, the filters are commonly applied with PID control which are designed based on the second order standard transfer function (Muminovic A. J. et al. 2014, p. 115):

$$G_{notch}(s) = \frac{s^2 + {\omega_{notch}}^2}{s^2 + 2 \cdot \xi_{notch} \cdot \omega_{notch} \cdot s + {\omega_{notch}}^2} \tag{3.10}$$

where ω_{notch} is the central frequency which corresponds to certain flexible mode critical speed of the rotor, while the width of the notch in the rotor's frequency response is controlled with the damping ratio denoted by ξ_{notch}. The number of notches is decided based on how many flexibles modes are required to be stabled.

When the rotor is balanced automatically with the notch filter and the applied phase shift, the control current of AMB needs to be reduced significantly. This is due to possible saturation of the power amplifier which can especially occur when UFCC control method is implemented for minimizing rotor's displacements which could then lead to high actuator forces. By decreasing the control current, saturation can be prevented which also leads to smaller vibration response of the rotor. (Liu et al. 2019, p. 1-2.) Another consideration is that the conditions for ensuring the stability of adapting synchronous injection signals to the present and changing unbalance conditions are heavily linked to the topology of selected control scheme and the rotation speed of the rotor (ISO 14389-4 2012, p. 39). Thus, the control topology should be chosen wisely while also considering what is the rotor's desired operation range in order for the unbalance control of AMB to work most effectively.

3.2.4 Load capacity of AMB

The performance of specific AMB is typically affected by the magnetic saturation of ferromagnetic material used in the bearing's stator and rotor core, and also by the amplifier's current and voltage limits. The actuator's coil temperature is also one factor which is limiting the performance. Any maximum load which AMB can apply on the rotor at its fixed middle position is specifically referred as load capacity of an AMB. (ISO 14389-1 2002, p. 11.)

When the rotor is passing its critical speed, the load capacity of AMB becomes important factor since the amplifier's voltage saturation may occur which would lead the rotor to become unstable. On such occasions, the performance of AMB deteriorates rapidly which could lead to higher whirling amplitudes. This is especially the case if the critical speed is at higher frequency than the knee frequency of the bearing which is the point in which the bearing load capacity is begun to be limited by the saturated voltage. (ISO 14389-2 2004, p. 19.) This is illustrated in Figure 28 where the knee frequency point is denoted by a_k.

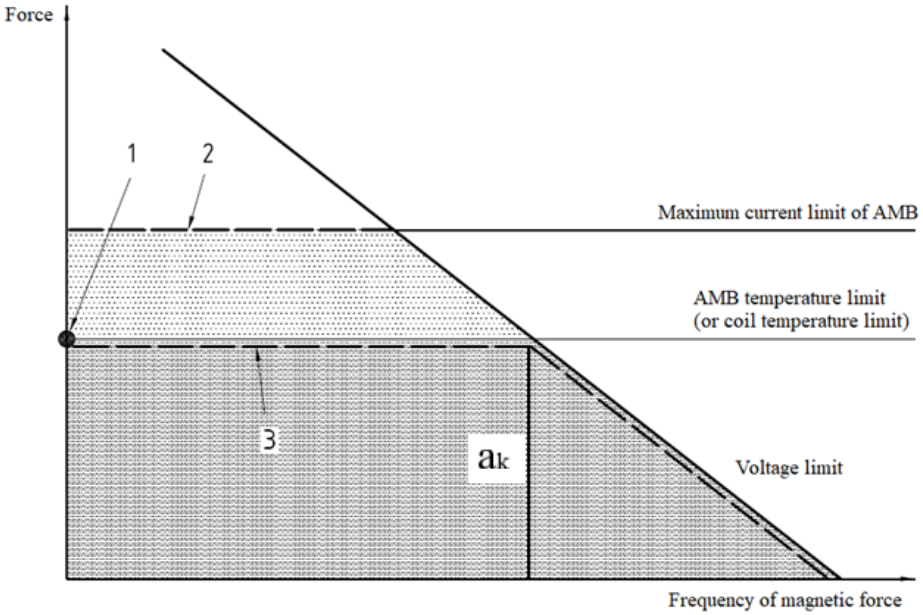

Figure 28. Load capacity of an AMB as a function of frequency of magnetic force (Mod. ISO 14389-1 2002, p. 12).

The load carrying performance of AMB can be characterized with three different types of capacities. In Figure 28, label 1 is referring to static load capacity of an AMB which is the bearing's maximum load capacity for certain constant load. Label 2 instead is referring to

peak transient load capacity of an AMB. It differs from the static load capacity in that aspect that it is measured over a limited time period whereas static capacity is measured for unlimited time period. Label 3 on the other hand is referring to dynamic load capacity of an AMB which dictates the maximum force the bearing is capable to apply on a rotor as a function of frequency. (ISO 14389-1 2002, p. 12.) In case of laminated bearings, the load capacity of AMB tends to decrease when frequency increases which is influenced by the actuator coil inductance. The reason for this is because the coil inductance becomes saturated due to large rotor motion which have an effect on creating currents in the actuator's coils which have improper magnitude and phase for controlling the rotor as intended. (ISO 14389-4 2012, p. 14.)

3.3 Vibration evaluation criteria

ISO 14389-2 is recognized as one suitable standard which provides general guidelines for measuring and evaluating displacement of a rotor system which is supported by AMBs. The standard is suited for rotating machines with a higher than 15 kW nominal power rate. Its applicability is also not limited by the size and operational speed range of the machine. The two evaluation criteria of ISO 14389-2 -standard are related to the allowed absolute maximum radial displacement value or the allowed maximum change in magnitude of vibration level. (ISO 14389-2 2004, p. 1.)

Reliable operation of the system equipped with AMBs is analyzed by comparing maximum displacement of a rotor D_{max} to the minimum clearance between rotor and AMB housing in both radial and axial directions. The equations to perform this analyze procedure are given as follows (ISO 14389-2 2004, p. 3):

$$D_{max} < C_{min-radial} \tag{3.11}$$

and

$$D_{max} = z_{max} < C_{min-axial} \tag{3.12}$$

in which $C_{min\text{-}radial}$ and $C_{min\text{-}axial}$ are typically the minimum radial and axial clearances of the air gap of an installed safety bearing while z_{max} is the maximum axial movement of the rotor.

Because AMBs are comparably soft and provide non-contact supporting action on the rotor, bearing dynamic forces and the force transfer to the stationary structures are not considered in the standard. Therefore, the displacement limit values are applied to the whole speed range of the rotor. Four different vibration evaluation zones have been established which are (ISO 14389-2 2004. p. 6):

- Zone A: displacements belonging to the machines which are new and have just been commissioned to the operation site.
- Zone B: displacements of machines which are at acceptable level and do not affect negatively on the machine's performance during its long-term operation.
- Zone C: displacements of machines which are considered to have a negative effect on the machine's performance during its long-term operation. Displacement is not severe if it is occurring only in the short term.
- Zone D: displacements of machines which are severe at any circumstance and have a high chance to damage the machine if preemptive actions are not taken.

By following the values which are listed in Table 2, it is possible to avoid larger deficiencies and any overestimated requirements regarding the system. The listed values are suitable for monitoring the machine's condition or while diagnosing a possible technical problem. The values can also be used for limiting the machine's operation based on the set requirements. (ISO 14389-2 2004, p. 6.)

Table 2. Proposed vibration zone limits based on ISO 14389-2 -standard (Mod. ISO 14389-2 2004, p. 7).

Zone limit	**Displacement** D_{max}
A/B	$< 0.3C_{min}$
B/C	$< 0.4C_{min}$
C/D	$< 0.5C_{min}$

In Table 2, C_{min} is the minimum value of radial $C_{min\text{-}radial}$ or axial $C_{min\text{-}axial}$ clearance values.

Figure 29 shows a graph which represents the four vibration zone limits described in table 1. In the figure, *X* is designated to minimum gap clearance C_{min}, whereas *Y* is designated to maximum vibration displacement D_{max}. Both values are in micrometers in the graph. The ratio D_{max}/C_{min} is dictated by *a*.

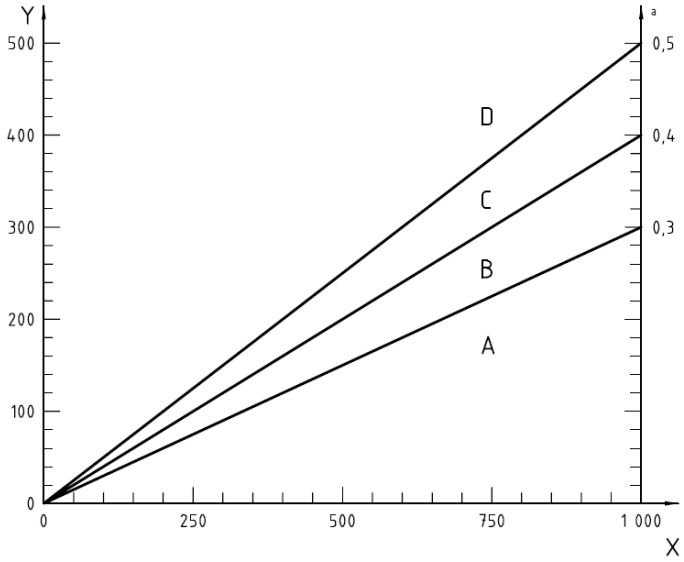

Figure 29. A graph representing the four vibration zone limits (ISO 14389-2 2004, p. 7).

4 ROBUSTNESS EVALUATION OF THE SELECTED SYSTEM TROUGH TIME DOMAIN SIMULATIONS

In this section the optimal performance of a chosen high-speed application is evaluated through time domain simulations in a safe virtual testing environment. To test the system's robustness over a certain period of time, unbalance and coupling misalignment faults are applied to simulation model of the studied system. The performed simulations provide information on whether the system could potentially maintain its stability even though the operation of the system is disturbed by excitations due to the mentioned fault types. If the simulation results are positive, it would indicate that it would be safe to advance in performing physical measurements on the real machine in order to replicate the same tests as done through simulations while also verifying the obtained results at a lab. The selected system which is named as MUSK drivetrain is a flexible rotor drivetrain of which radial displacements are controlled with the radial AMBs. The radial AMBs are located at the rotor which drives the system. The investigated drivetrain and its main components are shown in Figure 30.

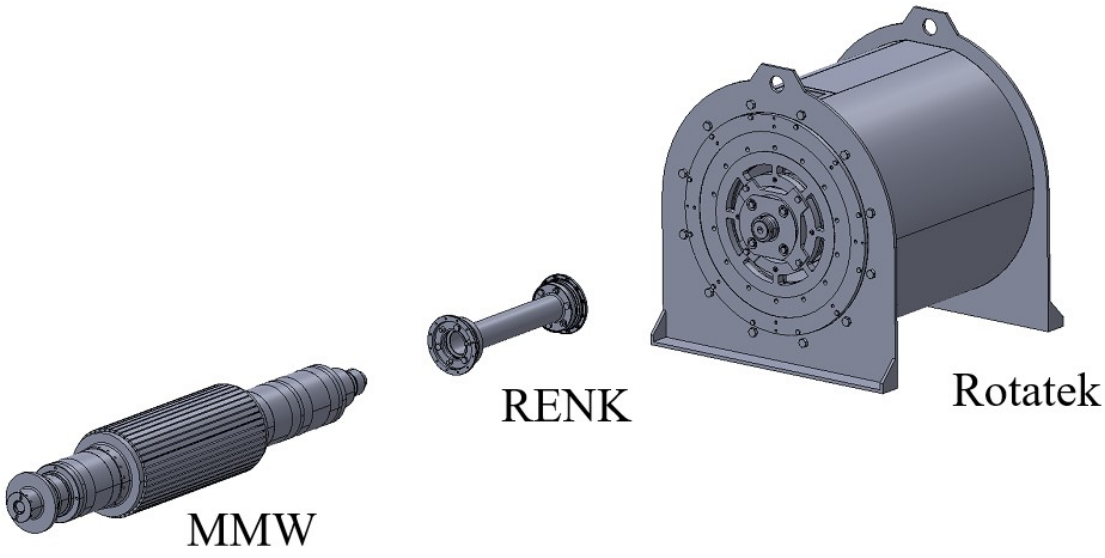

Figure 30. The investigated flexible AMB-rotor drivetrain and its main components.

4.1 Introduction of MUSK drivetrain

The mechanical construction of current MUSK drivetrain consists a driving rotor (MMW), a flexible disc coupling (RENK) and a driven test machine (Rotatek) which can be replaced by a compressor or turbine wheel for instance when the system is commissioned for industrial use. The operation speed of MUSK drivetrain has been rated as 12 000 rpm (200 Hz) whereas the rated power of the system is 2 MW. Both system values are dictated by the design specification of the coupling.

MMW, which is an induction motor rotor, is kept stable with three radial AMB and displacement sensor planes while the rotor is also supported axially with a separate single-axis axial AMB. The main purpose of using three different measurement and actuator planes is to allow each installed sensor-actuator pair to observe and control one of the first three flexible bending modes of the rotor (Jastrzebski, Kurvinen & Pyrhönen 2019, s. 811). In case when the radial AMBs are not active, the rotor is resting at its safety bearings of which air gap is 300 µm. The critical sections of MMW rotor are presented more detailly in Figure 31 from which it can also be seen that the rotor has drilled holes around its circumference at three different planes which are for inserting balancing weights on the rotor mechanically. Otherwise, the rotor has mostly a solid structure excluding the slits at its middle active part.

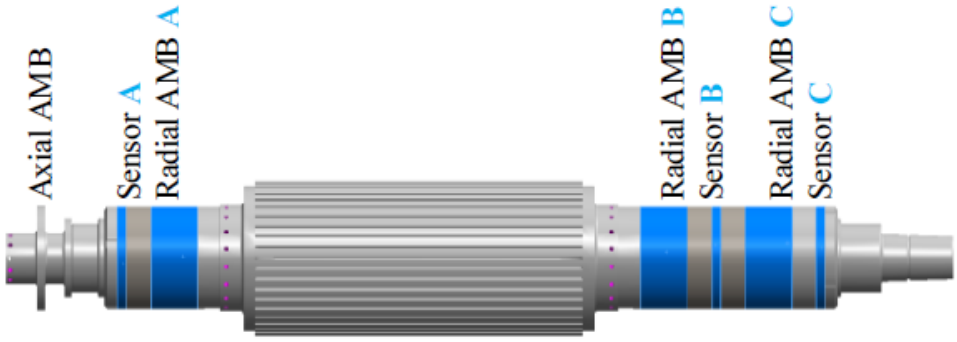

Figure 31. MMW rotor with three radial AMB and displacement sensor planes while also having one axial supporting plane provided by an axial AMB (Jastrzebski et al. 2019, p. 805).

The locations of the three radial AMB and sensor planes of MMW rotor which are measured from its left end are listed in Table 3. The utilized proximity sensors for measuring radial displacements of MMW are inductive type.

Table 3. The locations of the three sensor and radial AMB planes of MMW rotor measured from the left end.

Plane	Location [mm]
Sensor A / Radial AMB A	200 / 290
Sensor B / Radial AMB B	1225 / 1135
Sensor C / Radial AMB C	1405 / 1315

Wireframe plot of the corresponding MMW numerical model which is composed of 56 Timoshenko beam finite elements is shown in Figure 32. The length of numerical model is presented in the image with the label *X* which corresponds to *z*-axis of the rotor.

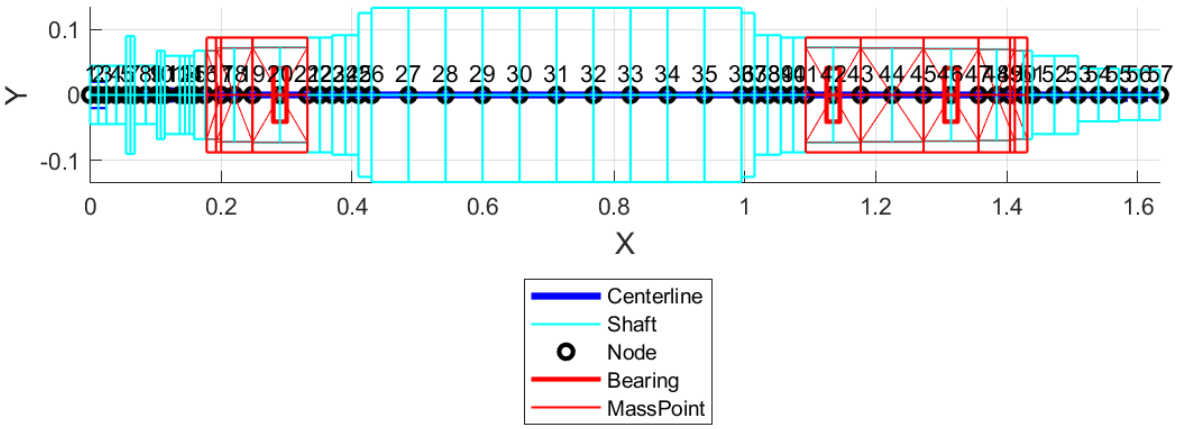

Figure 32. The numerical model of MMW rotor with a total length of 1630 mm.

Rotatek machine on the other hand is supported by its two own roller bearings in order to prevent any vibrations to be transmitted over the coupling to the machine. Like as MMW rotor, Rotatek machine also has mainly a solid structure. In case of RENK-coupling however, the spacer of the coupling is mostly hollow which is why most of the weight in the coupling is concentrated on the coupling halves or the flanges. The corresponding numerical models of Rotatek machine and RENK-coupling which are presented in Figures 33 and 34 consist of 30 and 24 finite beam elements, respectively.

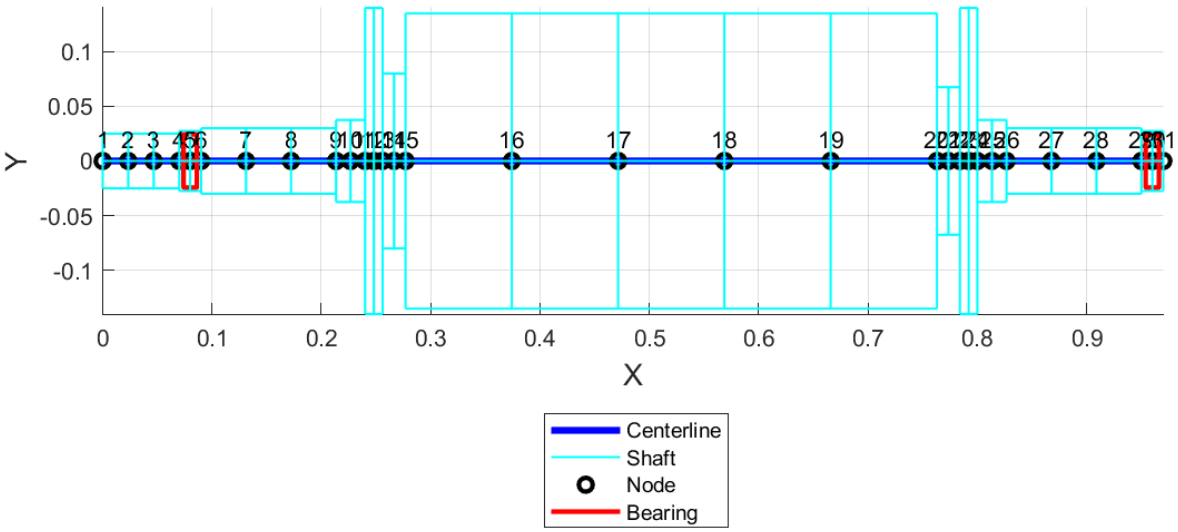

Figure 33. The numerical model of Rotatek machine with a total length of 970 mm.

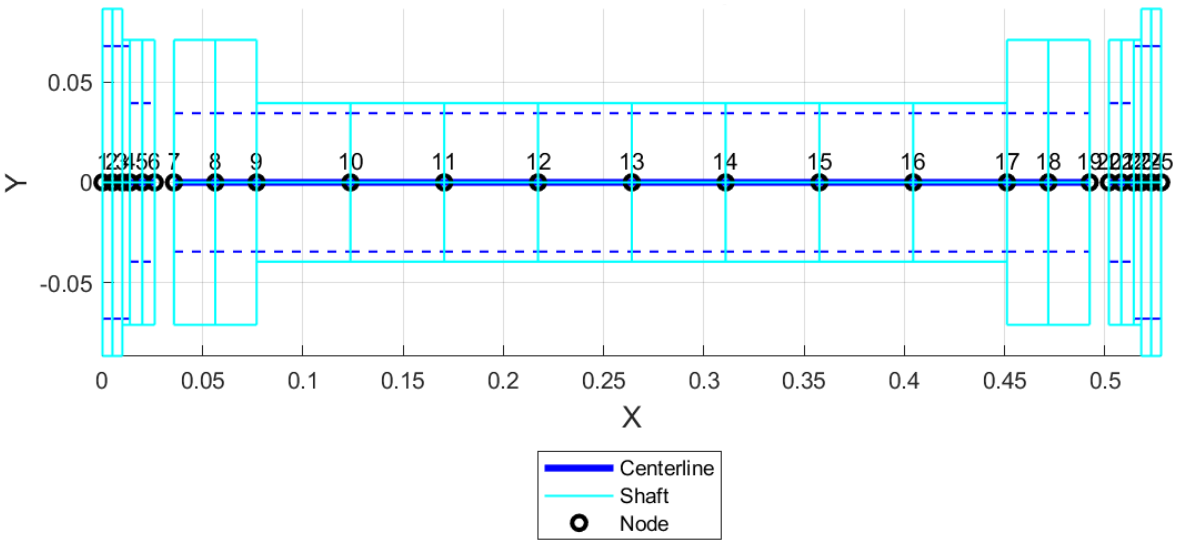

Figure 34. The numerical model of RENK-coupling with a total length of 520 mm.

The weight concentration points in the model of the coupling are located at nodes 4 and 22 of which node 4 is a loading machine side (side closer to MMW rotor) whereas node 22 is the coupling side which is closer to Rotatek machine. All presented numerical models have been created by using RoBeDyn (Rotor-Bearing Dynamics) software package which is used inside MATLAB (matrix laboratory) numerical computing environment.

The main material and inertia characteristics of MMW rotor, RENK-coupling and Rotatek machine are described in Table 4.

Table 4. The main material and inertia characteristics of the mechanical components of MUSK drivetrain.

Component	Material	Mass [kg]
MMW	S355	371.1
RENK	31CrMoV9V	10.3 (left flange); 9.8 (right flange)
Rotatek	S355	225

Rotatek machine also has cooling fans installed at both ends in its housing which are made of aluminum.

The translational, bending, and torsional stiffness parameters of RENK-coupling between its flange and spacer connection points are listed in Table 5. The value regarding translational stiffness applies in all axis directions of the coupling while the rotational stiffness value is only connected with radial axes. The torsional stiffness value instead applies along the length of the coupling.

Table 5. The different stiffness parameters of RENK-coupling.

Type of stiffness	Value
Translational [N/m]	7000
Rotational [Nm/rad]	650
Torsional [Nm/rad]	139 000

In the table, the torsional stiffness value of the coupling is provided by the manufacturer whereas both translational and rotational stiffnesses are estimated values. The approximated values are based on the first two flexible mode frequencies of the coupling which are presented later with MMW frequencies during this introduction chapter.

The nominal operational parameters of the radial AMBs which are used for supporting MMW rotor are shown on the other hand in Table 6. The values provide some insight to the load withstanding capabilities of the bearings and also to the possible reaction forces applied

by them. The nominal values are realized if the radial AMB is manufactured as per design instructions.

Table 6. The nominal operational parameters of the radial AMBs which are supporting MMW rotor.

Parameter	Value
Rated speed (max speed) [rpm]	12 000 (20 000)
Maximum payload [kg]	374
Current stiffness (large signals) [N/A]	764 (485)
Position stiffness (large signals) [N/m]	$1.18 \cdot 10^7$ ($1.33 \cdot 10^7$)
Maximum load capacity with 14 A max control current / with continuous current [N]	5685.5 / 4494
Peak current from the amplifier i_{max} [A]	21
Bias current i_o [A]	7
Inductance (large signal) [H]	0.039 (0.0339)
Resistance at 20 °C [Ω]	0.15

The radial controller of MMW rotor is based on the earlier presented MIMO centralized LQG control method which considers the dynamics of rigid and the first three bending modes of the rotor. The measured frequencies of the first three flexible modes of MMW rotor are presented in Table 7.

Table 7. The measured frequencies of the first three flexible modes of MMW rotor.

Flexible mode id	MMW - frequency [Hz]
1	478
2	680-700 (axis dependent)
3	907

The whole drivetrain has its first bending critical frequency at 405 Hz while the second mode occurs at 702 Hz due to the coupling. Both frequencies are measured values which have been obtained at the laboratory. Within the operation range of the system, the drivetrain has two important frequencies: 12 Hz and 38 Hz which are related to the flexible modes of RENK-coupling. At those frequencies MMW rotor tends to also experience vibration which is related to its rigid body modes because of the deforming coupling.

Currently, the radial position of MMW rotor in its *x*- and *y*-planes is controlled only with bearings A and C while displacement sensor B is used for measuring the lateral displacement of the rotor near to the location of bearing B. This is due to instability caused by the attempt to also control bearing B while the rotor is levitating. The 3AMB controller is however under continuous development at the research lab focused on the MUSK-project. For compensating unbalance excitations in MUSK drivetrain, an own implemented compensation solution is used which assist in minimizing displacements as by using UFCC balancing method. This should allow the system to adapt to the excitations due to uncertain residual unbalances to some extent. The specifics of the implemented balancing method can be found in the conference paper from Vuojolainen et al. (2018).

4.2 Implementing unbalance and misalignment on the simulation model

The simulation model of MUSK drivetrain is based on state-space representation which has been created with Simulink graphical programming environment. Simulink which works on top of MATLAB software is typically used for modelling and simulating dynamical systems in either frequency or time domain. The simplified topology model of MUSK drivetrain is presented in Figure 35. As can be seen from the figure, the simulation model can be considered to include three different matrices which store information of the properties of system inputs and outputs and also the properties related to the system itself. The properties for all these three matrices are processed with the corresponding vectors which are also shown in Figure 35.

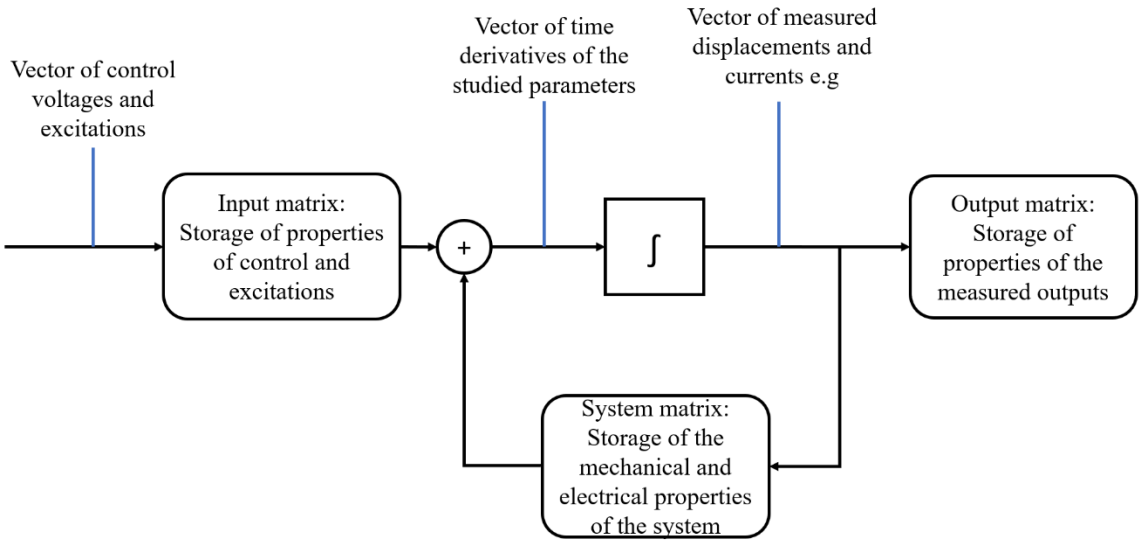

Figure 35. The topology of the mathematical model of MUSK drivetrain used in Simulink.

The measured states of the system which can include for instance the displacements of MMW rotor and the measured force-currents from radial AMBs are solved from the related time-derivatives which occurs after the effect of input parameters on the system's properties have been taken place. The solved states are then fed to the output matrix while the system matrix gets to be processed by the system states. The properties of excitation forces due to unbalance and misalignment are instead included in the input matrix of the model.

In previous studies related to the investigation of MUSK drivetrain, the magnitudes, and locations of permissible residual unbalances on the system have been identified based on SFS-ISO 21940-11 (2017) and API STD 617 (2002) standards. The parameters are measured for the system's rated operational speed 12 000 rpm and also according to the weight parameters of MMW, RENK and Rotatek components. Previously, the balancing quality grade has been set as G2.5 for MMW while the grade G1.5 has been given for Rotatek machine by its manufacturer. The procedure for calculating unbalance amount in case of both components is presented in SFS-ISO 21940-11 (2017, p. 14). The residual unbalances on RENK-coupling have been determined instead by API STD 617 standard (2002, p. 27).

In case of MMW and Rotatek, the location of unbalance has been selected on the closest local node to which the peak of the first possible excited mode due to unbalance is located. This is defined by API STD 617 standard. For the flexible coupling on the other hand, the unbalances have been placed where the coupling half weights are located according to the provided instruction by the coupling manufacturer. By placing unbalances at different locations in the drivetrain with different magnitudes makes the system as dynamically unbalanced. This is the most typical scenario as has also been explained in section 2.

It should be remarked that if AMBs are used specifically for supporting the drivetrain, balancing quality grades are usually too strict. This is true especially in cases where AMB control also includes UFRC control method or some other automatic compensation method for compensating excitations due to residual unbalances as is the case with the studied MUSK drivetrain. On the other hand, it is a good approach to be stricter with the system balancing if the rotor system is operating at close proximity to its bending critical frequency or above it. Stricter balancing is also helpful in situations where the rotor supported by its AMBs is dropped on its safety bearings during abnormal conditions. This minimizes wear of safety bearings while also helps the system to become stabilized sooner. (ISO 14389-4 2012, p. 16.)

To test if the system remains robust even though some additional amount of unbalance is built up on the system during its operation, balancing quality grade of MMW rotor is increased to G6.3 while the balancing grade of Rotatek machine is set to G2.5. Different unbalance distributions and their parameters which are going to be used during the simulation tests are presented in Table 8. For all simulation tests where the system is excited with unbalance excitations, a phase value of $\alpha = \pi$ rad is selected for each residual unbalance.

Table 8. Parameters of allowed residual unbalances in MUSK drivetrain based on SFS-ISO 21940-11 (2017) and API STD 617 (2002) standards. The magnitudes of modified unbalance distribution is also included to the table.

Component		**Nodal location of unbalance**	**Magnitudes of permissible distribution [kgm]**	**Magnitudes of modified distribution [kgm]**	**Phase [rad]**
MMW		39 (Fig. 32)	0.000738216	0.00186	π
RENK	MMW side	4 (Fig. 34)	0.000086868	0.000086868	π
	Rotatek side	22 (Fig. 34)	0.00008255	0.00008255	π
Rotatek		15 (Fig. 33)	0.0002685	0.0004484	π

Allowed misalignment magnitudes are provided by the manufacturer of RENK-coupling. Magnitudes for the allowed angular and radial misalignments are shown for example in Table 9. The allowed magnitudes have been measured for the same rated operational speed as with the case of allowed residual unbalances. In order to simulate misalignment in MUSK drivetrain model, misalignment is implemented at the first node of Rotatek machine.

Table 9. The maximum magnitudes of angular and radial misalignments specified by the manufacturer of RENK-coupling.

Type	**Magnitude**
Angular [°]	0.33
Radial [mm]	2.69

Since the magnitudes of allowed misalignment types are relatively small, the excitation loads on the coupling due to misalignment are linearized for the simulation model. The linearized equations for modelling misalignments with smaller magnitudes are presented in the journal paper published by Tiwari & Lal (2012, p. 91). It should be considered however that for larger magnitudes, a non-linear load vector equation like the equation (2.16) which has been presented during section 2 is needed. This is due to high-order terms in the equation which have potentiality to increase the excitation loads substantially when the magnitudes of misalignments are also large.

4.3 Case 1: With unbalance but without misalignment

This subcase focuses on simulating and analyzing the dynamic responses of the studied system in time domain when the unbalances have been imposed on the system as explained in chapter 4.2. The focus is especially on the radial displacement responses of MMW rotor and on the measured force-current responses of AMBs which are supporting MMW in radial directions. What is mainly studied is that if the AMBs are capable to handle excitations which are applied on the system due to permissible residual unbalances which are shown in Table 8. One of the study concentrations is also if the AMBs are additionally capable to handle uncertainties which may arise when the amount of unbalance on the system is unknown. Robustness of the system to the uncertainties is tested by using higher balancing grades for MMW and Rotatek than the defined ones. The responses of the system are studied by simulating the system with 0-5 s time interval and with a linear speed range of 0 – 10 000 rpm.

The simulations are performed in Simulink by using a numerical ordinary differential equation (ODE) solver with automatically variable time step. The ODE solver which has been used for solving the responses of the system is ode45 which is implemented in MATLAB while the maximum size of time step Δt has been set to $2.5 \cdot 10^{-5}$ seconds. While performing simulations, band-limited Gaussian noise has been enabled for considering some factors related to physical measurement and control setup uncertainties. Gravity of the system is also enabled for the simulations in order to include the effects due to the weight of the system components on the studied dynamical responses.

Other factors such as sensor runout and non-collocation have not been included to the simulations however since at the current stage the model of the controller is not capable to handle these measurement error sources. Therefore, during the following simulation runs it is required to assume for instance that the system has collocated AMB/sensor pairs. This assumption creates however only a small difference to the studied responses compared to the case if the control model which could handle non-collocation would be used for simulations. Thus, the made simplification is justifiable which is also supported by enabling Gaussian noise for the model.

The measured radial displacements of MMW rotor when the system is excited with the permissible unbalances according to Table 8 are shown in Figure 36. In main figure, the vertical axis represents the radial displacements of MMW rotor which are measured in millimeters whereas the horizontal axis shows the simulated time interval in seconds. The radial displacements have been measured in both *x*- and *y*-coordinates of the radial AMBs.

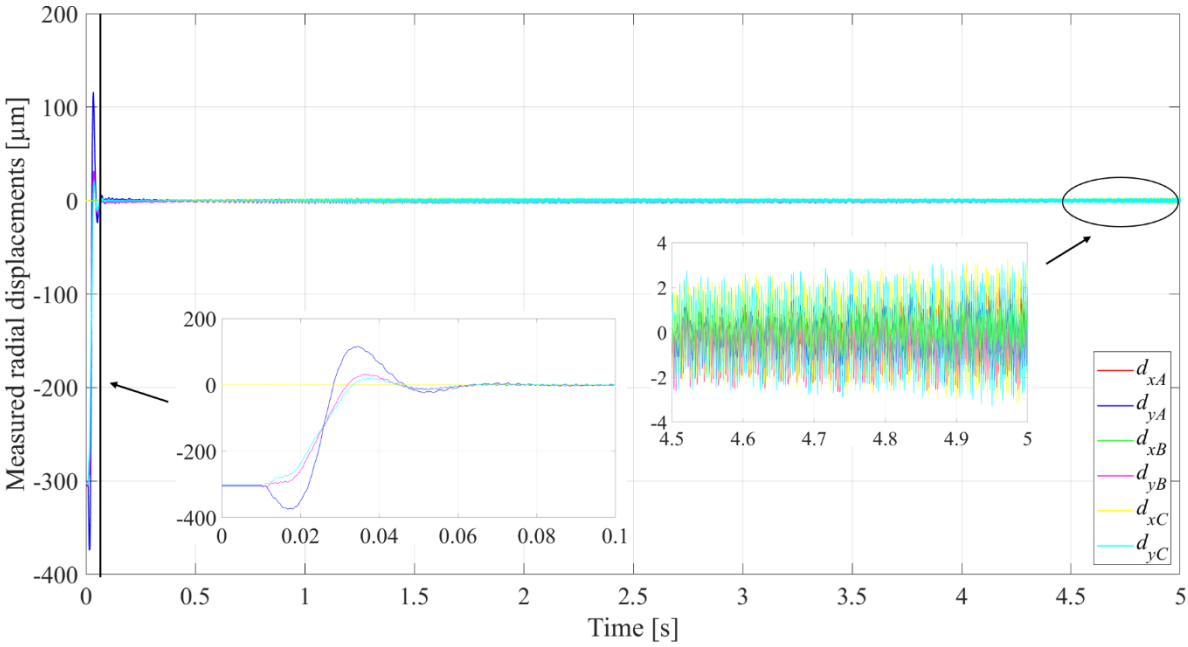

Figure 36. Measured radial displacements of MMW rotor at the bearing locations when the system has been excited with the defined permissible unbalances.

The responses of measured force-currents of radial AMBs are shown instead in Figure 37 in which the vertical axis represents the values of the measured currents in amperes. As with the case of harmonic radial displacements response plot, the horizontal axis is designated to

simulation time. All the currents in x- and y-directions have been measured from the two opposed actuators in each bearing. From Figure 37 it can also be verified that bearing B of which current values are approximately zero during the whole simulation does not participate in keeping MUSK drivetrain stable as has been dictated earlier.

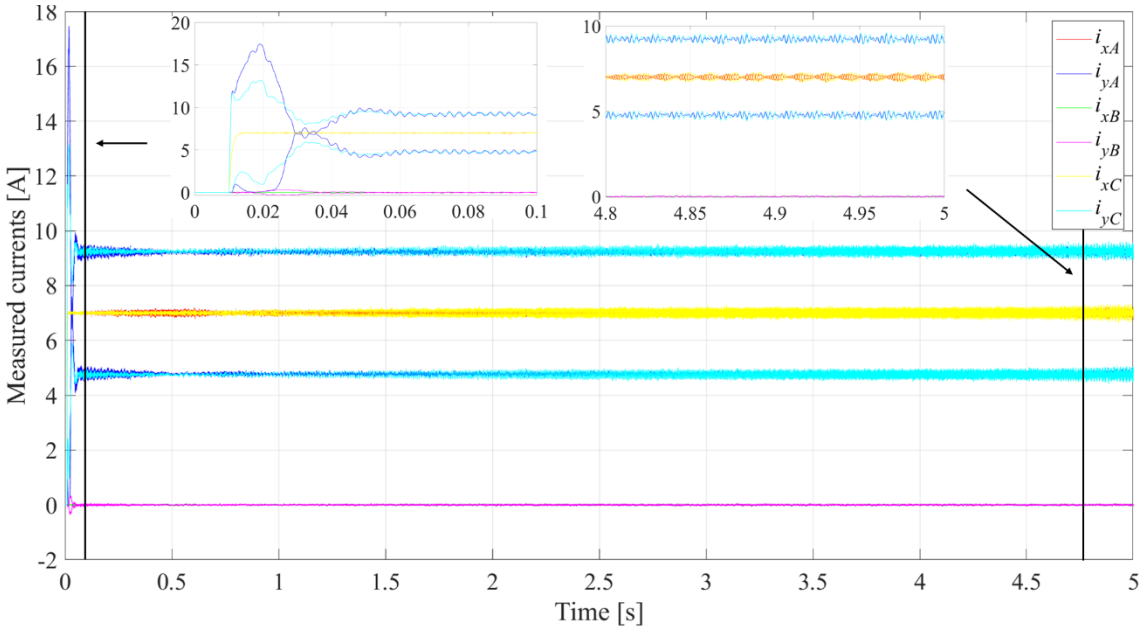

Figure 37. Measured force-currents of radial AMBs when the system has been excited with the defined permissible unbalances.

By looking at Figures 36 and 37, it is visible that the system can handle the earlier defined permissible unbalances by using the implemented compensation method. At time t = 0 s, MMW rotor is initially resting at the safety bearings since the measured initial displacement at the location of each vertical sensor plane is approximately d = 0.3 mm as is shown in Figure 36. When the radial AMBs are activated at t = 0.01 s, MMW rotor gets to be lifted up. But as can be seen from Figure 36, the rotor is not lifted straightforward but as tilted since the displacement of MMW rotor which is measured by sensor A in the negative y-axis direction is lower compared to the measurements from the other sensors.

This causes the rotor to collide with the safety bearing at the plane location of bearing A. The collision event can be seen as a vibration peak in the related displacement response while the same event also reflects to the measured currents of the AMBs at the beginning of

the simulation. The current of bearing A measured in *y*-axis direction especially increases significantly during this event to compensate the excitation due to collision. The controller of the radial AMBs is however capable to stabilize the system soon after the collision event has occurred while keeping the system stable for the rest of the simulation. The noise which is visible in both responses is due to simulated possible noise sources.

The response of radial displacements of MMW rotor and the bearing currents are next studied by using the larger unbalance distribution which has been defined in Table 8 while other simulation parameters are kept same as during the earlier simulation test. The measured radial displacements of MMW which have been obtained with the newly set balancing quality grades are shown in Figure 38 while the current responses of radial AMBs can be observed from Figure 39.

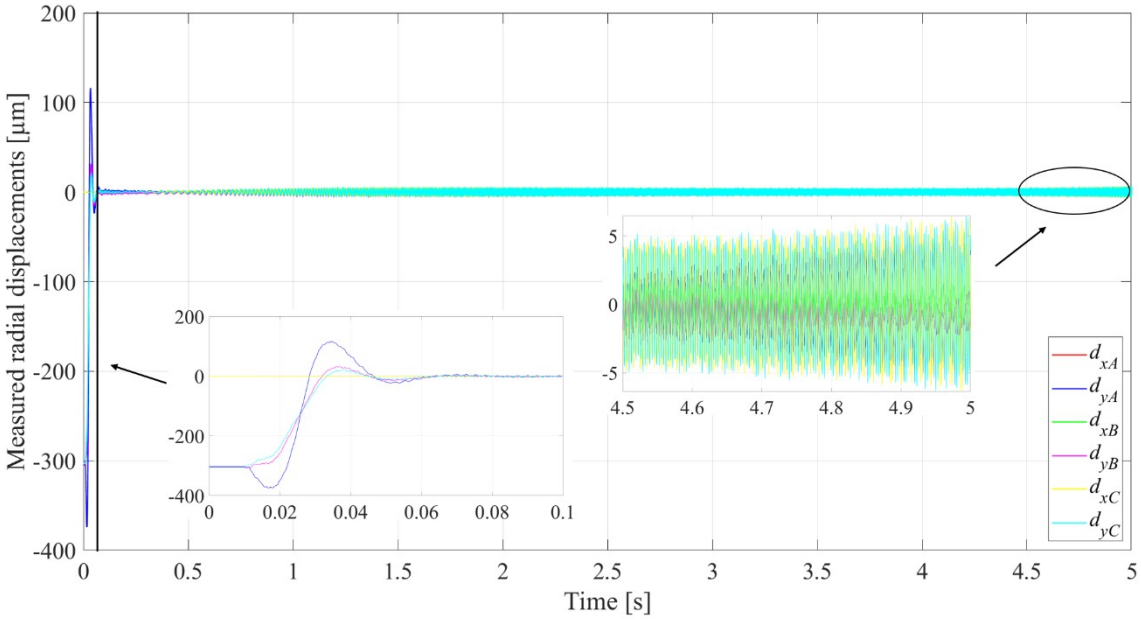

Figure 38. Measured radial displacements of MMW at the bearing locations with higher balancing grades: G6.3 for MMW and G2.5 for Rotatek.

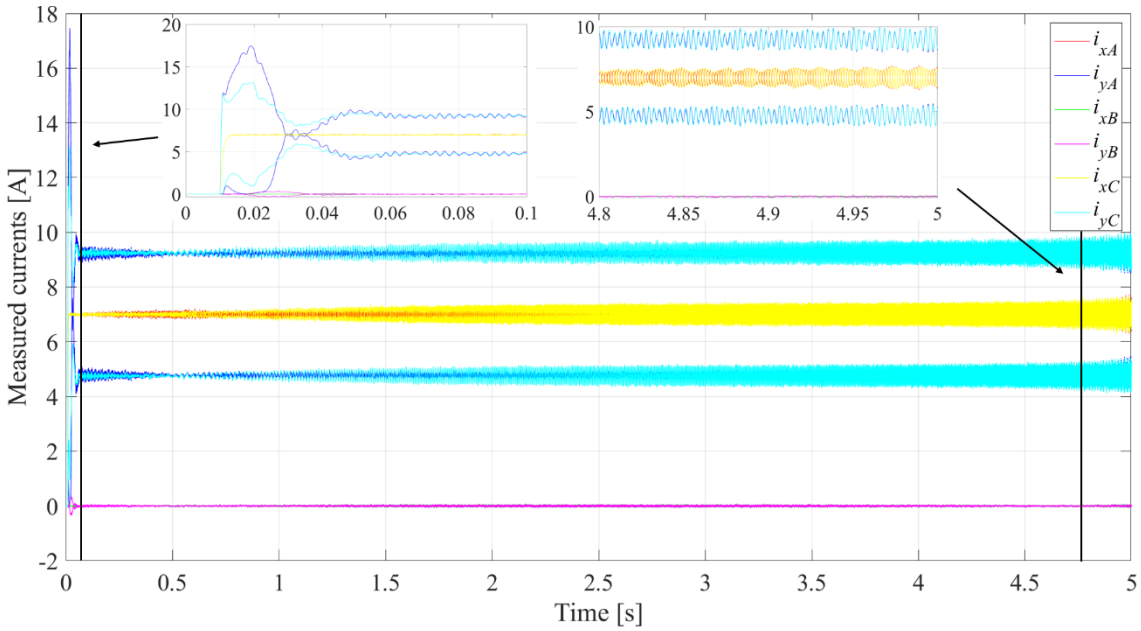

Figure 39. Measured force-currents of radial AMBs with higher balancing grades: G6.3 for MMW and G2.5 for Rotatek.

As can be seen from the measured response curves, the responses are changed only a little when higher residual unbalances have been placed on MMW rotor and Rotatek machine. In both figures, the responses are a bit higher which is expected since the system is subjected to higher unbalance excitation forces while the system is rotating. During the lift-off phase, larger unbalance distribution does not have much of an effect to the measured displacements since the system is mainly levitating with low rotation speed. It is also noticeable that radial AMBs provide efficient damping even though the system has more residual unbalance on it since the current variation is kept small.

Because of these observations, it can be concluded that the system is capable to adapt to uncertain conditions to some extent when the system is excited only with unbalance forces. This also verifies that the traditional method of using balancing quality grades for the application which is supported by AMBs is too strict. The method is commonly more suited for applications which are supported with conventional bearings such as journal or roller bearings.

To test the system robustness even further, additional test in which the operation of bearing A is disturbed by a step disturbance force at time t = 4 s is performed. The purpose of this

test is to evaluate if the system is capable to recover from a sudden disturbance which is applied to bearing A in positive *y*-direction while simultaneously the system is excited with unbalance forces at higher operation speeds. It is likely, that the source reason for this type of disturbance to occur could be related for example to gyroscopic forces, impulse force which is transferred through the base of the system or an impact force due to a debris particle collision. All these forces have potentiality to deviate the rotor from its stable position suddenly. For simulating this type of test case, the magnitude of disturbance force is set to 20 % of the maximum load capacity of the radial AMB while at time t = 4 s, the operation speed of MMW rotor is measured to be 8000 rpm. The resulted radial displacement response and the response of the bearing currents of MMW in this test case are shown in Figures 40 and 41 from which it is visible that the induced step disturbance event is affecting to both displacement and current responses at t = 4 s and also at t = 4.5 s.

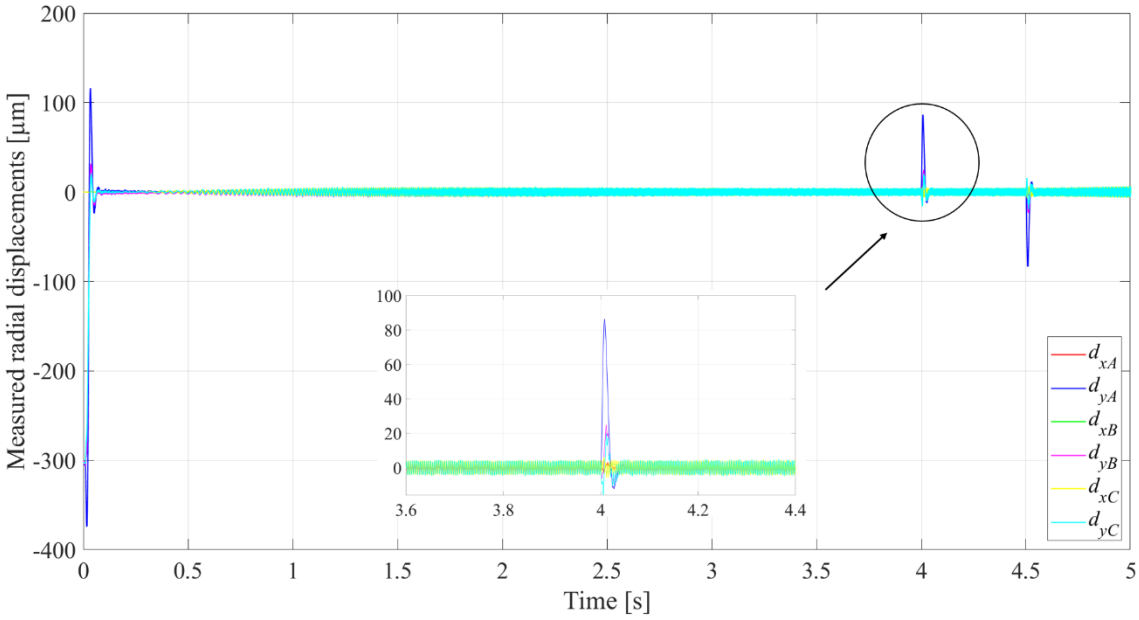

Figure 40. Measured radial displacements of MMW at the bearing locations with higher balancing grades and when a sudden step disturbance has been applied to bearing A in *y*-direction at t = 4.0 s.

In Figure 40, the measured radial displacement of bearing A in *y*-direction is increased approximately to the magnitude level of 85 µm because of the sudden disturbance. Based on the vibration zone limits shown in Table 2, this is however sufficient since the system can be considered to belong to zone limit A/B. This gives a value of 90 µm for the maximum allowed displacement D_{max} when the safety bearing clearance is 300 µm. Thus, the maximum

displacement in this case complies with the earlier mentioned limit: $D_{max} < 0.3C_{min}$, for a newly commissioned machine. After the step disturbance is eliminated at $t = 4.5$ s, the system is stabilized and operates smoothly to the end of the simulation.

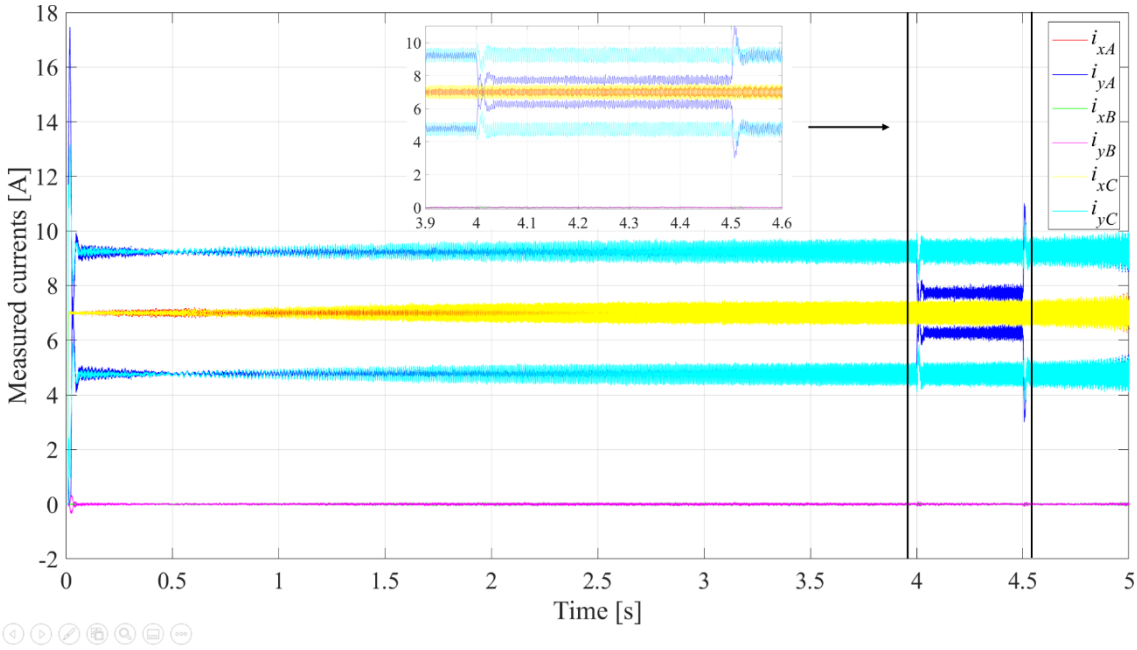

Figure 41. Measured force-currents with higher balancing grades and when a sudden step disturbance has been applied to bearing A in y-direction at $t = 4.0$ s.

Regarding the measured currents responses of bearing A, it can be seen that the related currents in y-direction are trying to keep the system stable while the induced disturbance is present at the system. This can be recognized as an increased activity in the corresponding responses in Figure 41 in which the activity period lasts 4 s – 4.5 s. During this activity period, the current of the actuator of bearing A which is responsible for lifting the rotor upwards is decreased while the current of the opposed actuator is increased. This occurs in order to compensate the sudden lifting force which tries to disturb the system. The opposite situation is occurring at $t = 4.5$ s when the disturbance is eliminated.

4.4 Case 2: With unbalance and misalignment

In this second subcase, the study is focused on whether a misalignment defect is possibly more critical for the investigated system than an unbalance defect. This study concern comes from the possibility, that the AMBs might not offer the same kind of adaptability to misalignment than with the case of unbalances. For this purpose, both parallel and angular

misalignments are imposed to the system while the unbalances and their parameters are kept the same as in the earlier subcase. Other simulation parameters which have been mentioned earlier have also not been varied for the following tests. The performed simulations are started with imposing a parallel misalignment defect with a magnitude of $\Delta y = 0.5$ mm at the coupling point between RENK and Rotatek in positive y-direction. The obtained radial displacement of MMW rotor and the bearing current responses from this test case are shown in Figure 42 and Figure 43, respectively.

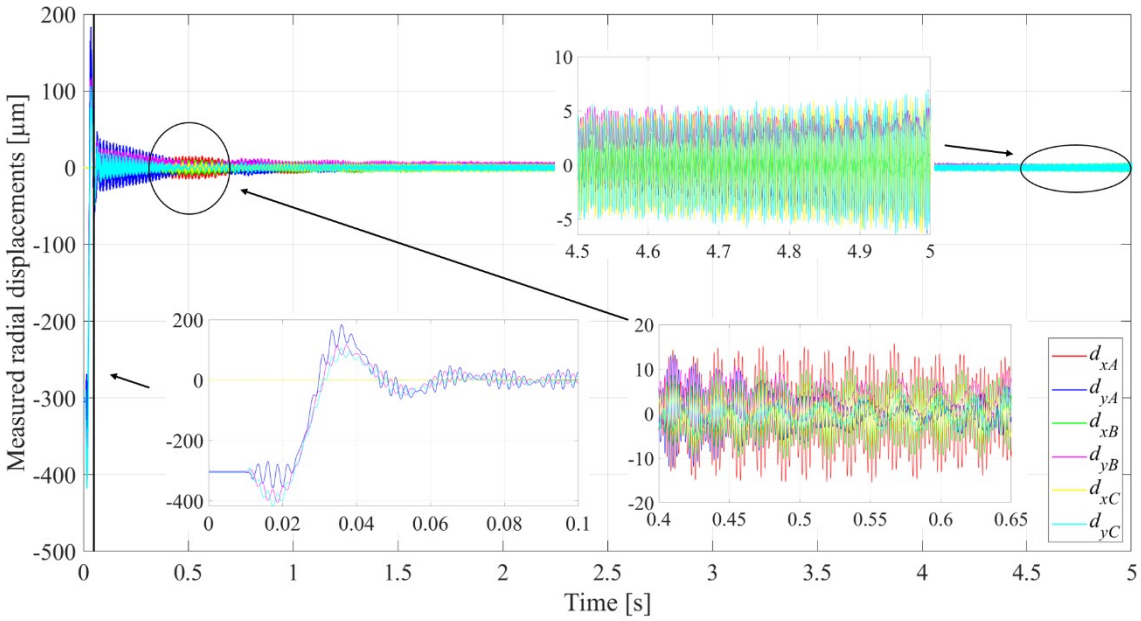

Figure 42. Measured radial displacements of MMW rotor at the bearing locations with the same higher residual unbalances imposed on MMW and Rotatek as during the earlier subcase while also the system has a parallel misalignment with a magnitude of $\Delta y = 0.5$ mm in the positive y-axis.

From Figure 42, it can be observed that the parallel misalignment between RENK-coupling and Rotatek machine causes MMW rotor to experience higher displacements near to the locations of bearing A and C compared to the earlier cases when the system has only been unbalanced. The rotor also experiences higher vibration at the direction of x-axis which has not been that visible only with the unbalance excitations. The collision between the rotor and its safety bearings is also more severe during the lift-off phase because of the imposed misalignment. Due to instability caused by the misalignment, it takes a longer time for the radial AMBs to stabilize MMW rotor than if the system would have only been excited with the forces created by the residual unbalances. Otherwise, the radial displacement responses

of MMW rotor measured by the three sensors are similar than with the earlier cases in which the parallel misalignment has not been present at the system.

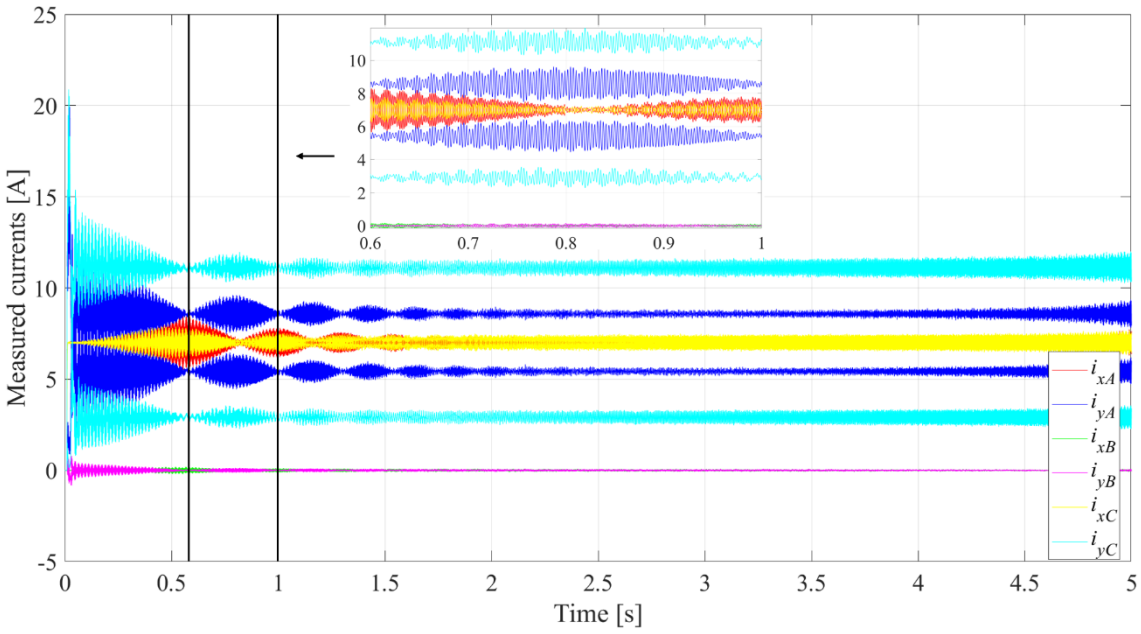

Figure 43. Measured force-currents of radial AMBs with the same higher residual unbalances imposed on MMW and Rotatek as during the earlier subcase while also the system has a parallel misalignment with a magnitude of $\Delta y = 0.5$ in the positive y-axis.

In Figure 43, a beating phenomenon can be seen occurring in the measured responses of the currents of the radial AMBs. The likely primary reason for this is the total effect of misalignment and unbalance excitations which is causing different components in the system to vibrate. Since the components are oscillating at different frequencies, this causes constructive and destructive wave interference which can be seen as a pulsation in the measured current responses due to vibration compensation by the radial AMBs. This phenomenon is also visible in the measured reaction force responses of the bearings which are shown in Figure 44. The force responses of bearing B are zero during investigated time period since bearing B is not active.

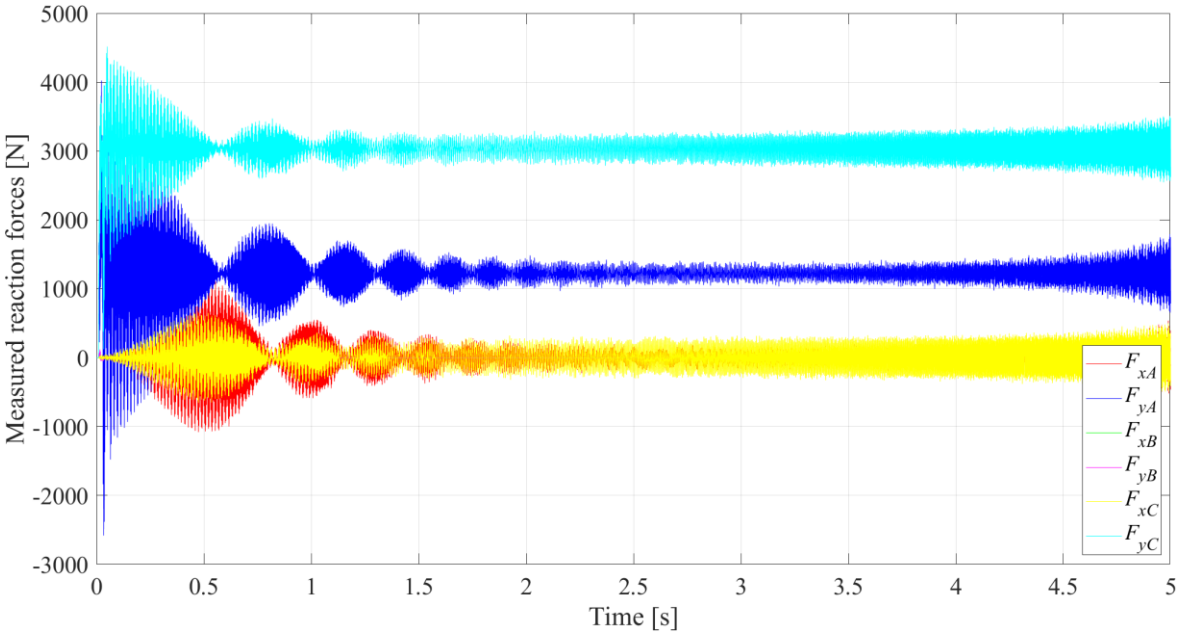

Figure 44. Measured reaction forces of radial AMBs with the same higher residual unbalances imposed on MMW and Rotatek as during the earlier subcase while also the system has a parallel misalignment with a magnitude of $\Delta y = 0.5$ in the positive y-axis.

While studying Figure 44, it is clearly seen that the measured radial force produced by bearing C in y-direction has the highest response of all the measured forces during the investigated time period. This is because bearing C is the one which is closest to the location of misalignment and thus has to be mainly responsible for keeping the drivetrain aligned. That is why bearing C has to produce forces with higher magnitudes compared to the other radial bearings. The load capacity of the bearing is not however over-reached since the magnitude of the reaction force is most of the time withing the range of 3000 - 4000 N. During the collision with the safety bearing, the measured reaction forces are however higher than 4000 N, but this lasts only for a brief time period and does not cause larger issues.

It is possible that the system can have an angular misalignment fault in addition to a parallel misalignment. Therefore, the next logical step is to test how the system behaves with a combined misalignment fault while the system is simultaneously dynamically unbalanced. To perform this test, the value of parallel misalignment is kept same as during the previous test but now additionally an angular misalignment which has a magnitude of $\beta = +\ 0.1°$ is imposed to the coupling point around the x-axis of the system. The measured radial displacements of MMW in this test case are shown in Figure 45.

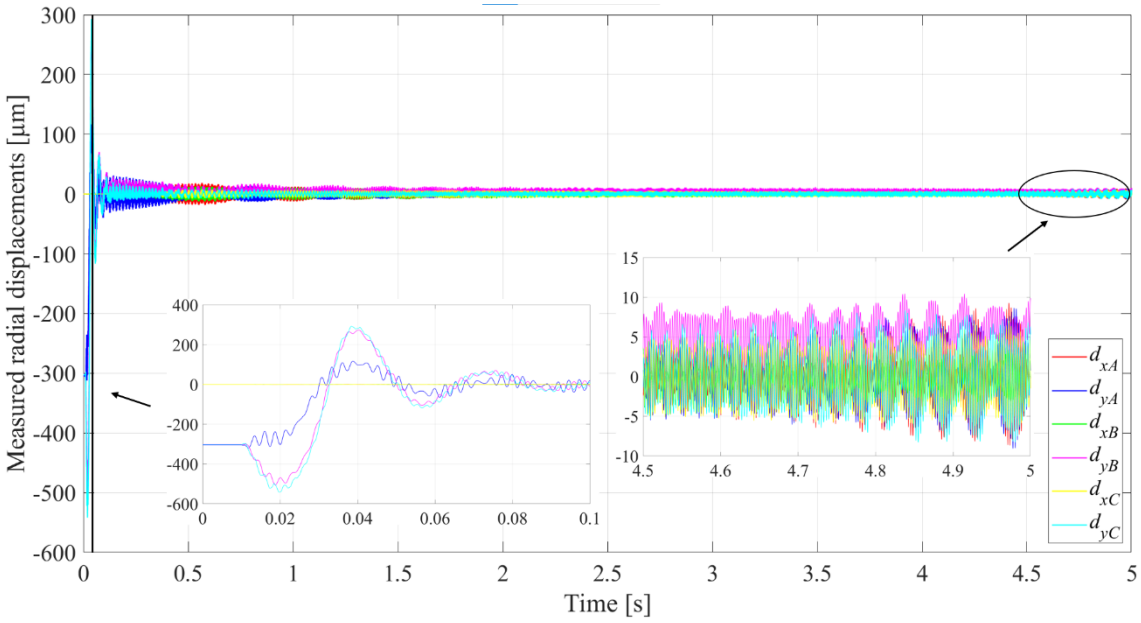

Figure 45. Measured radial displacements of MMW rotor at the bearing locations with the same higher residual unbalances imposed on MMW and Rotatek as during the earlier subcase. The system also has a combined misalignment which consists of parallel misalignment with a magnitude of Δy = 0.5 mm in the positive y-axis and an angular misalignment with a magnitude of β = + 0.1° around the system's x-axis.

From Figure 45, it can be noticed that MMW rotor has quite severe displacement peaks at the location of bearing C during the lift-off phase when the system has combined misalignment. Firstly, at this location, the rotor is colliding with its safety bearing while pushing the bearing more than 0.2 mm along the negative y-axis direction after which the rotor also contacts with the upper inner race of the bearing. Although the displacements are small in reality, in practice however the rubbing can still cause a fatigue to the safety bearing and also to the rotor itself which decreases the overall service-life of both components. If the safety bearing fails, in the worst case scenario this could then also lead to other system failures such as AMB failure as well because of the physical contact which the rotor takes with the stator. Therefore, it should be ensured that the vertical displacements of bearing C should be minimized during the lift-off phase.

The combined misalignment also compels bearing A and C to apply almost the maximum lift force on MMW during its lift-off which is seen from the measured current and force responses in Figure 46 and Figure 47. The response values are especially close to over-reach the performance capabilities of bearing C during this phase of the simulation. This is severe

since by almost reaching the load capacity of the bearing, it could lead to unstable condition from which the system may not recover. After the lift-off phase has ended, the currents and forces are stabilizing. The upper actuator of bearing C still draws however more current from the amplifier compared to other bearings to the end of the simulation. This is due to attempt of the bearing to keep the rest of the drivetrain aligned with the misaligned end at the proximity of Rotatek machine.

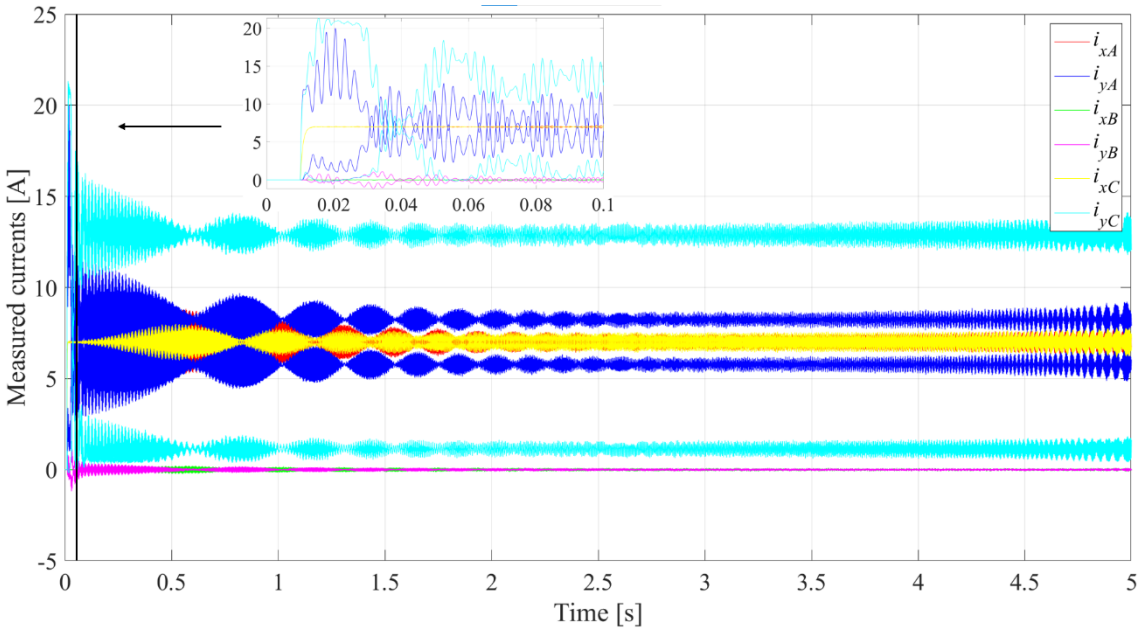

Figure 46. Measured force currents of radial AMBs with the same higher residual unbalances imposed on MMW and Rotatek as during the earlier subcase. The system also has a combined misalignment which consists of parallel misalignment with a magnitude of $\Delta y = 0.5$ mm in the positive y-axis and an angular misalignment with a magnitude of $\beta = +0.1°$ around the system's x-axis.

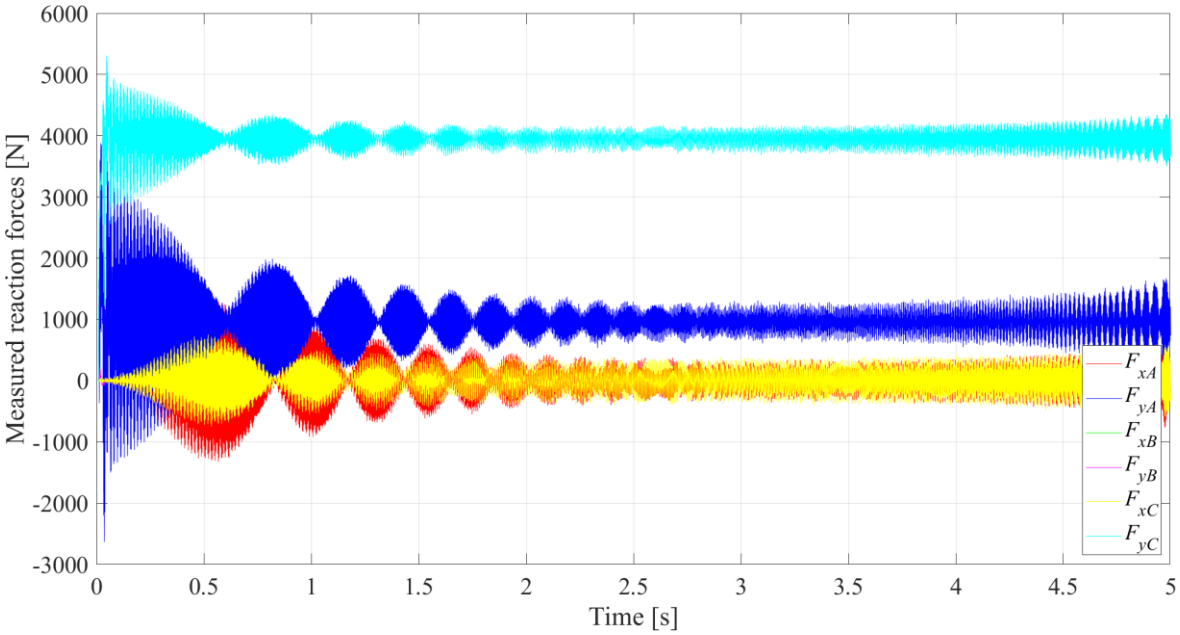

Figure 47. Measured reaction forces of radial AMBs with the same higher residual unbalances imposed on MMW and Rotatek as during the earlier subcase. The system also has a combined misalignment which consists of parallel misalignment with a magnitude of $\Delta y = 0.5$ mm in the positive y-axis and an angular misalignment with a magnitude of $\beta = +0.1°$ around the system's x-axis.

Overall, based on the simulated test cases where the misalignment has also been added to the system it can be pointed out that the effect of a misalignment fault to the measured responses of the system in time domain is more critical than the effect of an unbalance fault. Increasing the amount of unbalance in the system have not had as much of an effect to the measured responses as has been shown. But by adding different types of misalignments with small magnitudes to the coupling point between RENK-coupling and Rotatek machine, the responses have become evidently worse. This means that at least withing the current operation range of the system, the supporting radial AMBs are not as adaptable to the changing conditions caused by a misalignment fault than by an unbalance fault. Most of the undesired effect due to misalignment have seen to be occurring during the lift-off phase while the controller is capable to stabilize the system for the following operation phases. The lift-off phase is however one of the crucial phases during the operation cycle of the system, since if the system does not operate at stable condition when MMW is lifted, the probability for the system to operate safely after the lift-off also decreases. Stability of the drivetrain during the lift-off is also critical from the aspect of service-life of separate components in the system especially of the installed safety bearings.

5 DISCUSSION ABOUT THE RESULTS

The accuracy of the simulations results are highly dependent on the accuracy level of the simulation model. Therefore, the simulation results in this work have been obtained with the existing model of which validity level has been checked during former studies. To ensure that reliable simulation results can be obtained, the dynamical behavior of the system has been simulated by using the same steps as has been done before. The sensitivity aspects have also been dealt with by using a time step with proper size for the ODE solver which has been responsible for solving the dynamic responses of the studied system.

Still, the simulation results need to be verified by performing similar tests at the lab in order to verify the true validity level of the results. It is recommended while performing physical tests to add artificial defects to the system gradually as has been done during the simulation runs. After it has been ensured that the system can handle those defects which are first imposed to it then additional defects could be introduced. This would be the safest approach to test the system's robustness.

For ensuring reliable and valid measurements which can be compared with the simulation results, multiple measurements should be taken to eliminate any factors which could possibly distort the results. If the real measurements are deviating from the simulation results, then the reason for this deviation needs to be investigated. If the reason can be traced to some inaccuracies in the simulation model it is required to update the model after which the same simulations should be reperformed.

By using a collocated simulation model while performing simulations it acts as one possible source which can cause a difference between the simulation results and the measured results. This is due to the fact that the real system has non-collocated AMB/sensor pairs. Since non-collocation affects to the stability of the system it may also have an effect on the investigated responses. In reality, the surface quality of the rotor may also not be ideal but instead the surface could have some dirt, scratches, roughness, or some other deficiency on it. This could introduce some additional noise to the displacement sensor which would disturb the controller from keeping the system stable. The current control model has not however been

at that readiness level yet that it could handle non-collocation or sensor runout which is why it has been necessary to rely on a simpler model. Thus, to improve the validity of the results it is advised to introduce non-collocation and sensor runout factors to the simulation model for future simulations when the control model has been updated.

For future work, one aspect which should be studied is how the measured responses would change if unbalance would be more widely distributed along the drivetrain. Currently, unbalance is concentrated only at specific locations on the simulation model. This does not reflect the real system however that well since in reality unbalance would be distributed more unevenly with different magnitudes and phase values. One approach to make the model more realistic is to place different unbalances at several nodes in each mechanical component of the drivetrain.

Currently, the operation range of the machine is limited because of the flexible coupling. If at some point it is decided to extend this range by making new design iterations for the coupling, it should also be considered to use more precise automatic balancing method. The possible need for more precise unbalance compensation method arises from the fact that by increasing the operation range, the machine is also subjected to higher excitation forces which is influenced by residual unbalances in the system and because of the exponential relation between the magnitude of unbalance excitation and the rotation speed of the machine.

The current compensation solution might not be adequate in maintaining vibration at the suitable safety limit while the machine is operating at higher operation speeds than has been studied during this study. One solution is to design a general notch filter which can be used for compensating unbalance vibration at higher speeds. For this purpose, one can start the design process by using second order equation (3.10) which is suitable for designing notch filters to be implemented with the controller to keep vibration within appropriate limits.

For observing what are the main frequencies at which the drivetrain is oscillating when its rotation speed is changing as a function of time, a waterfall analysis could be applied in future studies. This analysis would provide useful information about the dominating frequencies at each rotation speed of the system. Based on the nature of observed frequency

distribution, it would be then possible to decide suitable design actions for developing the system further.

Other defects like rotor eccentricity and misalignment of AMBs have not been tested in this work because of the controller model not being able to handle these yet at this stage. After the model has been updated these deficiencies should also be tested because they might be present in the studied rotor drivetrain. To study how the responses of the system change due to the effect of misalignment between the supporting AMBs and MMW rotor, the force equation (2.27) which has been presented during section 2 can be implemented to the simulation model. Since it has been demonstrated that MMW rotor collides with the safety bearings during the lift-off, it is required to model and study more carefully how large contact forces are formed during this event and how they are affecting to the system's overall reliability and service-life.

After the design process of a controller which could also control bearing B has finalized, it could be studied if any benefits can be acquired related to the responses due to coupling misalignment. It is possible that the third controlled AMB could assist bearing C to align the drivetrain which would allow to obtain better responses during the lift-off. Different arrangement regarding the location of the bearings may also have a positive effect to the responses. Therefore, it is also worth to investigate if more optimal location can be found for some bearing.

The research which has been made during this thesis work contributes to provide information on how AMBs can be harnessed for performing ACM for the high-speed rotating machines. This has been done by studying optimal performance of a chosen sustainable machine of which rotor has been supported by radial AMBs. In addition to the provided supporting action, the machine's condition has also been monitored and attempted to kept stable by the radial AMBs in real time while its operation has been disturbed by excitations due to unbalances and misalignment faults. Based on the studied responses of the system, the most severe fault of the two fault types has been identified for this specific system. Some insight to which operation cycle of the machine is critical from the aspect of the prolonged system reliability has also been acquired.

The collected research results are also contributing positively to the development stage of the investigated machine. The main observations of this research can be used specifically for designing and developing the studied machine to operate even more optimally in the future. One application area in which the results can be used is to validate the complete simulation model of the investigated machine. The main benefit of this complete simulation model called as Digital Twin of the physical system is that it provides a safe and accurate virtual design and testing environment. This reduces the possible risks that are normally related to design processes. The Digital Twin is also suitable for providing remote access to monitor the performance of the machine predicatively after it has been commissioned to the operation site which decreases maintenance personnel and equipment transportation costs.

From the society point of view, this research is contributing to the global issue of diminishing natural resources by being involved in the design process of energy-efficient machines. Since AMBs do not require lubrication the machines which utilize these devices have also an environmental value. Also, the growing interest and demand for more sustainability-oriented machines have created commercial value for the applications such as one studied in this research. This on the other hand has a cumulative impact by raising a common research interest towards sustainability-oriented machines by other scientists and R&D departments of industrial companies. By including the process of how to utilize AMBs as tools in ACM of the high-speed applications to this work, it is hoped that it would advance ACM becoming a new norm in condition monitoring of such machines.

6 FINAL CONCLUSIONS

In this thesis work, the main source reasons why vibration can occur in AMB-rotor systems have been studied. It has been found that most probable causes are related to residual unbalances and misalignment faults of which there exist different varieties. The main focus of this work has been on dynamic unbalance and coupling misalignment faults which both of them can be present in a studied application and subject it to excessive vibration.

To compensate vibration in AMB supported rotors, different control algorithms can be utilized. When only rigid rotors are considered, a simple PID controller is sufficient. For flexible rotors however, a more sophisticated controller is needed because of more complex dynamics related to these types of rotors. A more sophisticated controller is also capable to handle general uncertainties and external/internal noises to some extent which allows the controller to keep the levitated rotor stable even though these factors may be present. But because of the complex abstract level which is required to understand the working principle of these types of controllers, PID controllers are more commonly used in commercial applications. Adaptable controllers provide however a better reliability and robustness for applied system which is why the research revolving around these types of controllers should be continued. Additional unbalance control methods can also be used specifically to compensate unbalance excitations.

During the case-study section of this work, robustness level of the selected flexible AMB-supported rotor drivetrain system (MUSK) has been studied against unbalance and coupling misalignment faults through time domain simulations. The study has been performed by using the simulation model of the physical counterpart to which unbalance and misalignment faults have been imposed virtually by utilizing Simulink testing environment. To study severity of different faults, the mentioned faults have been introduced to the system gradually. Residual unbalances have been first imposed to the system after which it has been analyzed what kind of system dynamic responses are caused due to this defect. Then, the research focus has been shifted to the investigation of the dynamic responses of the system due to combination of unbalance and misalignment faults.

Based on the obtained results, it can be concluded that the system is capable to adapt to changing unbalance conditions within the studied operation range 0 rpm – 10 000 rpm. This is achieved by the implemented control methods and by the capabilities of radial AMBs which are supporting driving MMW rotor. It has been evidenced that a misalignment fault is more severe in the investigated AMB-supported rotor drivetrain than an unbalance fault. This is most evident during the lift-off phase which is one of the critical phases of the system. The magnitude of misalignment is critical during this phase since the severity level of the collision between MMW rotor and the safety bearings is highly dependent on how largely the drivetrain is misaligned. It is noteworthy however that the control is capable to stabilize the system after the lift-off phase regardless of whether the system is unbalanced, misaligned or both.

Since the lift-off phase has been recognized to be critical operation phase of the drivetrain, it should be ensured that the controller is capable to compensate vibration due to misalignment. However, it should not be solely dependent on the controller's performance to handle the mentioned defect because the controller has also its own limitations. This is true even if the controller is capable to handle uncertainties to some extent. Additionally, the radial AMBs also have their own physical limitations. Therefore, one should foremost take care of to minimize all different factors which could lead the system to have misalignment in the first place. This would also help in minimizing the total measured vibration level in the system.

For example, RENK-coupling which is used for connecting MMW rotor with a driven machine can act as one source which could cause the rotor drivetrain to become misaligned. Coupling misalignment can also lead to other possible deficiencies such as rotor eccentricity which itself on the other hand can cause UMP to occur. This causes the system to experience more excessive vibration which decreases the service-life of the machine while also increases its life-cycle costs. Because of the flexible modes of the coupling which have frequencies that are included in the operation range of the drivetrain, the whole system is also flexible and for this reason is susceptible to severe vibration. Thus, it is recommended to consider if the coupling is really needed and if it could be possibly removed from the system. Alternatively, a more robust coupling solution is required to be invented for improving the overall reliability of the whole drivetrain.

LIST OF REFERENCES

Adams Jr., M. L. 2007. Rotor Balancing and Unbalance-Caused Vibration. In: Crocker, M. J. (editor). Handbook of Noise and Vibration Control. 1st edition. Hoboken, New Jersey. 2007. John Wiley & Sons Inc. Pp. 753-760.

API STD 617. 2002. Axial and Centrifugal Compressors and Expander-compressors for Petroleum, Chemical and Gas Industry. 7th. edition. Washington D.C: American Petroleum Institute. 234 p.

Behera, D. P., Behera, R. & Naikan, V. N. A. 2014. Virtual Fault Simulation for Diagnosis of Shaft Misalignment of Rotating Machine. 2014 International Conference on Advances in Computing, Communications and Informatics (ICACCI). Delhi, India. 24-27 Sept. 2014. IEEE. P. 2476-2480.

Bloch, H. P. & Geitner, F. K. 2019. Machinery Component Maintenance and Repair. Vol. 3, 4th. edition. Elsevier. 668 p.

Bouaziz, A., Bouaziz, S., Hentati, T., Cholley, J. Y. & Haddar, M. 2015. Vibrations monitoring of high speed spindle with AMBs in presence of defects. International Journal of Applied Electromagnetics and Mechanics, Vol. 49. IOS Press. Pp. 207-221.

Chiba, A., Fukao, T., Ichikawa, O., Oshima, M., Takemoto, M. & Dorrell, D. 2005. Magnetic Bearings and Bearingless Drives. 1st edition. Amsterdam, Netherlands. Newnes. 400 p.

Corne, B., Knockaert, J. & Desmet, J. 2017. Misalignment and Unbalance Fault Severity Estimation Using Stator Current Measurements. Proceedings of the 2017 IEEE 11th International Symposium on Diagnostics for Electrical Machines, Power Electronics and Drives (SDEMPED 2017). Tinos, Greece. 29 Aug.-1 Sept. 2017. IEEE. P. 247-253.

Darbandi, S. M., Habibollahi, A., Behzad, M., Salarieh, H. & Mehdigholi, H. 2016. Sensor runout compensation in active magnetic bearings via an integral adaptive observer. Control Engineering Practice, Vol. 48. Elsevier. Pp. 111-118.

Desouki, M., Sassi, S., Renno, J. & Gowid, S. A. 2020. Dynamic Response of a Rotating Assembly under the Coupled Effects of Misalignment and Imbalance. Shock and Vibration, Vol. 2020. Hindawi. Pp. 1-26.

Diouf, P. & Herbet, W. 2014. Understanding Rotor Balance for Electric Motors. Conference Record of 2014 Annual Pulp and Paper Industry Technical Conference. Atlanta, GA, USA. 22-26 June 2014. IEEE. P. 7-17.

Donát, M., 2012. Computational Modelling of the Unbalanced Magnetic Pull by Finite Element Method. Procedia Engineering, Vol. 48. Elsevier. Pp. 83-89.

Gerada, D., Mebarki, A., Brown, N. L., Gerada, C., Cavagnino, A. & Boglietti, A. 2014. High-Speed Electrical Machines: Technologies, Trends, and Developments. Transactions on Industrial Electronics, Vol. 61, No. 6. IEEE. Pp. 2946–2959.

Halminen, O., Kärkkäinen, A., Sopanen, J. & Mikkola, A. 2015. Active magnetic bearing-supported rotor with misaligned cageless backup bearings: A dropdown event simulation model. Mechanical Systems and Signal Processing, Vol. 50-51. Elsevier. Pp. 692-705.

Huang, T., Zheng, M. & Zhang, G. 2019. A Review of Active Magnetic Bearing Control Theory. The 31th Chinese Control and Decision Conference (2019 CCDC). Nanchang, India. 3-5 June 2019. IEEE. P. 2888-2893. [Referred 25.10.2020]. Available in PDF-file: https://ieeexplore.ieee.org/abstract/document/8833062. Requires a password.

Jastrzebski, R., Kurvinen, E. & Pyrhönen, O. 2019. Design, Modelling and Control of MIMO AMB System with 3 Radial Bearing Planes for Megawatt-Range High-Speed Rotor. 2019 IEEE International Electric Machines and Drives Conference. San Diego, California, United States. 12–15 May 2019. IEMDC 2019. P. 805–811.

Kim, H., Sikanen, E., Nerg, J., Sillanpää, T. & Sopanen, J. T. 2020. Unbalanced Magnetic Pull Effects on Rotordynamics of a High-Speed Induction Generator Supported by Active Magnetic Bearings – Analysis and Experimental Verification. IEEE Access, Vol. 8. IEEE. Pp. 212361-212370.

Kulesza, Z. 2015. Virtual collocation method for a flexible rotor supported by active magnetic bearings. Journal of Vibration and Control, Vol. 21, No. 8. SAGE Publications Inc. Pp. 1522-1538.

Kumar, B. K., Diwakar, D. & Satyanarayna, M. R. S. 2012. Determination of Unbalance in Rotating Machine Using Vibration Signature Analysis. International Journal of Modern Engineering Research, Vol. 2, No. 5. IJMER. Pp. 3415-3421. [Referred 26.01.2021]. Available in PDF-file: http://www.ijmer.com/papers/Vol2_Issue5/BT2534153421.pdf.

Kumar, P. & Tiwari, R. 2020. Development of a Novel Approach for Quantitative Estimation of Rotor Unbalance and Misalignment in a Rotor System Levitated by Active Magnetic Bearings. Iranian Journal of Science and Technology, Transactions of Mechanical Engineering. Springer. Pp. 1-18.

Kumar, P. & Tiwari, R. 2021. Dynamic Response Analysis of an Unbalanced and Misaligned Rotor Supported on Active Magnetic Bearings and Touchdown Bearings. Proceedings of the 6th National Symposium on Rotor Dynamics. Springer. Pp. 407-418.

Kuppa, S. K. & Lal, M. 2019. Dual flexible rotor system with active magnetic bearings for unbalance and misalignment faults analysis. Sadhana – Academy Proceedings in Engineering Sciences, Vol. 44, No. 8. Springer. Pp. 1-16.

Kärkkäinen, A. 2007. Dynamic simulations of rotors during drop on retainer bearings. Doctoral Thesis. Lappeenranta-Lahti University of Technology. 91 p. + appendixes 4 p.

Lijesh, K.P. & Hirani, H. 2015. A Comparative Study on Shaft Alignment Systems (SAS). International Journal of Current Engineering and Technology, Vol. 5., No. 2. InPressco. Pp. 1142-1147. [Referred 09.02.2021]. Available in PDF-file: https://inpressco.com/a-comparative-study-on-shaft-alignment-systems-sas/.

ISO 14839-1. 2002. Mechanical vibration – Vibration of rotating machinery equipped with active magnetic bearings – Part 1: Vocabulary. 1st. edition. Genève: International Organization for Standardization. 30 p.

ISO 14839-2. 2004. Mechanical vibration – Vibration of rotating machinery equipped with active magnetic bearings – Part 2: Evaluation of vibration. 1st. edition. Genève: International Organization for Standardization. 20 p.

ISO 14839-4. 2012. Mechanical vibration – Vibration of rotating machinery equipped with active magnetic bearings – Part 4: Technical guidelines. 1st. edition. Genève: International Organization for Standardization. 41 p.

Liu, Y., Ming, S., Zhao, S., Han, J. & Ma, Y. 2019. Research on Automatic Balance Control of Active Magnetic Bearing-Rigid Rotor System. Shock and Vibration, Vol. 2019. Hindawi. Pp. 1-13.

Mogal, S. P. & Lalwani, D. I. 2015. Experimental investigation of unbalance and misalignment in rotor bearing system using order analysis. Journal of Measurements in Engineering, Vol. 3, No. 4. JVE International Ltd. Pp. 114-122. [Referred 26.01.2021]. Available in PDF-file: https://www.jvejournals.com/article/16117.

Muminovic, A. J., Braut, S., Muminovic, A., Saric, I. & Roncevic, G. S. 2020. Improvement of Flexible Rotor/Active Magnetic Bearings System Performance Using PI-D Controller. Engineering Review, Vol. 40, No. 2. Pp. 112-123. [Referred 24.10.2020]. Available in PDF-file:
https://www.researchgate.net/publication/340350094.

Ozoegwu, C. C., Nwangwu, C. C., Uzoh, C. F. & Ogunoh, A. V. 2012. zPure Analytical Approach to Rotational Balancing. Journal of Safety Engineering, Vol. 1, No. 4. Scientific & Academic Publishing. Pp. 50-56. [Referred 26.01.2021]. Available in PDF-file: https://www.researchgate.net/publication/271101265.

Ran, S., Hu, Y. & Wu, R. 2018. Design, modeling and robust control of the flexible rotor to pass the first bending critical speed with active magnetic bearing. Advances in mechanical engineering, Vol. 10, No. 2. SAGE Publications Inc. Pp. 1-13.

Safa, H. H., Ebrahimi, M., Davoudi, A. & Pouramin, A. 2014. Analytical Derivation of Induction Motors Inductances under Eccentricity Conditions. Progress in Electromagnetics Research B, Vol. 60. PIER. Pp. 95-110.

Saleem, A., Diwakar, G. & Satyanarayana, M.R.S. 2012. Detection of Unbalance in Rotating Machines Using Shaft Deflection Measurement during Its Operation. Journal of Mechanical and Civil Engineering, Vol. 3, No. 3. IOSR Journal. Pp. 8-20. [Referred 26.01.2021]. Available in PDF-file: https://www.researchgate.net/publication/313557404.

Schlensok, C. & Henneberg, G. 2004. Comparison of static, dynamic, and static-dynamic eccentricity in induction machines with squirrel-cage rotors using 2D-transient FEM. The International Journal for Computation and Mathematics in Electrical and Electronic Engineering, Vol. 23, No. 4. Emerald Group Publishing Limited. Pp. 1070-1079.

Schweitzer, G. & Maslen, E. H. 2009. Magnetic Bearings. Theory, Design, and Application to Rotating Machinery. 1st edition. Heidelberg, Berlin. Springer. 535 p.

Scopus. 2021. Scopus document search. Database. [Accessed on 13.05.2021].

SFS-ISO 21940-11. 2017. Mechanical vibration. Rotor balancing. Part 11: Procedures and tolerances for rotors with rigid behaviour. 1st. edition. Helsinki: Finnish Standards Association. 29 p.

Shabaninia, F. & Jafari, K. 2012. Using LQG/LTR Optimal Control Method to Improve Stability and Performance of Industrial Gas Turbine System. ISRN Electronics, Vol. 2012. International Scholarly Research Network. Pp. 1-8.

Skogestad, S. & Postlethwaite, I. Multivariable Feedback Control: Analysis and Design. 2nd edition. Hoboken, New Jersey. Wiley-Interscience. 608 p.

SpinDrive. 2021. Benefits of Active Magnetic Bearing System. [SpindDrive webpage]. [Referred 25.01.2021]. Available: https://spindrive.fi/benefits-of-active-magnetic-bearing-system%E2%80%AF/

Srinivas, R. S., Tiwari, R. & Kannababu, Ch. 2018. Application of Active Magnetic Bearings in Flexible Rotordynamic Systems – A State of the Art Review. Mechanical Systems and Signal Processing, Vol. 106. Elsevier. Pp. 537-572.

Subbiah, R. & Littleton, J., E. 2018. Rotor and Structural Dynamics of Turbomachinery: A Practical Guide for Engineers and Scientists. Applied Condition Monitoring, Vol. 11. Cham, Switzerland. Springer. 289 p.

Tiwari, R. 2018. Rotor Systems: Analysis and Identification. 1st edition. Boca Raton, Florida. CRC Press. 1092 p.

Tiwari, R. & Lal, M. 2012. Multi-fault identification in simple rotor-bearing coupling systems based on forced response measurements. Mechanism and Machine Theory, Vol. 51. Elsevier. Pp. 87-109.

Vaughan, J. 2013. Static and Dynamic Balancing. [Web document]. [Referred 16.03.2021]. Brüel & Kjær. 2nd edition. 20 p. Available in PDF-file: https://pearl-hifi.com/06_Lit_Archive/15_Mfrs_Publications/10_Bruel_Kjaer/04_App_Notes/Static_and_Dynamic_Balancing_2nd_Edn.pdf

Verma, A. K., Sarangi, S. & Kolekar, M. H. 2014. Experimental Investigation of Misalignment Effects on Rotor Shaft Vibration and on Stator Current Signature. Journal of Failure Analysis and Prevention, Vol. 14, No. 2. Springer. Pp. 125-138.

Vuojolainen, J., Jastrzebski, R. & Pyrhönen, O. 2018. Balancing of a Rotor with Active Magnetic Bearing System: Comparison of One-and Two-Plane Balancing Procedures. 2018 20th European Conference on Power Electronics and Applications (EPE'18 ECCE Europe). Riga, Latvia. 17-21 Sept. 2018. IEEE. P. 1-8.

Vuojolainen, J. 2020. Identification of Magnetically Levitated Machines. Doctoral Thesis. Lappeenranta-Lahti University of Technology. 133 p.

Wang, H. & Gong, J. 2019. Dynamic analysis of coupling misalignment and unbalance coupled faults. Journal of Low Frequency Noise, Vibration and Active Control, Vol. 38, No. 2. SAGE Publications Inc. Pp. 363-376.

Wroblewski, A. C. 2011. Modeling and Identification of Active Magnetic Bearing High-Speed Machining Spindle for High-Speed Precision Machining Operation. Doctoral Thesis. Cleveland State University. 120 p. [Referred 25.01.2021]. Available in PDF-file: https://www.researchgate.net/publication/281936470.

Yoon, S.Y., Lin, Z. & Allaire, P.E. 2013. Control of Surge in Centrifugal Compressors by Active Magnetic Bearings – Theory and Implementation. 1st edition. London, United Kingdom. Springer. 275 p.

Zhang, S.Y., Pan, W., Wei, C.B. & Wu, J.H. 2017. Structure design and simulation research of active magnetic bearing for helium centrifugal cold compressor. IOP Conference Series Materials Science and Engineering, Vol. 278, No. 1. Madison, Wisconsin, USA. 9-13 July 2017. IOP Publishing. P. 1-8.